Spring 2019

Studying Carbon Dioxide Solvent Properties by Microwave Spectroscopic Investigations of Vinyl Fluoride/Carbon Dioxide Clusters and Developing New Approaches to Decode Rotational Spectra

Prashansa Kannangara
Eastern Illinois University

The Graduate School
EASTERN ILLINOIS UNIVERSITY

Thesis Maintenance and Reproduction Certificate

FOR: Graduate Candidates Completing Theses in Partial Fulfillment of the Degree
Graduate Faculty Advisors Directing the Theses

RE: Preservation, Reproduction, and Distribution of Thesis Research

Preserving, reproducing, and distributing thesis research is an important part of Booth Library's responsibility to provide access to scholarship. In order to further this goal, Booth Library makes all graduate theses completed as part of a degree program at Eastern Illinois University available for personal study, research, and other not-for-profit educational purposes. Under 17 U.S.C. § 108, the library may reproduce and distribute a copy without infringing on copyright; however, professional courtesy dictates that permission be requested from the author before doing so.

Your signatures affirm the following:

- The graduate candidate is the author of this thesis.

- The graduate candidate retains the copyright and intellectual property rights associated with the original research, creative activity, and intellectual or artistic content of the thesis.

- The graduate candidate certifies her/his compliance with federal copyright law (Title 17 of the U. S. Code) and her/his right to authorize reproduction and distribution of all copyrighted materials included in this thesis.

- The graduate candidate in consultation with the faculty advisor grants Booth Library the nonexclusive, perpetual right to make copies of the thesis freely and publicly available without restriction, by means of any current or successive technology, including but not limited to photocopying, microfilm, digitization, or internet.

- The graduate candidate acknowledges that by depositing her/his thesis with Booth Library, her/his work is available for viewing by the public and may be borrowed through the library's circulation and interlibrary loan departments, or accessed electronically. The graduate candidate acknowledges this policy by indicating in the following manner:

_____Yes, I wish to make accessible this thesis for viewing by the public

__X__No, I wish to quarantine the thesis temporarily and have included the ***Thesis Withholding Request Form***

- The graduate candidate waives the confidentiality provisions of the Family Educational Rights and Privacy Act (FERPA) (20 U. S. C. § 1232g; 34 CFR Part 99) with respect to the contents of the thesis and with respect to information concerning authorship of the thesis, including name and status as a student at Eastern Illinois University. I have conferred with my graduate faculty advisor. My signature below indicates that I have read and agree with the above statements, and hereby give my permission to allow Booth Library to reproduce and distribute my thesis. My adviser's signature indicates concurrence to reproduce and distribute the thesis.

Prashansa Kannangara
Printed Name
07/09/2019
Graduate Degree Program

Faculty Adviser Signature
Rebecca Peebles
Printed Name
7/9/19
Date

Please submit in duplicate.

Studying carbon dioxide solvent properties by microwave spectroscopic investigations of vinyl fluoride/carbon dioxide clusters and developing new approaches to decode rotational spectra

(TITLE)

BY

Prashansa Kannangara

THESIS

SUBMITTED IN PARTIAL FULFILLMENT OF THE REQUIREMENTS
FOR THE DEGREE OF

Masters of Science in Chemistry

IN THE GRADUATE SCHOOL, EASTERN ILLINOIS UNIVERSITY
CHARLESTON, ILLINOIS

2019

YEAR

I HEREBY RECOMMEND THAT THIS THESIS BE ACCEPTED AS FULFILLING
THIS PART OF THE GRADUATE DEGREE CITED ABOVE

THESIS COMMITTEE CHAIR	4/18/19 DATE	DEPARTMENT/SCHOOL CHAIR OR CHAIR'S DESIGNEE	4/18/19 DATE
THESIS COMMITTEE MEMBER	4/18/19 DATE	THESIS COMMITTEE MEMBER	4/18/19 DATE
THESIS COMMITTEE MEMBER	4/18/19 DATE	THESIS COMMITTEE MEMBER	DATE

Studying CO_2 solvent properties by microwave spectroscopic investigation of vinyl fluoride/CO_2 clusters and developing new approaches to decode rotational spectra

Dedicated to God and my parents

Acknowledgements

I want to acknowledge my research supervisor Dr. Rebecca Peebles and Dr. Sean Peebles, for their continuous support, guidance, and all the opportunities gave me during this period and also, their assistance and help in correcting English and grammatical errors in my thesis.

Special thanks to Dr. Brooks Pate for allowing me to visit his lab and use the great instrument in his lab. I want to thank his graduate student Channing West, for collecting all the scans for us. I would also like to thank Dr. Steve Scheiner for helping us with the AIM analysis.

I would also like to express my gratitude to my thesis committee, Dr. Douglas G. Klarup, Dr. Daniel J. Sheeran and Dr. Edward M. Treadwell, for taking a careful look at my thesis and their wonderful suggestions. They helped me to produce a much better thesis.

I would also like to thank my friend Tulana Ariyaratne, for his moral support. I would also like to thank Cori Christenholz for carrying out VF...CO_2 dimer studies, they helped and guided me a lot to initiate the study of VF...CO_2...CO_2 trimers; thanks to past students in our group, Asela Dikkumbura and Ashley Anderton, I used their theses as a guide when I write my dissertation. Thanks also to the Chemistry and Biochemistry faculty and students in the Eastern Illinois University.

I also want to acknowledge the financial support given by the National Science Foundation grants, RUI 1664900 (EIU) and CHE 1531913 (UVa). Lastly, I want to thank my parents, sister and brother, for their support and encouragement.

Abstract

Supercritical carbon dioxide (sc-CO_2) is an excellent green solvent, but its properties are not thoroughly understood. For example, fluorinated compounds have higher than expected solubility in sc-CO_2. Microwave spectroscopy is one way to learn more about sc-CO_2 because it can be used to determine detailed structures of small clusters of molecules. The purpose of this investigation was to study weak hydrogen bonding interactions in complexes of fluorinated ethylene (solute) with carbon dioxide (CO_2, solvent). Investigations on dimers with one CO_2 molecule and fluorinated ethylene were carried out previously and found two different structures for vinyl fluoride (VF)...CO_2, one structure for 1, 1-difluoroethylene...CO_2 and one structure for trifluoroethylene...CO_2. In this study, the trimer VF...CO_2...CO_2 has been studied using chirped-pulse Fourier-transform microwave (CP-FTMW) spectroscopy. Four structures were predicted using theoretical calculations and two of these possible structures were observed experimentally. Based on measured rotational constants, and comparing intensities with predicted dipole components, the actual structures were predicted well by theoretical calculations. Both observed trimer structures have CH...O interactions that are similar to the observed dimers. Weakly bound tetramers were the next step in the series of complexes of CO_2 with fluorinated ethylene. But before going to the next step, we were able to observe 5 constant difference patterns from original scans which were not previously assigned. Then these 5 patterns were fully assigned and the experimental rotational constants for the spectra were found. But the cluster formulas and structures associated with them were unknown. Then to find the structures for these unknown molecular clusters we collected additional scans with different CO_2 concentrations. These

data helped us to develop different analytical tools using MathCAD program for identifying the formulas for assigned spectra as well as extracting 5 more unknown molecular clusters. We were able to come up with some possible matches for the unknown clusters, ranging from trimers up to pentamers with the aid of Gaussian and ABCluster program. Future work will involve finding molecular structures for unknown cluster and finding ways to better mimic CO_2 solvation of VF.

Table of Contents

List of Figures

List of Tables

Abbreviations

1. *sc*-CO_2 - Supercritical CO_2
2. μ - Reduced mass
3. ω - Angular velocity
4. J - 0, 1, 2, 3.... (Rotational quantum number of the molecule)
5. $\hbar$ - $h/2\pi$ (h is Planck's constant)
6. B' - Rotational constant (Units of B'=Joules)
7. B - Rotational constant (Units of B = Hertz)
8. κ - Kappa (the Ray's asymmetry parameter)
9. A,B,C – Rotational constants along the three principal axes
10. P_{aa}, P_{bb}, P_{cc} - Planar moment for a axis, b axis and c axis, respectively
11. μ_a, μ_b, μ_c - Dipole components along the three principal axes
12. Int_{max} - Maximum intensity
13. CP-FTMW - Chirped-pulse Fourier-transform microwave
14. UVa - University of Virginia
15. VF - vinyl fluoride (C_2H_3F)
16. DFE - 1,1-difluoroethylene ($C_2H_2F_2$)
17. TFE - trifluoroethylene (C_2HF_3)
18. AIM - Atoms in Molecules
19. BCPs - Bond critical points
20. XCC - Extended cross correlation
21. DFT - Density functional theory

CHAPTER 1

Introduction

1. I. Supercritical carbon dioxide and fluorinated ethylene complexes

(What is basis of the research project?)

The ultimate goal of this research project is to determine the solvation sphere of supercritical CO_2 (*sc*-CO_2) around vinyl fluoride (VF) which gives an idea of how many CO_2 molecules should combine and weakly interact. *sc*-CO_2 is a fluid state of CO_2 which can be found in high temperatures (304 K) and high pressure (83.8 bar) conditions.[1] *sc*-CO_2 is an environmentally friendly solvent and it can be used as a coffee decaffeinating agent, extraction solvent for essential oils and dry-cleaning agent, etc.[2, 3] Even though *sc*-CO_2 is used in various industries the properties of *sc*-CO_2 are not fully resolved. The ultimate goal of this research series is to give insight on the properties of *sc*-CO_2. CO_2 is a greenhouse or heat trapping gas, which contributes to climate change. If *sc*-CO_2 is capable of being used as an organic solvent, it would provide a way to reuse captured CO_2 from industrial processes before it is released, and avoiding using more toxic or damaging chemicals.

This research series primarily studies gaseous phase CO_2 complexes using microwave spectroscopy and, through these findings, provide information about *sc*-CO_2 solvation properties. This fundamental chemical research uses microwave spectroscopy to study and understand weak interactions between molecules. The major purpose is to determine the detailed molecular structures and to learn about the weak hydrogen bonding interactions in complexes of fluorinated ethylenes with carbon dioxide (CO_2). The interactions within the complexes of the smallest fluoroalkene molecules, consisting of two C atoms, and CO_2 were studied by using microwave spectroscopy. Studying the weak interactions between these molecules permits investigation of the solvation properties of supercritical CO_2.

Previous investigations have found that fluorinated hydrocarbons have increased solubility in *sc*-CO_2.[1] Most non-polar solutes have the ability to dissolve in *sc*-CO_2 because of its non-polar nature. Even though the CO_2 molecule has zero dipole moment, it has nonzero bond dipoles. Hence, it also has some ability to form solvent...solute interactions in a polar media. Because of this ability to form interactions, fluorinated hydrocarbons have increased solubility in *sc*-CO_2 compared to the hydrogen substituted equivalent compounds. For example, Krytox 16350 and Teflon AF are fluorinated polymers which can be dissolved in *sc*-CO_2 (Fig. 1.1.a and 1.1.b).[4]

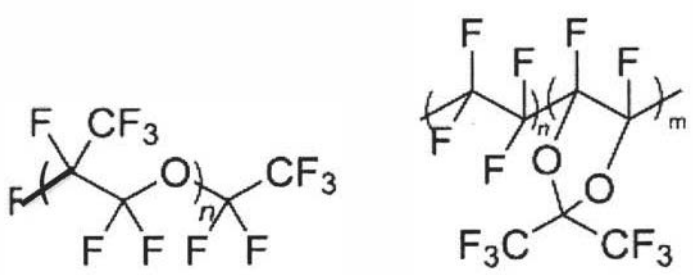

a). Krytox 16350 **b). Teflon AF**

Figure 1.1: Fluorinated polymers which can dissolve in *sc*-CO_2 a). Krytox 16350 b). Teflon AF[4]

1. II. Introduction to microwave spectroscopy

Microwave spectroscopy is the study of the interaction of matter and electromagnetic radiation in the microwave region (300 MHz to 300 GHz) of the spectrum (Fig. 1.2). When a molecule is irradiated with excited photons, it may absorb the radiation and undergo an energy transition. When a molecule with a permanent dipole moment absorbs microwave radiation, the molecule starts to rotate.

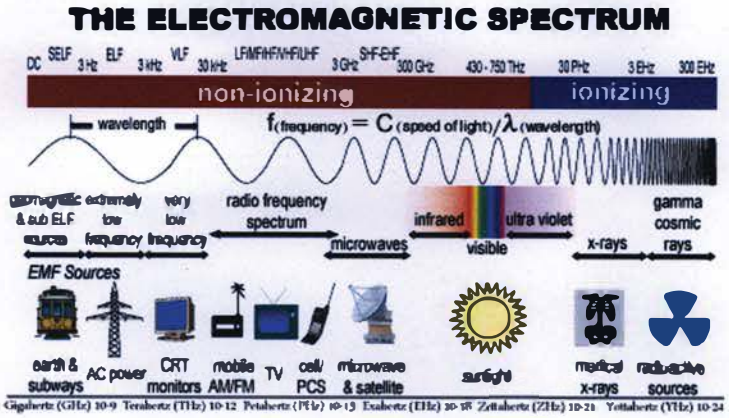

Figure 1.2: The electromagnetic spectrum[5]

Microwave spectroscopy is used for fundamental chemical research studies such as investigating the detailed structures of molecules and noncovalent interactions within molecular clusters. The knowledge gained from microwave spectroscopy studies can help to learn more about the different systems, but they cannot be studied directly by microwave spectroscopy, themselves. The knowledge gained from microwave spectroscopy can be used in structure-based drug design processes by helping understand the noncovalent interactions between a ligand and its receptor.[6] Also, it can be used in studying the interaction between CO_2 and metal-organic frameworks (MOFs) which are capable of capturing CO_2.[7] In the present research, microwave spectroscopy is being used to study weak interactions within the fluoroethylene and CO_2 molecular clusters to help understand *sc*-CO_2 solvation properties.

1. III. Theory of microwave spectroscopy

The basis of microwave spectroscopy is that in order for a molecule to rotate it needs to have a discrete amount of energy. When a polar molecule sits in its J=0 energy level there is no rotation at all (Fig. 1.3), where J is the quantum number used to denote the amount of rotational angular momentum.

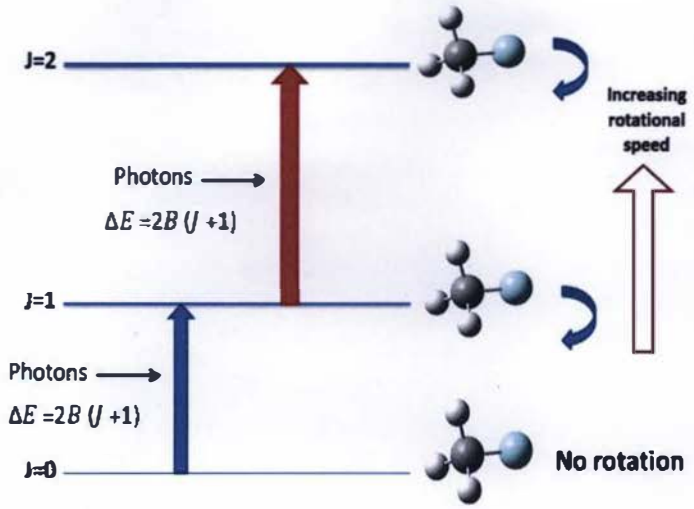

Figure 1.3: Energy transitions between adjacent energy levels[8]

When the molecule has a permanent dipole moment it can absorb the energy from the microwave region of the electromagnetic spectrum. Hence, when photons shine on the molecule it absorbs energy from the microwave region and moves higher energy levels. The exact frequency that it needs to rotate and jump to the next energy level is associated with the molecular structure of the rotating molecule. When the molecule moves to the higher energy levels, its rotational speed also becomes higher. Absorbing a specific amount of energy means it absorbs a specific frequency of radiation since the energy and frequency are related to each other (Eq. 1.1).

$$\Delta E = h\nu \qquad \textbf{Equation 1.1}$$

ΔE=Energy difference
h=Planck's constant
ν=Frequency

The frequency needed to jump to the next energy level is directly related to the mass distribution of the molecule and different molecules have different mass distributions. Hence, the absorbed frequency should be specific to a certain molecule,

making this absorbed frequency completely unique depending on the structure and the mass of the molecule. So, the generated rotational spectrum for a specific molecule is unique for it and it is like a molecular fingerprint of the molecule.

The theory of microwave spectroscopy can be explained mathematically. To explain the theory behind the microwave spectroscopy, the rigid rotator model is used, which is a simple model for a rotating diatomic molecule (Fig. 1.4). This model is the rotational equivalent of the harmonic oscillator. In this diatomic molecule there are two atoms which have masses of m_1 and m_2 (Fig. 1.4). The two atoms are connected with a bond which does not have weight. The distance between two atoms is r and this diatomic molecule rotates around the center of mass with the angular velocity ω. Atoms 1 and 2 are located at r_1 and r_2 distances from the center of mass, respectively.

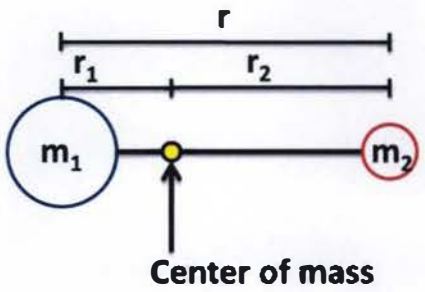

Figure 1.4: Rigid rotator model for a diatomic molecule[9]

For a diatomic molecule the total mass is calculated as the reduced mass, μ, using equation 1.2. Hence, in the rigid rotator model it is assumed the reduced mass is rotating around the center of mass with the angular velocity of ω.

$$\mu = \frac{m_1 m_2}{m_1 + m_2} \qquad \textit{Equation 1.2}$$

When masses and distances from the center of mass are available the moment of inertia of the molecule can be calculated. Equation 1.3 and 1.4 can be used to calculate

the moment of inertia for diatomic molecules and polyatomic molecules, respectively. Moment of inertia is the measurement of the resistance against angular acceleration and it is also the angular equivalent of mass in microwave spectroscopy. The moment of inertia depends on the axis of rotation.

$$I = \mu r^2 \qquad \textit{Equation } 1.3$$

$$I = \sum_{i=1}^{n} m_i r_i^2 \qquad \textit{Equation } 1.4$$

i=sum over each atom
m_i=atomic mass
r_i=distance of the atom from the axis of rotation

Equation 1.5 can be obtained after solving the Schrödinger equation, and used to calculate total rotational energy in a diatomic molecule. This equation can also be used to calculate the total rotational energy of any rigid linear molecule.

$$E_J = \frac{\hbar^2}{2I} J(J+1) = B'J(J+1) \qquad \textit{Equation } 1.5$$

J=0, 1, 2, 3.... (Rotational quantum number of the molecule)
$\hbar = h/2\pi$ (h is Planck's constant)
B'=Rotational constant= $\hbar^2/2I$ (Units of B'=Joules)

Rotational constants are the most important parameter that can be found in microwave spectroscopy. As mentioned in the beginning of this section, depending on the mass distribution of a molecule it absorbs discrete amounts of energy. Since the energy and the rotational constant are related (Eq. 1.5), the rotational constant is a unique parameter for a specific molecule. Rotational constants can be measured in Joules (Eq.

1.6) and Hertz (Eq. 1.7) though usually in microwave spectroscopy Hertz is used to measure the rotational constants.

$$B' = \frac{h^2}{8\pi^2 I} \qquad \textbf{Equation 1.6}$$

$$B = \frac{h}{8\pi^2 I} \qquad \textbf{Equation 1.7}$$

When considering a diatomic molecule, it should have different energy levels in order to produce a rotational spectrum with $\Delta J=\pm 1$. The energy for a certain energy level with a quantum number J can be calculated using Equation 1.5. The energy of the transition between two energy levels must be equivalent to the energy of the photon absorbed according to the Planck's equation (Eq. 1.1). For a diatomic molecule the rotational energy on specific energy level (J) and its adjacent level (J+1) can be calculated by equations 1.8 and 1.9. The rotational energy difference between adjacent rotational levels (J to J+1) can be calculated by equation 1.10 (Fig. 1.5). Therefore the irradiated frequency of the absorbed photon can be calculated using equation 1.11.

$$E(J) = B'J(J+1) \qquad \textbf{Equation 1.8}$$

$$E(J+1) = B'(J+1)(J+2) \qquad \textbf{Equation 1.9}$$

$$E(J+1) - E(J) = B'(J+1)(J+2) - B'J(J+1)$$

$$\Delta E = 2B'(J+1) \qquad \textbf{Equation 1.10}$$

$$\nu = 2B(J+1) \qquad \textbf{Equation 1.11}$$

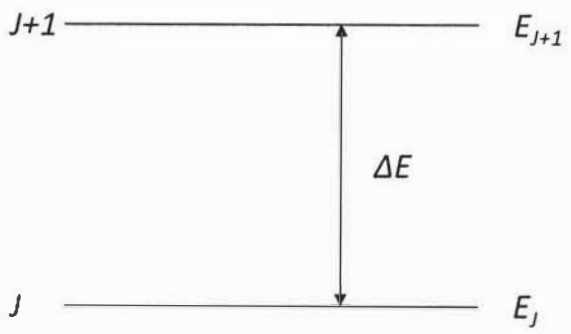

Figure 1.5: Energy difference between two adjacent energy levels

According to equations 1.10 and 1.11, when energy transfers from one energy level to an adjacent energy level, the frequency difference is directly proportional to twice the rotational constant (Fig. 1.6). Hence by using the frequency difference between two adjacent energy levels, for a diatomic molecule the rotational constant can be obtained. If the rotational constant is known then the moment of inertia (I) can be calculated by using equation 1.7. After finding the moment of inertia, equation 1.3 or 1.4 can be used to calculate the bond distances for the diatomic molecule or polyatomic molecules. Therefore, by using the B and I, molecular structural parameters can be obtained for a rigid molecule. Hence, microwave spectroscopy is a very important and reliable method to determine the molecular structure for rigid molecules.

In microwave spectroscopy, three principal axes are defined a, b and c (Fig. 1.7). All the axes originate from the molecule's center of mass. Hence, whenever the molecule rotates around the center of mass, these three rotational axes are considered. The axis which has the minimum moment of inertia is defined as the a axis. The axis which has maximum moment of inertia is defined as the c axis. The axis perpendicular to both a and c axes is the b axis. The mass distribution of the molecule is considered along these three

axes and therefore whenever structural calculations are being done all the moments of inertia (I_a, I_b and I_c) around the three axes are accounted for.

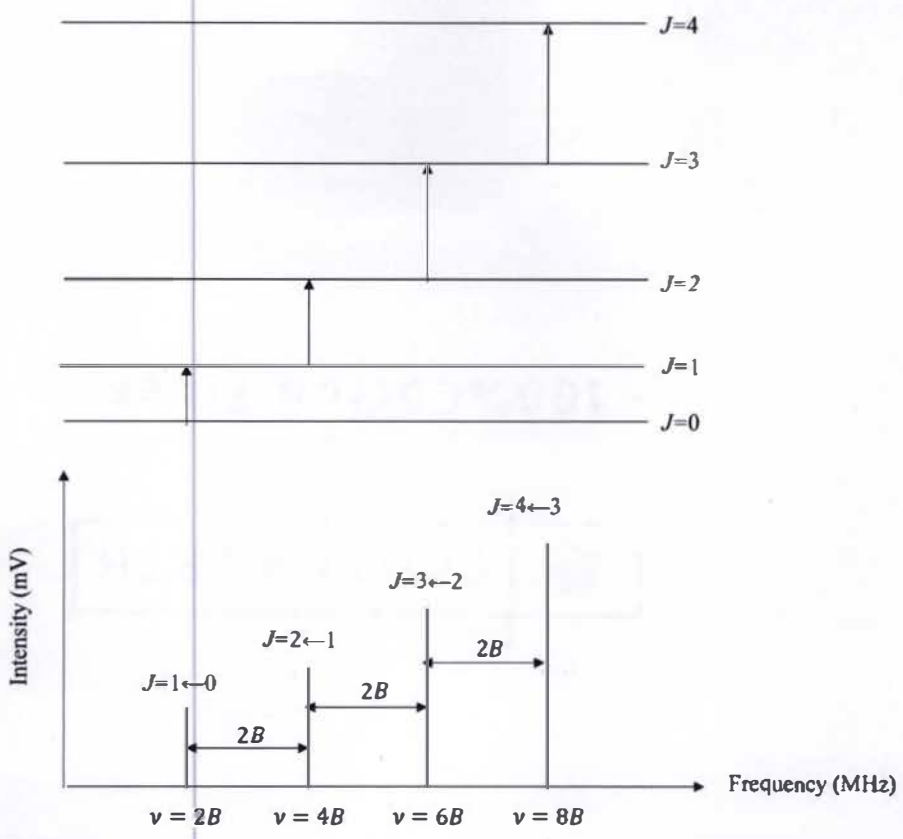

Figure 1.6: The energy transition and corresponding rotational spectrum for the energy transitions[10]

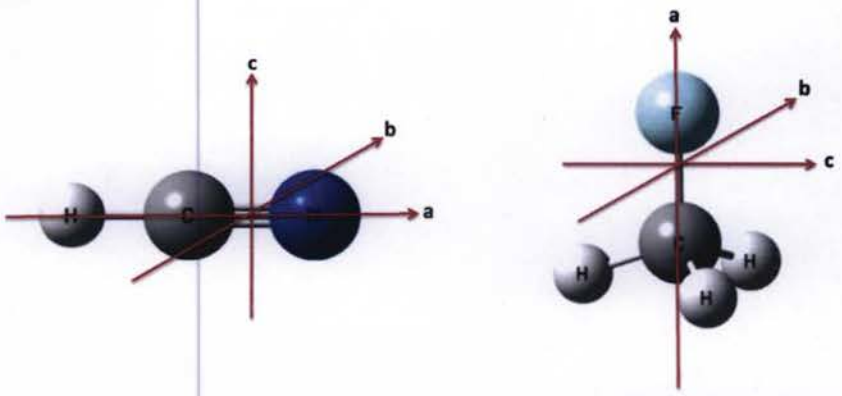

Figure 1.7: The principal axes for a linear molecule and for a non-linear polyatomic molecule[11]

A molecule that behaves according to the actual rigid rotator model has multiples of $2B$ ($2B$, $4B$, $6B$ etc.) frequency spacing between two adjacent energy levels and also $2B$ spacing between lines in the spectrum (Fig. 1.6). But a real molecule does not behave as predicted as the rigid rotator model and the transitions for a real molecule do not have the $2B$ frequency spacing in a microwave spectrum. That happens because the bonds between the atoms are not rigid, and change when the molecules rotate. When the rotational speed becomes higher, the centrifugal force acting on the molecule's bonds becomes higher. Because of that, bond lengthening occurs. Hence, the moment of inertia for a molecule can be changed according to equations 1.3 and 1.4 since the bond length changes with the rotational speed. The change in moment of inertia affects the rotational constants according to equations 1.6 and 1.7. Because of that, a constant called the centrifugal distortion constant (D) (Eq. 1.12) has to be added to equation 1.8, in order to get the correct rotational energy (Eq. 1.13) and also to get the correct transition frequency (Eq. 1.14).

$$D = \frac{4B^3}{\omega^2} \qquad \textbf{Equation 1.12}$$

$$E(J) = B'J(J+1) - D'J^2(J+1)^2 \qquad \textbf{Equation 1.13}$$

$$\nu = 2B(J+1) - 4D(J+1)^3 \qquad \textbf{Equation 1.14}$$

The above equations (Eq. 1.13 and 1.14) are valid for a linear or diatomic system. But when it comes to the nonlinear molecule system, it gets more complicated. As discussed above, a linear or nonlinear molecular system has three major axes and along these three axes they have three different moments of inertia (I_a, I_b and I_c), needed to describe the mass distribution through each axes. When it comes to nonlinear molecular systems, it requires two additional quantum numbers to the J quantum numbers to explain

the rotational energy levels, and these are designated K_a and K_c. The J quantum numbers represent the total angular momentum, while the K_a and K_c quantum numbers represent the projection of angular momentum vector on the a and c molecular principal axes, respectively.

Figure 1.8 shows how the J=2 energy level associates with the K_a and K_c energy levels. In this energy level diagram, the J=2 rotational energy state has five corresponding energy levels. The general nomenclature for these energy levels follows the $J_{K_aK_c}$ order. Hence, we can see the five different energy levels with the 2_{20}, 2_{21}, 2_{11}, 2_{12} and 2_{02} notations.

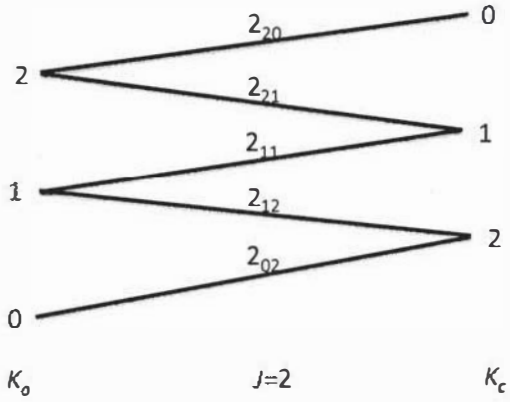

Figure 1.8: Correlation diagram for J=2 rotational energy levels (the spacing between the energy levels is not to scale, but does show the correct order)

According to the mass distribution along the axes of a molecule (in other words according to the moments of inertia) and the shape of the molecule, they can be divided into four categories, which are linear or diatomic molecules, spherical tops, symmetric tops and asymmetric tops. Moments of inertia for linear or diatomic molecule are I_a=0 and I_b=I_c since the mass distribution around the a axis is zero. In spherical tops the three

moments of inertia are equal to each other (I_a=I_b=I_c). There are two types of symmetric tops: prolate and oblate symmetric tops. The prolate symmetric tops are molecules which have cigar shaped body types (*e. g.* CH_3I, NH_3). The moments of inertia around the *b* and *c* axes are equal to each other (I_b=I_c) while the moment of inertia around the *a* axis is less than I_b and I_c. The oblate symmetric tops have pancake shaped body types (*e. g.* C_6H_6, XeF_4) and equal moments of inertia along the *a* and *b* axes (I_a=I_b) while the moment of inertia along the *c* axis is higher than the I_a and I_b. The asymmetric tops have different mass distributions around all three axes and they have lower I_a values, higher I_c values and I_b values which lie in between I_a and I_c (I_a<I_b<I_c).

Asymmetric top molecules are being studied in this research project. Unlike in the diatomic or linear molecular systems, the multi-atomic and multi-molecular asymmetric top systems need more distortion constants in order to obtain the correct energies of the rotational energy levels (eq. 1.15).[12] Usually for molecular systems in this study, even more distortion constants are added and Equation 1.15 shows a simplified version of the full energy expression.

$$E(J,K) = B'J(J+1) + (A' - B')K_a^2 - D'_J J^2(J+1)^2 - D'_{JK}J(J+1)K_a^2 + D'_K K_a^4 \qquad \textbf{Equation 1.15}$$

A and *B* are the rotational constants around the *a* and *b* axes, respectively. D_J, D_{JK} and D_K are the distortion constants.

When considering an asymmetric molecule, it has three unique moments of inertia, which mean it has three unique rotational constants (*A*, *B*, *C*) around the three axes. Rotational energies can be given by the energy level expressions shown in Table 1.1 for an asymmetric molecule. Table 1.1 only shows a few energy levels and there are

many other possible expressions that can be obtained. The energy differences between two energy levels can be worked out through the energy expressions. When calculating the energy differences the ΔK_a and ΔK_c should be 0 or ±1 to go with the J values. For example, the energy difference between 2_{21} and 1_{10} energy levels, $(4A+B+C)-(A+B)$ is $3A+C$ and this is an allowed transition, since K_a changes by 1 and K_c changes by 1. A transition such as 2_{21}-1_{01} would not be allowed, since K_a changes by 2.

Table 1.1: Rotational energy levels and corresponding energy expressions for first four rotational states[13]

Energy level ($J_{K_aK_c}$)	Energy expression
0_{00}	0
1_{10}	$A+B$
1_{11}	$A+C$
1_{01}	$B+C$
2_{21}	$4A+B+C$

To measure the degree of asymmetry of a molecule Ray's asymmetry parameter (κ) can be used. Using equation 1.16, the degree of asymmetry of a molecule can be measured quantitatively. For a prolate top molecule κ=-1 and for an oblate top molecule κ=+1.

$$\kappa = \frac{2B - A - C}{A - C} \qquad \textbf{Equation 1.16}$$

There is one more important parameter in microwave spectroscopy, which is the planar moment. The planar moment is important to help describe the shape of a molecule and gives an idea of the mass distribution of the molecule along each axis. For example, if the value of the planar moment along a certain axis is 0 or close to 0, that means there is no mass distribution along that axis. The planar moment for a axis (P_{aa}), b axis (P_{bb}) and c axis (P_{cc}) can be calculated using equation 1.17, 1.18 and 1.19, respectively.

$$P_{aa} = \frac{I_b + I_c - I_a}{2} = \sum m_i a^2 \qquad \textit{Equation 1.17}$$

$$P_{bb} = \frac{I_a + I_c - I_b}{2} = \sum m_i b^2 \qquad \textit{Equation 1.18}$$

$$P_{cc} = \frac{I_a + I_b - I_c}{2} = \sum m_i c^2 \qquad \textit{Equation 1.19}$$

m_i=sum of the mass along the axis
a=distance along a axis
b=distance along b axis
c=distance along c axis

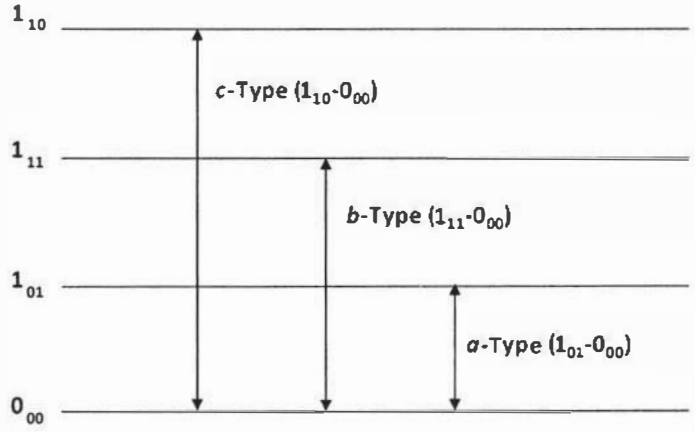

Figure 1.9: Occurrence of *a*-type, *b*-type and *c*-type transitions

When it comes to the microwave spectroscopy, the dipole moment components play a very important role. There are a possible maximum of three dipole components along the three principal axes, which are μ_a, μ_b and μ_c. The square root of the sum of the squares of each component gives the total dipole component of the molecule. There are three different types of rotational transitions called *a*-type, *b*-type and *c*-type transitions. Figure 1.9 shows example *a*-type, *b*-type and *c*-type transitions. These transitions are allowed, if there is a dipole component along a particular principal axis of the molecule. The intensity of a transition is directly proportional to the square of the dipole component. The selection rules for all three transitions are shown in the Table 1.2.

Table 1.2: Selection rules for *a*-type, *b*-type and *c*-type transitions

Type of transition	ΔJ	ΔK_a	ΔK_c
a-type	$0, \pm 1$	0	± 1
b-type	$0, \pm 1$	± 1	± 1
c-type	$0, \pm 1$	± 1	0

1. IV. Isotopic substitutions and importance

Isotopes contain different amounts of neutrons and the same amounts of electrons and protons for a specific element. Isotopologues are the group of molecules of a given compound which have different isotopic compositions. Hence, the isotopologues have different masses. When the mass differs the moment of inertia will vary according to equations 1.3 and 1.4. A change in moment of inertia causes a change in rotational constants in the molecule. Therefore, isotopologue species will produce different rotational spectra for a specific molecule. These different rotational spectra will give different rotational constants for each molecule. One microwave spectrum will provide, at most, three moments of inertia, which allow three structural parameters to be precisely determined, but most molecules have more than three structural parameters. Hence, by measuring isotopes additional moment of inertia (three more from each isotope) can be obtained. Therefore, measuring additional isotopic spectra will provide extra information on the structural parameters, making it possible to derive the moment of inertia for the molecule and the bond distances as well as bond angles. These bond angles and distances are the same for each isotopologue species and it helps to confirm the measurements are correct. Getting the same bond distances and angles with different isotopologues determines the structure of the molecule precisely.

This experiment used gaseous samples containing vinyl fluoride (VF, C_2H_3F) and CO_2. For example, considering the VF...CO_2 dimer, there are various combinations for isotopologues from ^{13}C and ^{18}O. It is possible to obtain different combinations of isotopologues such as $^{13}C^{12}CH_3F...^{12}C^{16}O^{16}O$, $^{12}C^{12}CH_3F...^{12}C^{18}O^{16}O$, $^{12}C^{12}CH_3F...^{13}C^{16}O^{16}O$, etc. along with the parent isotopologue $^{12}C^{12}CH_3F...^{12}C^{16}O^{16}O$.

The natural abundance of the isotopes is also important in rotational spectroscopy, because the peak intensities of the transitions related to isotopic substitutions are directly proportional to the abundance. For example, the ratio of ^{12}C: ^{13}C is 99:1. Hence the peak intensities for ^{13}C isotopic transitions are comparatively very weak.

1. V. Instrumentation and Experimental setup

A chirped-pulse Fourier-transform microwave spectrometer (CP-FTMW) located at University of Virginia (UVa) which operates at 2-8 GHz region was used to obtain all the spectra.[14] A gas sample containing 1% VF and 1% CO_2 with 98% Ne gas was injected into the vacuum chamber; then these gas pulses expanded supersonically inside the vacuum chamber and formed the molecular clusters. The temperature becomes very low (~2 K) inside the vacuum chamber when the gas expansion occurs. The supersonic expansion helps to keep the weak interactions between the molecules intact and helps to measure the rotational spectrum of the molecule effectively. The resulting scan is an emission spectrum of the molecular cluster.

When microwave radiation shines on the molecular clusters they absorb the radiation and initiate the rotation. The interaction between the microwave radiation and the molecular cluster aligns the dipole moments of the molecular clusters with the electric field of the radiation. Therefore, in the vacuum chamber a huge polarization can be

observed with time. When the microwave radiation is ceased the polarization decays with the time and the molecules come back to the initial state. This process is called a free induction decay (FID). The FID is recorded in the time domain but in microwave spectroscopy using the scan in the frequency domain is desired. Therefore, to obtain a spectrum with a frequency domain the Fourier-transform (FT) is applied to the time domain spectrum (Fig. 1.10).

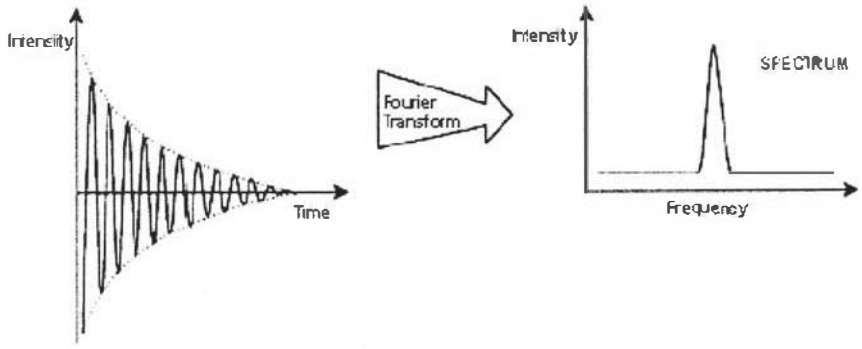

Figure 1.10: Fourier transformation from time domain to frequency domain[15]

1. VI. Objectives and Goals

The main objectives of this project are,

- To find spectra of the isomers for VF...CO_2...CO_2 trimer (Chapter 2)
- To determine the possible structures for the VF...CO_2...CO_2 trimer (Chapter 2)
- To find isomers for tetramers containing VF and CO_2 (Chapter 3)

In this study, five different spectra for unknown structures were extracted from the experimental data. After recording more data, different analytical tools were developed to extract more spectra from the collected scans. The objectives of the second half of this study were,

- To develop analytical tools to identify spectra from the collected scans (Chapter 3)

- To find the formulas and molecular structures for the assigned spectra (Chapter 3)

1. VII. References

[1]https://www.energy.gov/supercritical-co2-tech-team, accessed 01/10/2019.

[2]P. Raveendran, Y. Ikushima, S. L. Wallen, Polar attributes of supercritical carbon dioxide. *Acc. Chem. Res.*, **2005,** 38, 478-485.

[3]X. Zhang, S. Heinonen, E. Levanen, Applications of supercritical carbon dioxide in materials processing and synthesis. *RSC Adv.*, **2014,** 4, 61137-61152.

[4]J. Peach, J. Eastoe, Supercritical carbon dioxide: a solvent like no other. *Beilstein J Org Chem.* **2014,** 10, 1878-1895.

[5]https://churchofthecosmos.wordpress.com/2012/12/05/%EF%BB%BFthe-electromagnetic-radiation-spectrum-and-its-health-risks/electromagnetic-spectrum/, accessed 01/10/2019.

[6]S. Sarkhel, G. R. Desiraju, N-H...O, O-H...O, and C-H...O hydrogen bonds in protein-ligand complexes: Strong and weak interactions in molecular recognition. *Proteins: Structure, Function and Bioinformatics*, **2004,** 54, 247-259.

[7] https://commons.lbl.gov/display/neatongroup/Carbon+Capture, accessed 01/08/2019

[8] S. A. Peebles, Personal communication, **2019**

[9] http://hyperphysics.phy-astr.gsu.edu/hbase/cm.html, accessed 01/10/2019.

[10]https://chem.libretexts.org/Bookshelves/Physical_and_Theoretical_Chemistry_Textbook_Maps/Supplemental_Modules_(Physical_and_Theoretical_Chemistry)/Spectroscopy/Rotational_Spectroscopy/Microwave_Rotational_Spectroscopy. accessed 01/10/2019.

[11]M. J. Hollas, Basic Atomic and Molecular Spectroscopy. 4th edition, John Wiley & Sons, Inc., West Sussex, **2004**. Ch. 4.

[12]M. J. Hollas, Basic Atomic and Molecular Spectroscopy. 4th edition, John Wiley & Sons, Inc., West Sussex, **2004**. Ch. 5.

[13]W. Gordy, R. L. Cook, Microwave Molecular Spectra, 3rd edition, John Wiley and Sons, New York, **1984**, Ch. 7.

[14]G. G. Brown, B. C. Dian, K. O. Douglass, S. M. Geyer, B. H. Pate, A Broadband Fourier Transform Microwave Spectrometer Based on Chirped Pulse Excitation. *Rev. Sci. Instrum*, **2008**, 79, 053103.

[15]http://triton.iqfr.csic.es/guide/man/beginners/chap3-9.htm, accessed 02/17/2019.

CHAPTER 2

Studying CO_2 solvent properties by microwave spectroscopic investigation of $VF\ldots CO_2\ldots CO_2$ trimers

2. I. Introduction

The ultimate goal of this research series is to find the weak interactions within fluoroethylene and CO_2 complexes. Previously the research group carried out experiments on vinyl fluoride...CO_2 dimer complexes.[1] Hence, in this chapter, the findings of a new trimer, vinyl fluoride...CO_2...CO_2 using CP-FTMW spectroscopy will be discussed and variations in the CH...O interaction strength and orientation in VF/CO_2 molecular clusters will be compared.

In 1995, Bemish *et al* found a complex of ethylene and CO_2 (Fig. 2.1).[2] In this ethylene...CO_2 the CO_2 molecule is positioned above the ethylene molecule in a stacked structure and aligned in a parallel fashion.

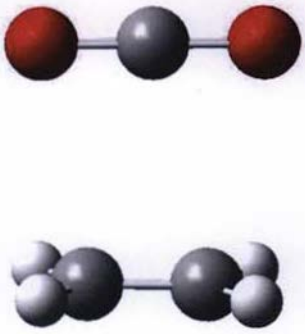

Figure 2.1: Ethylene...CO_2 dimer structure[2]

In this research series fluorinated ethylene compounds with its CO_2 complexes were studied. The fluorinated ethylene...CO_2 complexes have F atoms substituted in the place of H atoms. The first and simplest fluorinated ethylene in the series is vinyl fluoride (VF, C_2H_3F). Investigations of dimers with one CO_2 molecule and one VF molecule were carried out previously.[1] Three theoretical structures were simulated and two different planar isomers which are Side and Top dimers for VF...CO_2 (Fig. 2.2.a and 2.2.b, respectively) were observed experimentally. In the Side dimer, the CO_2 molecule lies in

the same plane as the VF and also nearly perpendicular to the double bond. In the Top dimer, the CO_2 molecule is lying in the same plane approximately parallel to the double bond of the VF molecule and also on the side with the F in the VF molecule. The Above structure is non planar and it was not observed experimentally (Fig. 2.2.c). In the Above dimer, the CO_2 molecule lies on top of the C-F bond and also it is perpendicular to the C-F bond of the VF molecule.

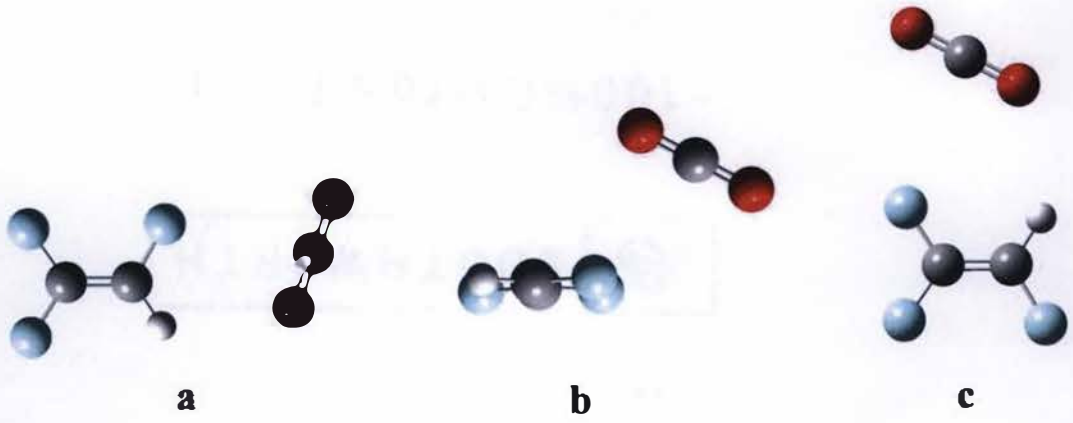

Figure 2.2: TFE...CO_2 dimers a). Side b). Above c). Top[1]

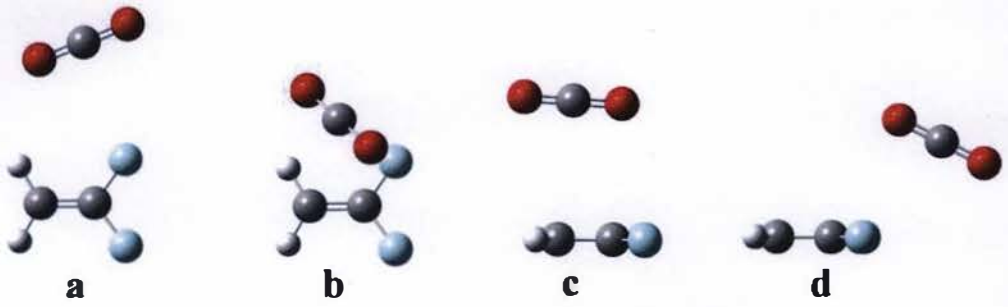

Figure 2.3: DFE...CO_2 dimers[3]

Studies on CO_2 complexes of 1,1-difluoroethylene (DFE, $C_2H_2F_2$) (Fig. 2.3) and trifluoroethylene (TFE, C_2HF_3) (Fig. 2.4) were also carried out.[3, 4] For DFE...CO_2 dimer studies four different theoretical structures were simulated and only one dimer structure (the Top) was observed experimentally (Fig. 2.3.a). In TFE...CO_2 dimer studies, three different theoretical structures were simulated and only one isomer (the Side) was experimentally observed (Fig. 2.4.a).

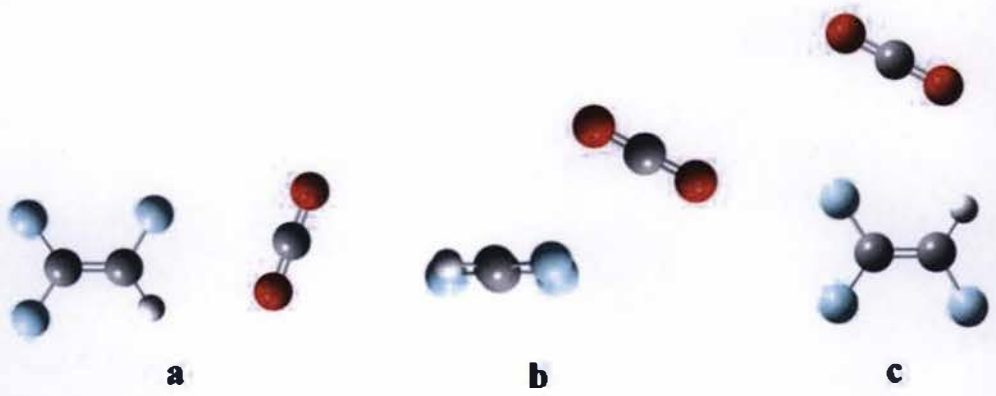

Figure 2.4: TFE...CO_2 dimers[4]

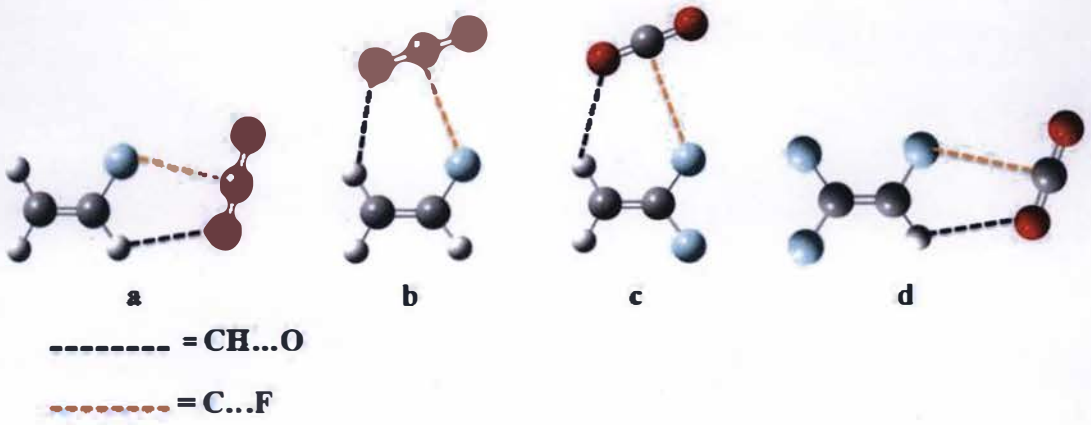

Figure 2.5: Experimentally observed fluoroethylene...CO_2 dimers a). VF...CO_2 Side dimer b). VF...CO_2 Top dimer c). DFE...CO_2 Top dimer d). TFE...CO_2 Side dimer[1, 3, 4]

Intermolecular interactions are important in molecular clusters because these interactions hold the molecules together within a cluster. When the cluster size increases, the both strength and number of interactions between atoms also increases. Hence, studying interactions in these molecular clusters is very important since the ultimate goal of this project is to study the solvation properties of the *sc*-CO_2 by examining these fluoroethylene/CO_2 complexes. All the studied dimers, which are VF...CO_2, DFE...CO_2 and TFE...CO_2, had two types of non-covalent interactions. One type was CH...O interactions and other type was C...F interactions (Fig. 2.5). The goals of this study were to investigate weak non-covalent interactions in VF...CO_2...CO_2 using CP-FTMW spectroscopy, to compare variations in CH...O interaction strength and orientation in VF/CO_2 molecular clusters and also to study the structural changes that occur within the complexes when the VF/CO_2 molecular cluster gets larger.

To study the weak interactions within these molecular clusters more quantitatively and precisely Atoms in Molecules (AIM) analysis via the AIMAll program was used.[5,6] This theoretical model determines the weak interactions and bonding nature between atoms in molecules by using electron densities of the atoms in the molecular cluster. AIM is used to study the atom...atom, covalent and non-covalent interactions in molecules or molecular clusters.

2. II. Experimental

2. II. A. Predicting possible structures and rotational constants

The initial structures of Top-Side, Top-Above and Side-Above, Above-Above (Fig. 2.6) were predicted using the previously studied VF...CO_2 dimer structures; Top,

Side and Above (Fig. 2.2).[7] All the initial structures were optimized using Gaussian 09 at the MP2 level and 6-311++G(2d,2p) basis set to obtain theoretical rotational constants.[8]

2. II. B. Microwave spectroscopy

The experimental microwave spectrum was obtained from the chirped-pulse Fourier-transform microwave (CP-FTMW) spectrometer at the University of Virginia (UVa) which operated in the region of 2-8 GHz. The gas sample used to acquire the spectrum contained 1% VF and 1% CO_2. The remaining 98% was filled with 2 atm of Ne buffer gas. To obtain one scan 1 million spectra were averaged.

2. II. C. Spectral assignment

Using the theoretical rotational constants from the Gaussian optimizations, the SPCAT program was run to obtain the theoretical rotational spectrum for each optimized structure.[9] The theoretical rotational spectrum acts as a guide to identify patterns in the experimental spectrum. At the very beginning of the process of assigning spectra, these theoretical and experimental rotational spectra were not lining up with each other, because the theoretical rotational constants were different from the experimental rotational constants and the resulting theoretical rotational spectrum is different from the experimental rotational spectrum. Hence, to align the theoretical transition frequencies with the experimental transition frequencies the SPFIT program was used. The SPFIT program uses the experimental line frequencies to update the rotational constants based on the Watson A-reduction Hamiltonian.[10] Then, the SPCAT program was rerun which allows prediction of a theoretical spectrum that reproduces the experimental rotational spectra better.[8,9] Then, gradually, the distortion constants were added until a better fit was obtained. After lining up the theoretical spectrum of a specific experimentally likely

structure to the experimental spectrum, the experimental rotational constants can be obtained from the fit file which is produced by the SPFIT program.

2. III. Results and Discussion

2. III. A. Initial guesses for trimers

Previously studied VF...CO_2 dimer structures Above, Top and Side (Fig. 2.2) were used as building blocks to generate initial trimer structure guesses (Fig. 2.6).[4] To begin, two experimentally favorable dimer structures were combined together to give the Top-Side trimer. Even though the Above structure was not observed experimentally, it was used as a building block to get the initial guesses for the trimers where the Top and Side structures both were combined with the Above structure separately to give the Top-Above and Side-Above structures. Finally the Above structure was combined with itself to give the Above-Above trimer structure.

2. III. B. Structural optimizations

From the relative energies of the optimized structures it was found that the Top-Above and Side-Above structures are energetically more likely to be experimentally observed since they had low energies compared to the other two structures (Table 2.1).

2. III. C. Spectral assignments

From the experimental spectrum, two recognizable constant difference patterns were found (Fig. 2.7). Constant difference patterns are useful in assigning spectra as the frequency difference between a and b was equal to the frequency difference between c and d and also the same for the e and f difference and g and h difference. These constant difference patterns were matched with the patterns of predicted spectra of the Side-Above and Top-Above structures. Then the quantum numbers were assigned for the patterns and

SPFIT program was run in order to provide the experimental rotational constants (Table 2.1).

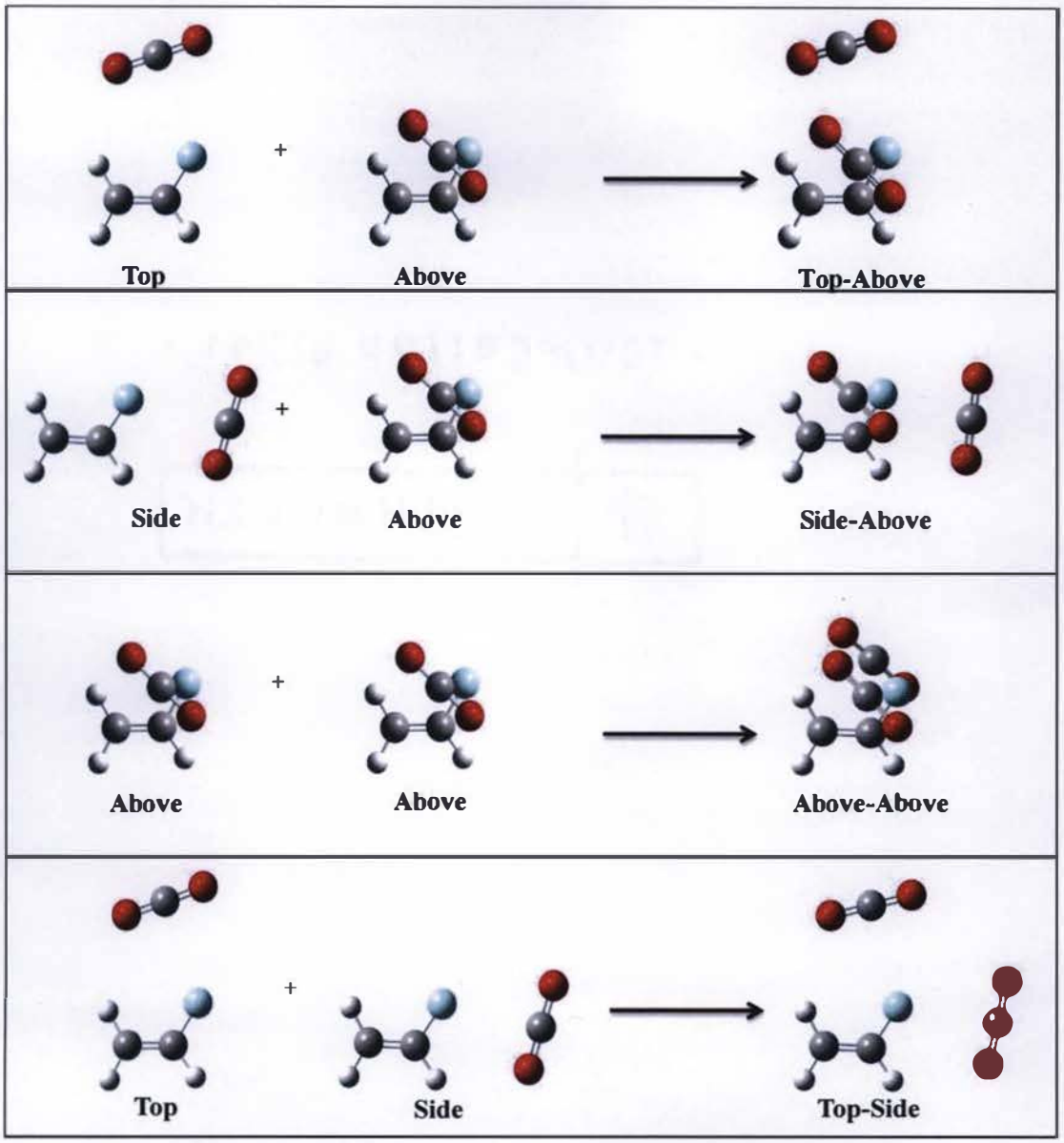

Figure 2.6: Guessing of initial structures for VF...CO_2...CO_2 trimers using previously studied VF...CO_2 dimers

Table 2.1: Theoretical and experimental constants and energies for the ab initio and experimentally observed VF...CO_2...CO_2 trimer structures

	Side-Above	Top-Above	Above-Above	Top-Side	Isomer I (Side-Above)	Isomer II (Top-Above)
A/MHz	1734.3	1618.7	2933.3	1626.9	1660.35121(8)	1552.10543(12)
B/MHz	1107.4	1174.0	643.5	922.8	1109.76469(6)	1169.46004(11)
C/MHz	808.4	881.9	609.4	588.8	785.77728(6)	847.25679(12)
Δ_J/kHz					1.5373(10)	2.143(4)
Δ_{JK}/kHz					−0.3410(18)	−4.0883(26)
Δ_K/kHz					4.1842(17)	7.577(3)
δ_J/kHz					0.3739(3)	0.6035(4)
δ_K/kHz					1.4606(17)	0.3219(18)
P_{aa}/amu Å^2 [a]	395.1	345.7	721.2	547.7	397.08512(4)	351.51361(8)
P_{bb}/amu Å^2 [a]	230.1	227.4	108.1	310.7	246.07296(4)	244.97498(8)
P_{cc}/amu Å^2 [a]	61.3	84.8	64.2	0.0	58.30782(4)	80.63370(8)
μ_a/D	0.84	1.16	0.00	0.03	Medium	Strong
μ_b/D	0.78	0.98	0.73	1.53	Medium	Medium
μ_c/D	1.08	0.68	1.37	0	Strong	Medium
N[b]					136	83
RMS/kHz[c]					1.4	1.5
$\%\Delta B_{rms}SA$[d]					2.95	7.41
$\%\Delta B_{rms}TA$[d]					7.16	3.25
$\%\Delta B_{rms}AA$[d]					51.5	58.9
$\%\Delta B_{rms}TS$[d]					22.6	29.8
ΔE/cm^{-1} [e]	0.0	24	311	387		

[a]Planar moment $= P_{aa} = \frac{(I_b+I_c-I_a)}{2} = \sum m_i a_i^2$

[b]N= number of transitions in the fit.

[c]$RMS = \sqrt{\frac{\Sigma(\upsilon_{obs}-\upsilon_{calc})^2}{N}}$ (Frequencies used to calculate RMS for each isomer can be found in Appendix I)

[d]root-mean-square percent differences between observed and calculated rotational constants (A, B, C)

$$\%\Delta B_{rms}x = \sqrt{\frac{\Sigma\left(\left(\frac{(Bx_{(calc)} - Bx_{(exp)})}{Bx_{(calc)}}\right) \times 100\%\right)^2}{3}}$$

x=SA, TA, AA, TS (rotational constant differences between Side-Above (SA), Top-Above (TA), Above-Above (AA) and Top-Side (TS) ab initio structures).

[e]ΔE is the relative energy of each structure, compared to the minimum energy structure.

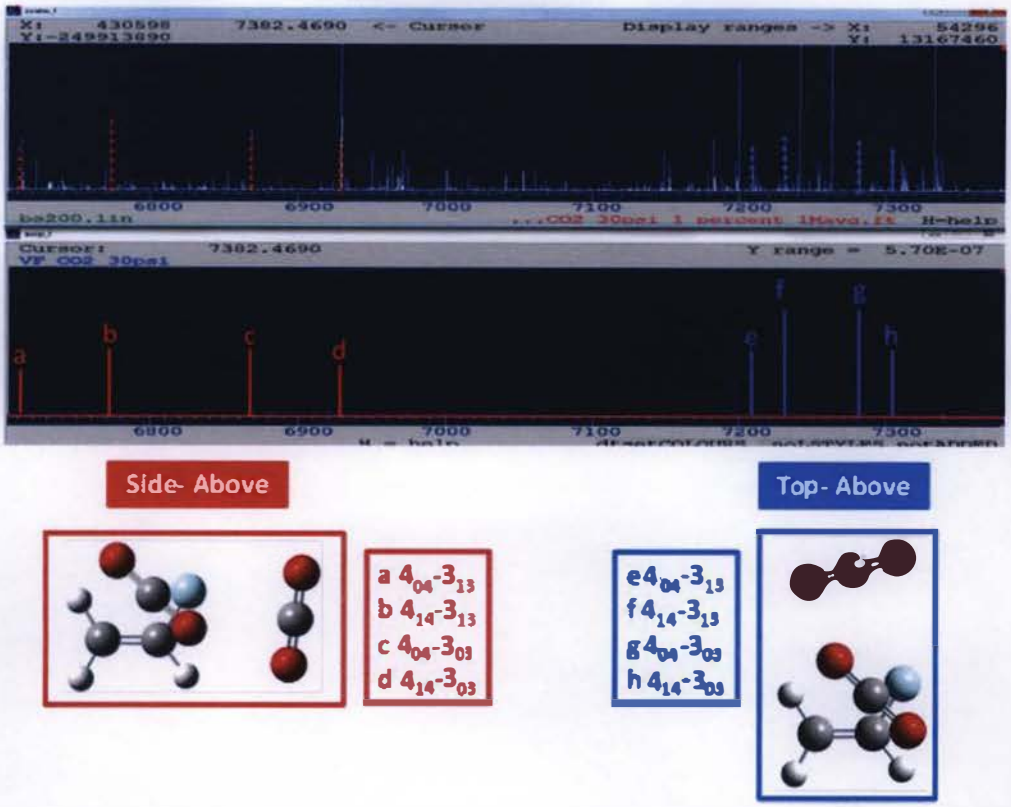

Figure 2.7: Constant difference patterns related to Side-Above and Top-Above VF...CO_2...CO_2 trimer structures (Top spectrum-experimental microwave spectrum for VF/CO_2 and Bottom spectrum- simulated spectra for Side-Above and Top-Above VF...CO_2...CO_2 trimer structures)

2. III. D. Comparison of theoretical and experimental rotational constants

The rotational constants and planar moments were compared with the experimental rotational constants for the experimentally likely structures to confirm that they matched. For example, one could argue that the Top-Side theoretical rotational constants are similar to the isomer I experimental rotational constants, since the *A* rotational constant for Top-Side is 1626.9 MHz and *A* rotational constant for the Isomer I is 1660.35121 MHz. But when comparing the planar moments for both the structures, Top-Side has a P_{cc} of 0 amu Å^2 while the isomer I has a P_{cc} of 58.31 amu Å^2. Those

values showed disagreement of the theoretical and experimental constants for the Top-Side structure and confirmed the assignment as Side-Above is correct.

A quantitative comparison method was also used in addition to the rotational constants and planar moment comparison between the structures. The root-mean-square percent differences ($\%\Delta B_{rms}$) were compared between observed (experimental) and calculated (theoretical) rotational constants (A, B, C). The lower value indicated the best correlation between the observed and predicted constants and structures.

In Table 2.1, the $\%\Delta B_{rms}$ values for rotational constants of all four predicted structures with Isomer I give the lowest value (2.95%) with the Side-Above structure, while the Isomer II gives lowest value (3.25%) with the Top-Above structure. Hence, these $\%\Delta B_{rms}$ values confirmed that the assignments based on comparing the rotational constants were correct.

Dipole moment comparisons can also be used to confirm that the theoretical and experimental structural assignments were correct. The intensity of a peak is proportional to the square of dipole moment. For both the isomer I and II spectra *a*-type, *b*-type and *c*-type transitions were observed. For isomer I there were medium sized *a*-type and *b*-type transitions with strong *c*-type transitions. In isomer II, there were strong *a*-type and *b*-type transitions with medium sized c-type transitions.

There is no *a* dipole component for the Above-Above structure and also no *c* dipole component for the Top-Side structure. Hence, the dipole components of isomer I and II do not agree with the Above-Above and Top-Side dipole components. The relative intensities are consistent with the predicted dipole components for Side-Above and Top-Above, respectively. For instance, the Side-Above has largest *c* dipole and because of

that it has intense *c*-type transitions. Also, the Top-Above has similar *a* and *b* dipoles and they are larger than *c*. Hence, the spectrum has intense *a*-type and *c*-type transitions that *c*-type transitions.

2. III. E. Comparison of theoretical dimer and trimer structures

The ab initio structural parameters of VF...CO_2...CO_2 trimers such as atom...atom distances (Fig. 2.8), bond angles and the dihedral angles were compared with the ab initio structural parameters of the previously studied VF...CO_2 dimers and CO_2...CO_2dimer structures (Fig. 2.9).[1, 11, 12]

Atom...atom distances of VF...CO_2 dimers and VF...CO_2...CO_2 trimers were compared. Shortening of atom...atom distances from VF...CO_2 dimers was observed when it comes to the VF...CO_2...CO_2 distances. For example, the C...F atom...atom interaction distances in VF...CO_2 dimers range between 2.98 Å - 3.11 Å, but in the VF...CO_2...CO_2 trimers it ranges between 2.90 Å - 2.97 Å. Also, the trimers form roughly barrel shaped structures. Within them, the dimer structures can be observed, and the energetically unfavorable Above dimer is also a part of the trimer structures. The Above dimer did not change much within the trimer structures. The O=C...F-C dihedral dimer angle of 33° is not changed much within the trimer structures, where there was deviation of only about 1°.

The experimentally observed dimer structures are planar, with the CO_2 molecule in the same plane of the VF molecule.[1] Within the trimers O=C...F-C dihedral angles show that these experimentally observed dimer fragments are no longer planar. The O=C...F-C dihedral angle for Top-Above and Side-Above structures were 16.12° and 7.52°, respectively..

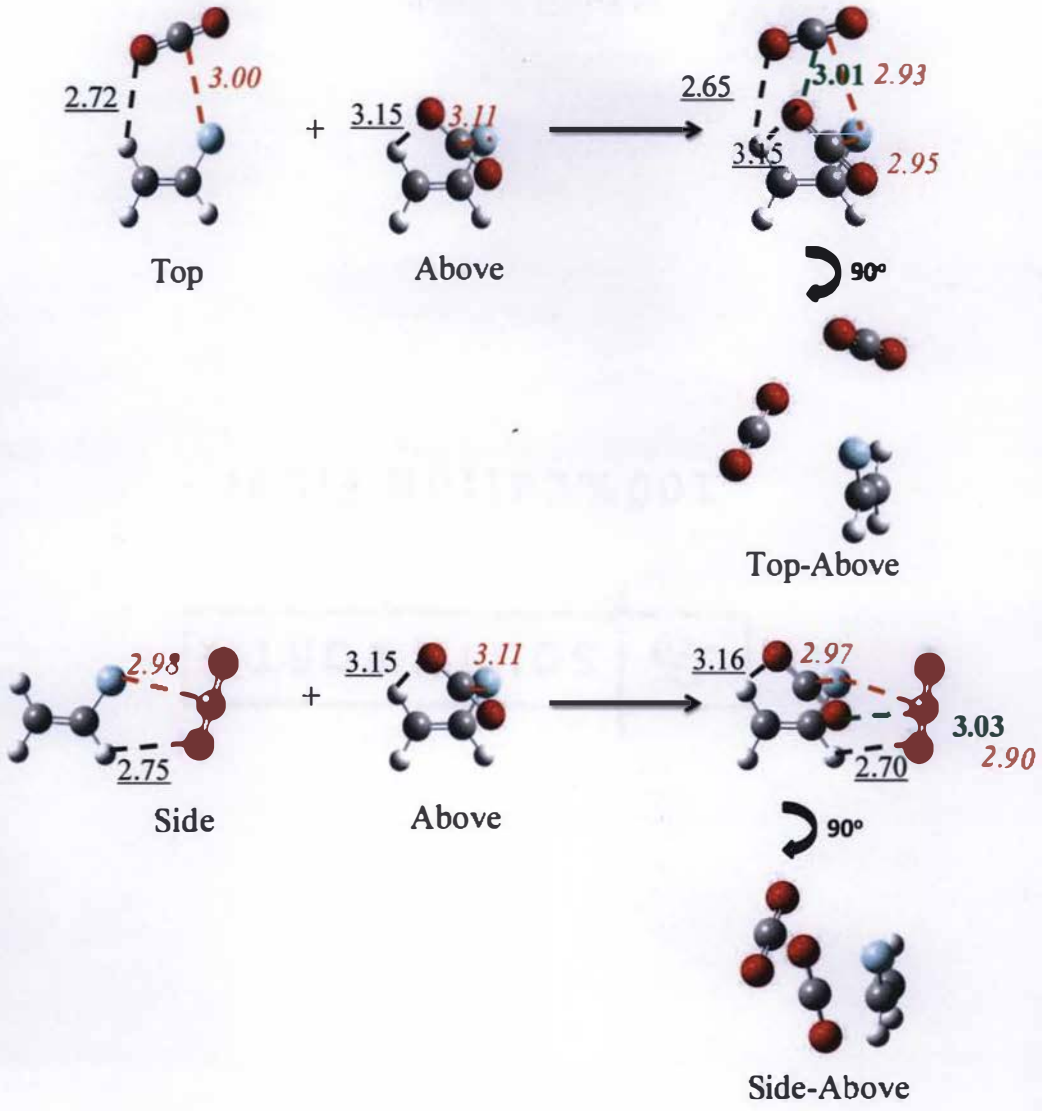

Figure 2.8: Comparison of atom...atom interaction distances in VF...CO_2 dimer structures and VF...CO_2...CO_2 trimer structures (the distances in italic (orange) = O...H, underline (Black) = C...F, bold (Green) = C...O) [Units for the bond distances=Å] (the distances shown are theoretical and the optimizations were carried out at the MP2/6-311++G(2d,2p) level)[1]

Both CO_2 molecules in the side position and the top position of the Top-Above and Side-Above structures were lifted upwards from the VF plane. The Above CO_2 molecule within both experimentally observed trimers remained the same as the Above dimer structure. This movement slightly upwards from the VF plane happened because

one CO_2 molecule is likely to form interactions with the other CO_2 molecule within the trimer structure. Within these VF...CO_2...CO_2 trimer structures the two CO_2 molecules are trying to form a CO_2 dimer like structure

The two conformations of CO_2 dimer are T shaped (Fig. 2.9.a) and slipped parallel (Fig. 2.9.b). The slipped parallel structure is the experimentally observable structure and the T shaped structure has higher energy and it is not experimentally observable.[11] The ab initio C...O atom...atom interaction distance within slipped parallel structure is 3.11 Å and within T shaped structure it is 3.01 Å. Within the VF...CO_2...CO_2 trimer structures it can be observed that the CO_2 molecules are trying to form a CO_2 dimer and these dimers are more close to a T shaped CO_2 dimer structure since the C...O atom...atom interaction distance is in between 3.01-3.03 Å. The ab initio C...O=C angle in CO_2 dimers and VF...CO_2...CO_2 trimers were compared. The bond angle within T shaped CO_2 dimer is 90° and within slipped parallel structure it is 101°. Within both Top-Above and Side-Above structures the C...O=C bond angle is 80°. This bond angle value within experimentally observed trimer structures is closer to the C...O=C angle within T shaped CO_2 dimer value. This observation shows that two CO_2 molecules within trimers are trying to form T shaped CO_2 dimer within the VF...CO_2...CO_2 trimers.

Within the VF...CO_2...CO_2 trimer structure both the energetically higher and experimentally not observed VF...CO_2 Above dimer structure and the CO_2...CO_2 T shaped dimer structures were observed. These structures are less stable as dimers, but they are stable within VF...CO_2...CO_2 trimer structure. When these unstable complexes combine with each other it stabilizes the higher energies and forms more stable structures by lowering the energy.

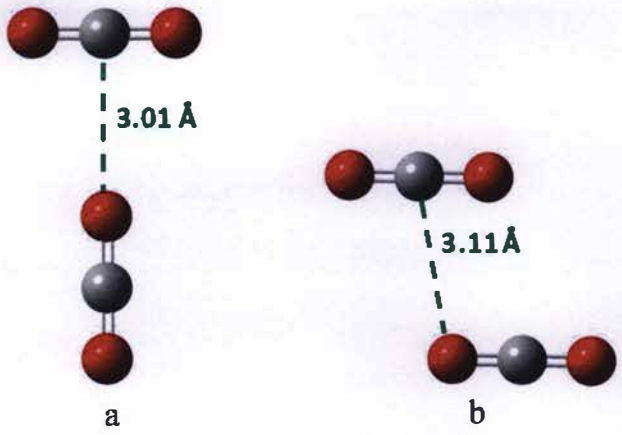

Figure 2.9: CO_2...CO_2 dimer structures a). T shaped structure b). **Slipped parallel structure (the distances shown are theoretical and the optimizations were carried out at the MP2/6-311++G(2d,2p) level)**[11]

When comparing the VF...CO_2...CO_2 trimer structures with the VF...CO_2 dimer structures, the trimer structures are forming more compact and packed barrel type structures. Formations of compact structures are due to more interactions within the VF...CO_2...CO_2 trimers than the VF...CO_2 dimers. In the VF...CO_2 dimers there are two types of interactions (C...F interactions and O...H), but within the trimers they have one more interaction, which is C...O. That means whenever the solvation sphere around the VF increases the interactions increase as well, as they can make more stabilized and compact structures too. Moreover, within the VF...CO_2...CO_2 trimer structures the unstable dimer structures became more stabilized.

2. III. F. Atoms in Molecules (AIM) analysis

The AIM analysis was carried out to observe the interactions between atoms in the studied molecular clusters.[5] The interactions in VF...CO_2 dimers, $(CO_2)_2$ dimers and VF...CO_2...CO_2 trimers were observed in this section. For all the molecular clusters,

bond critical points (BCPs) were analyzed (Fig. 2.10). BCPs give the value of the minimum electron density in between atoms but along a path of maximum density.

The dotted lines or the thick black lines in Fig. 2.10 show the maximum electron density paths between the atoms. The dotted lines show interactions and the thick black lines represent the covalent bonds between the atoms. The red dots in between the atoms represent the BCPs which are minimum electron density value in between atoms. Figs. 2.10, 2.11 and 2.12 show the BCPs for VF...CO_2 dimers, $(CO_2)_2$ dimers and VF...CO_2...CO_2 trimers.

BCPs for all the VF...CO_2 dimer structures were analyzed since the dimer structures are the building blocks of the experimentally observed VF...CO_2...CO_2 trimer structures. Side and Top VF...CO_2 dimer structures have two types of interactions. The Top VF...CO_2 dimer structure has CH...O and C...F interactions while the Side structure has a CH...O interaction and an F...O interaction, but this O...F interaction is bending towards the C atom in the CO_2 molecule. The energetically unstable Above VF...CO_2 dimer structure does not have CH...O interactions. It only shows one type of interaction, and that is between the F atom and the C=O bond of the CO_2 molecule. For all three VF...CO_2 dimer structures the BCP value for the interaction between F atom and the other bond or atom is nearly the same although in the Above structure it is slightly less than the planar structures.

BCPs for the VF...CO_2...CO_2 trimers were also investigated using AIM analysis. BCPs of the experimentally observable VF...CO_2...CO_2 Top-Above and Side-Above trimer structures were compared with the BCPs of the VF...CO_2 dimers, $(CO_2)_2$ dimers and theoretical Top-Side VF...CO_2...CO_2 trimer structure, which is energetically

unstable. Both the Top-Above and Side-Above structures have four interactions in between the atoms in the molecules. There are one CH...O interaction, two C...F interactions and C...O interactions in between the atoms. The CH...O and C...F interactions are the same as the VF...CO_2 dimer interactions. In the VF...CO_2...CO_2 trimer structures, they are forming C...O interactions since it has two CO_2 molecules in the cluster.

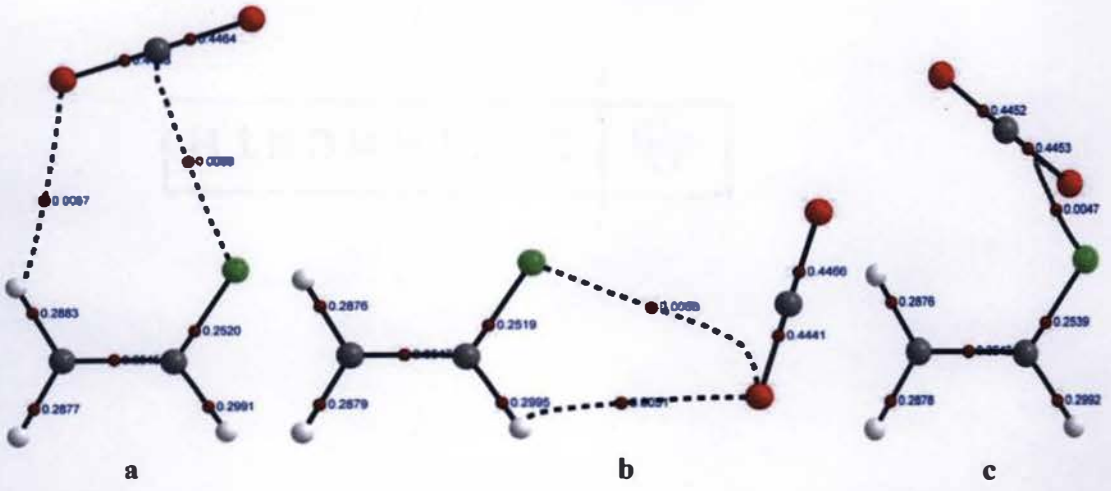

a b c

Figure 2.10: Electron densities at BCPs for studied VF...CO_2 dimer structures a). Top b). Side c). Above [Units for the BCP= atomic units (e/bohr^3)]

When comparing the electron densities at BCPs of the $(CO_2)_2$ dimer structures the slipped parallel structure which is experimentally observable, has a higher value for BCP (0.0072 u) (Fig. 2.12.b) compared to the energetically unstable T shaped structure (0.0054 u) (Fig. 2.12.a). Within both VF...CO_2...CO_2 trimer structures C...O interactions are having the BCP value nearly 0.0060 u and this value is much closer to the C...O interaction BCP value of the T shaped CO_2...CO_2 dimer structure. This

observation proves the presence of a more T shaped $CO_2...CO_2$ dimer structure fragment within both $VF...CO_2...CO_2$ trimer structures.

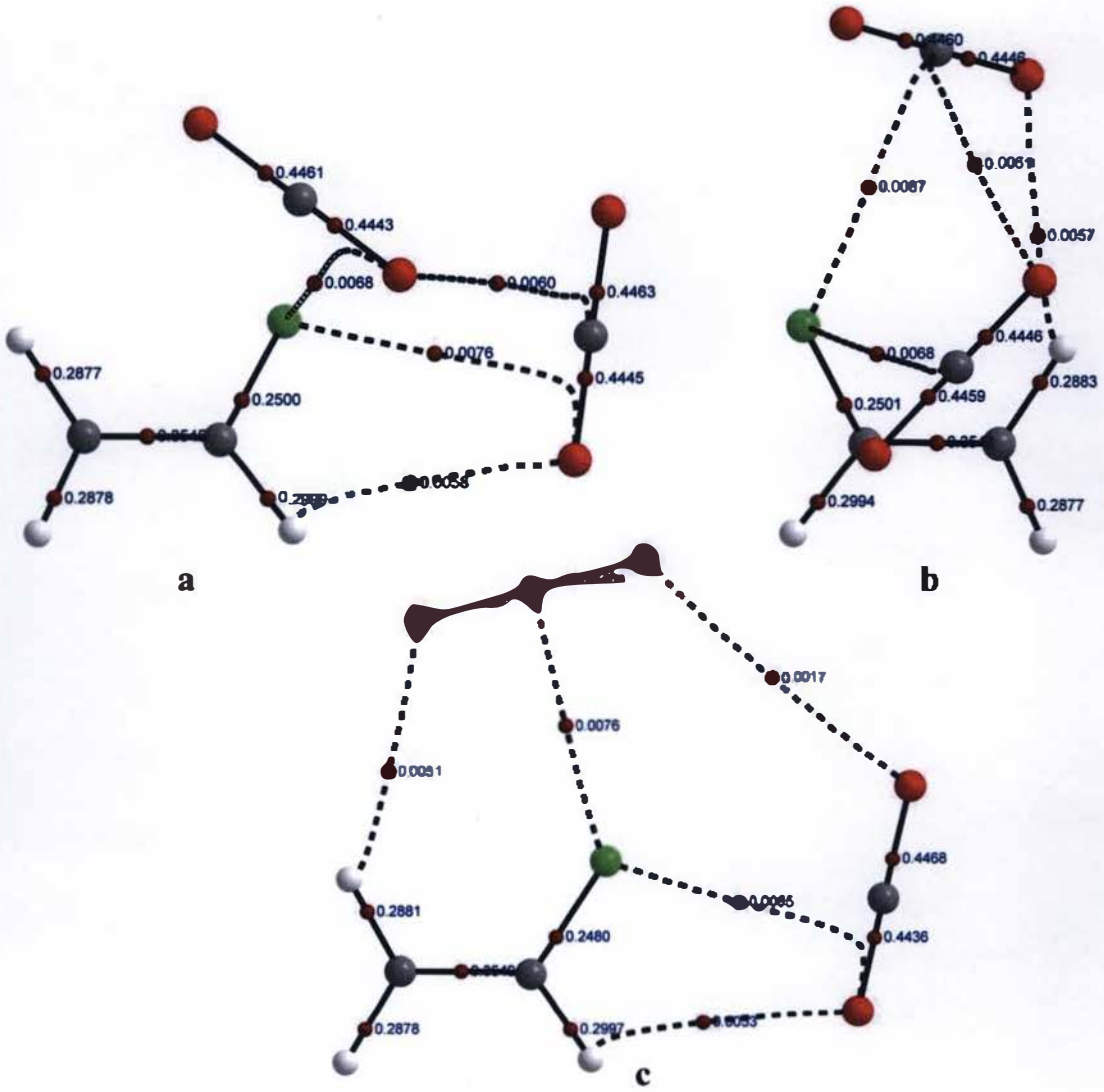

Figure 2.11: Electron densities at BCPs for $VF...CO_2...CO_2$ trimer structures a). Side-Above b). Top-Above c). Top-Side [Units for the BCP= atomic units ($e/bohr^3$)]

When comparing the interactions and the electron densities at BCPs for all the studied $VF...CO_2...CO_2$ trimer structures, five interactions were observed within the

energetically unfavorable Top-Side structure. The additional interaction was between the O atoms in two CO_2 molecules. These two interactions might be more repulsive since both O atoms are having the same charge in this structure and this might be one reason for the higher energy in this structure.

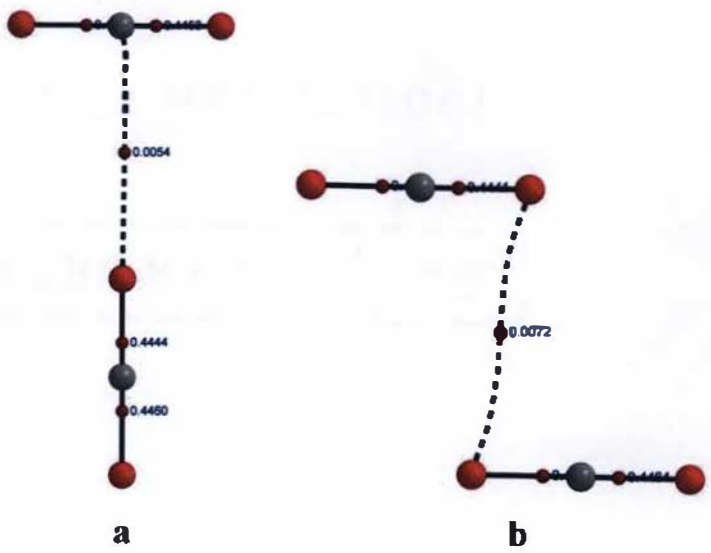

Figure 2.12: Electron densities at BCPs for $CO_2...CO_2$ dimer structures a). T shaped structure b). Slipped parallel structure [Units for the BCP= atomic units ($e/bohr^3$)]

Two conformers, which are Top-Above and Side-Above were found as $VF...CO_2...CO_2$ trimers. These trimer structures had weak interaction between atoms and the $VF...CO_2...CO_2$ trimers formed more compact structures than that of the $VF...CO_2$ dimers. Since the ultimate goal of this project is to investigate the solvation properties of *sc*-CO_2, this study gave insight to the weak interactions within the fluoroethylene$...CO_2$ complexes.

2. IV. References

[1] C. L. Christenholz, R. E. Dorris, R. A. Peebles, S. A. Peebles, Characterization of Two isomers of the Vinyl Fluoride—Carbon Dioxide complex. *J. Phys. Chem. A* **2014**, 118, 8765–8772.

[2] R. J. Bemish, P. A. Block, L. G. Pedersen, R. E. Miller, The ethylene–carbon dioxide complex: A double internal rotor. *J. Chem. Phys.* **1995**, 103, 7788-7795.

[3] A. M. Anderton, R. A. Peebles, S. A. Peebles, Rotational Spectrum and structure of the 1, 1-Difluoroethylene...Carbon Dioxide Complex. *J. Phys. Chem. A* **2016**, 120, 247-253.

[4] R. A. Dorris, W. C. Trendell, R. A. Peebles, S. A. Peebles, Rotational Spectrum, Structure, and Interaction Energy of the Trifluoroethylene...Carbon Dioxide Complex. *J. Phys. Chem. A* **2016**, 120, 7865-7872.

[5] AIMAll (Version 17.11.14), Todd A. Keith, TK Gristmill Software, Overland Park KS, USA, 2017 (aim.tkgristmill.com)

[6] R. F. W. Bader, Atoms in molecules: a quantum theory, Oxford University Press, Oxford, UK, **1990**.

[7] GaussView 5.0.9, Gaussian, Inc., Wallingford, CT. **2000-2008**.

[8]Gaussian 09, Revision A.02, M. J. Frisch, G. W. Trucks, H. B. Schlegel, G. E. Scuseria, M. A. Robb, J. R. Cheeseman, G. Scalmani, V. Barone, G. A. Petersson, H. Nakatsuji, X. Li, M. Caricato, A. Marenich, J. Bloino, B. G. Janesko, R. Gomperts, B. Mennucci, H. P. Hratchian, J. V. Ortiz, A. F. Izmaylov, J. L. Sonnenberg, D. Williams-Young, F. Ding, F. Lipparini, F. Egidi, J. Goings, B. Peng, A. Petrone, T. Henderson, D. Ranasinghe, V. G. Zakrzewski, J. Gao, N. Rega, G. Zheng, W. Liang, M. Hada, M. Ehara, K. Toyota, R. Fukuda, J. Hasegawa, M. Ishida, T. Nakajima, Y. Honda, O. Kitao, H. Nakai, T. Vreven, K. Throssell, J. A. Montgomery, Jr., J. E. Peralta, F. Ogliaro, M. Bearpark, J. J. Heyd, E. Brothers, K. N. Kudin, V. N. Staroverov, T. Keith, R. Kobayashi, J. Normand, K. Raghavachari, A. Rendell, J. C. Burant, S. S. Iyengar, J. Tomasi, M. Cossi, J. M. Millam, M. Klene, C. Adamo, R. Cammi, J. W. Ochterski, R. L. Martin, K. Morokuma, O. Farkas, J. B. Foresman, and D. J. Fox, Gaussian, Inc., Wallingford CT, 2016.

[9]H. M. Pickett, The Fitting and Prediction of Vibration-Rotation Spectra with Spin Interactions,*J. Mol. Spectros.* **1991**, 148, 371-377.

[10]J. K. G. Watson, Aspects of quadratic and sextic centrifugal effects on rotational energy levels. *Vib. Spectra Struct.* **1977**, 6, 1-89.

[11]K. W. Jucks, Z. S. Huang, D. Dayton, R. E. Miller, The structure of the carbon dioxide dimer from near infrared spectroscopy. *J. Chem. Phys.* **1987**, 86, 4341.

[12]P. B. Kannangara, C. T. West, S. A. Peebles, R. A. Peebles, Towards microsolvation of fluorocarbons by CO_2: Two isomers of fluoroethylene-$(CO_2)_2$ observed using chirped-pulse Fourier-transform microwave spectroscopy. *Chem. Phys. Lett.* **2018**, 706, 538-542.

CHAPTER 3

Developing new approaches to decode rotational spectra and to find the structures of unknown molecular clusters

3. I. Introduction

The previous chapter discussed the findings of VF...CO_2...CO_2. After that molecular structures for another trimer (VF...VF...CO_2) and tetramers (VF...CO_2...CO_2...CO_2, VF...VF...CO_2...CO_2 and VF...VF...VF...CO_2) were sought. However, before starting those clusters there was a huge breakthrough which was identifying constant difference patterns (discussed in Chapter 2) from the 1 million average VF/CO_2 and VF-only scans in which nearly 4000 peaks (52% of all the peaks in the scan) have signal to noise ratio more than 2.5. These identified patterns were assigned and the experimental rotational constants for many new spectra were found, but the cluster formulas and structures associated with them were unknown. Then more scans from the UVa instrument were collected to help find the structures for these unknown molecular clusters.[1] In this attempt the same gases in the gas mixture as in Chapter 2 were used, but now the concentration of CO_2 gas was changed while the VF concentration was kept constant. These data helped identify the formulas for assigned spectra as well as extracting spectra for more unknown molecular clusters using two methods. An Excel program was used to find the *J* values associated with a specific group of lines identified in the scan. A MathCAD based program developed at UVa was also implemented to identify spectra of more molecular clusters from the scans using their intensity behaviors over different CO_2 concentrations.[2]

Initially, the Gaussian 09 program with DFT (Density Functional Theory) level calculations ωB97X-D and 6-31+G(d,p) basis set was used to predict the structures of the unknown molecular clusters.[3] In this approach, the molecules in a cluster were positioned by considering electronic charge distribution and bond polarity, and the previously studied structures of smaller clusters. In this method (which will be referred to as the

Gaussian 09 approach), it was hard to guess the most likely structure or to ensure that the lowest energy structures were considered for the optimizations, since the larger clusters have more permutations for arranging the molecules around each other. To help find the structures more efficiently the ABCluster program, which is used to predict structures based on global as well as local minima of the molecular clusters, was used.[4,5]

The ABCluster program follows the artificial bee colony algorithm, which is introduced briefly here, with results presented later in this chapter. In the artificial bee colony (ABC) algorithm, it considers a bee colony which is composed of three types of bees; employed bees (EMs), onlooker bees (OLs) and scout bees (SCs). These bees are looking for the best quality nectar around the bee colony. In the ABC system, each artificial employee bee is assigned for one nectar source. Hence in the ABC system, the number of artificial employee bees equals the food sources or nectars around the bee colony. The task of the EMs is to find the food source and come back to the beehive. After that, they have to dance in front of the OLs. OLs have to watch the EMs dance and select the corresponding food source or nectar depending on the dance. Then they evaluate all the selected food sources and find the best food source that is registered as the best source. All the other EMs which were abandoned due to the low-quality nectar have to become SCs and they have to start finding new food sources. This process repeats until the desired number of quality food sources is fulfilled.[4]

In the ABCluster program, the number of artificial employee bees and food sources or nectars around the bee colony is the analog of the number of calculation cycles (the number of structures considered for a given sized cluster). In the case of searching for cluster structures, the analog of the nectar quality is the potential energy and the

analog of the best quality nectar is the global minimum (most stable) structure. A set of calculations occurs within the program and acts as the EMs, OLs and SCs. This ensures that a series of random structures are considered and the program can use the results of the potential energy to seek out lower energy structures. This makes sure that the program (a) samples a large number of possible structures for each cluster size and (b) makes it much more likely that it will not be biased in the starting structure selection, making it much more likely that the global minimum will be identified. The first round of calculations acts as EMs which give basic information about the structures. Then this information is given to the next level calculations which are OLs. They select the good structures with the minimum energies and pass them to the next level calculation which is SCs. This will give the final output with the minimum potential energy.[4]

In the ABCluster program, there were two approaches which were used to calculate the energies for each structure considered. One approach was the ab initio method, which calculates the energy of the cluster by doing ab initio calculations. This method was time consuming since in the ABCluster approach, lots of calculations have to be run to ensure the lowest energy structure has been considered. Also, since energy is calculated using the same method as the Gaussian 09 approach, when the molecular clusters are getting larger it consumes a lot of time to give the output. A second ABCluster approach used force fields to calculate the energies of the molecular clusters much more quickly. This method primarily used intermolecular Coulomb interactions and Lennard-Jones potentials to calculate these energies. The force field is what describes the distribution of charge within each molecule, and the sizes of the atoms. Then that force field is used in the Coulomb and Lennard-Jones based energy calculations. The

force field provides the charge on each atom, and the Coulomb calculation calculates the interaction energy between the charges on each pair of atoms.[6,7,8] The first half of equation 3.1 gives the intermolecular Coulomb interactions which give the quantitative amount of the electrostatic attractions and the repulsions of the molecular system. In here, a distributed atomic charges model is being used to mimic the electronic charge distribution on each molecule. The second half of the equation 3.1 gives the Lennard-Jones interactions which quantitatively approximates the amount of repulsive and attractive interactions between the atoms or molecules in the system. This repulsion is the repulsion from the overlap of the electron clouds on the different molecules and the attraction is due to the London dispersion forces operating as a result of the motion of the electrons within the electron charge cloud.

$$U(Q) = \sum_{I=1}^{N}\sum_{I<J}^{N}\sum_{i_I \in I}\sum_{j_J \in J}\left(\frac{e^2}{4\pi\epsilon_0}\frac{q_{i_I}q_{j_J}}{r_{i_I j_J}}\right) + 4\epsilon_{i_I j_J}\left(\left(\frac{\sigma_{i_I j_J}}{r_{i_I j_J}}\right)^{12} - \left(\frac{\sigma_{i_I j_J}}{r_{i_I j_J}}\right)^{6}\right) \quad \textbf{Equation 3.1}$$

$U(Q)$ = Potential energy

q_i, q_j= Magnitude of charges of each atom; used to represent electronic charge distribution of each monomer

r= distance between the two atoms

ε= depth of the potential well; used to scale the dispersion and repulsion contribution

σ= finite distance at which the inter-particle potential is zero; used to represent the effective size of each atom

This method does not rely on time consuming ab initio calculations and within a very small time duration (within few seconds) can provide a lot of lower energy structures for molecular clusters. When the ABCluster program is compared with the Gaussian 09 program, lots of differences between them are observed. The ABCluster program keeps positioning the molecules in different orientations based on application of

the artificial bee colony algorithm to test hundreds of possible structures of the desired molecular clusters, but in the initial Gaussian 09 approach, the molecular clusters were created by positioning by hand, based on chemical intuition and previous experimental results, allowing only a limited number of structures to be acquired.

Some structures for the unknown molecular clusters were found by using both the Gaussian 09 approach and ABCluster force field methods. The rest of this chapter describes how the unknown molecular clusters were identified by looking at the spectroscopic patterns, and also by the Excel and Mathcad analytical techniques collectively. Moreover, this chapter describes the use of analytical tools to suggest the composition of the unknown molecular clusters and use of different computational programs to find the structures of them.

The Experimental section will explain how (a) the microwave scans were collected, (b) molecular clusters were found by looking at the scans, (c) the MathCAD program was used to identify related transitions (d) spectra were assigned and (e) possible structures were predicted. The Results and Discussion section will explain (a) the identification of structures for the assigned molecular clusters with Gaussian 09 (b) how the concentration dependence studies helped to identify possible molecular formulas for clusters, including discussing the molecular clusters that were obtained by the MathCAD based program, and (c) how ABCluster was used to identify the molecular structures.

3. II. Experimental

3. II. A. Microwave spectroscopy

The experimental microwave spectra were obtained from a chirped-pulse Fourier-transform microwave (CP-FTMW) spectrometer at the University of Virginia (UVa) which operated in the region of 2-8 GHz.[1] The gas samples used to obtain the VF+CO_2 spectra contained 1% VF (Synquest Laboratories) and four different concentrations of CO_2 (Sigma Aldrich) (0.5%, 1%, 2% and 4%). The rest was filled with 2 atm of the buffer gas, Ne (Praxair). To get one scan, 400,000 spectra were averaged. The original 1% VF and 1% CO_2 scan with 1 million spectral averages (discussed in Chapter 2) was used to find molecular clusters using the Excel and visual pattern identification. The VF-only scan was also used to find molecular clusters. The gas sample used to get the VF-only scan contained 1% VF with 2 atm of Ne buffer gas, and 1 million spectra were averaged.

3. II. B. Constant difference pattern finding

Constant difference patterns were visually identified from the VF-only scan and VF/CO_2 scan. The easily observable initially found constant difference patterns were called the "mother pattern" for a specific molecule (Fig. 3.1). Additional transitions/frequencies related to a specific molecule were identified by finding trends and additional patterns in the constant differences related to the mother patterns. The constant difference frequency extraction method was developed by using the Excel program to find more frequencies related to the mother patterns (See 3.III for more details).

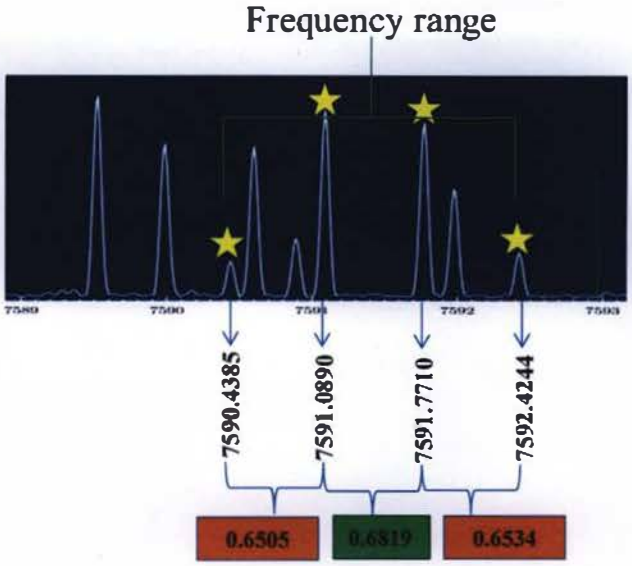

Figure 3.1: "Mother constant difference pattern" of the BS200 molecular cluster

The initial frequencies were predicted by using frequency predicting plots. Then the observed transition frequencies in a certain range around the predicted frequency were entered in the first row and column of the Excel sheet. Then the differences between each observed frequency were calculated. Finally, the constant differences were located within the spectrum near the predicted frequencies by using the "find" tool in Excel.

3. II. C. Related frequency extraction by MathCAD program

Five spectra were assigned by using the MathCAD based program.[2] This MathCAD approach extracted the frequencies which show similar intensity behavior over the different CO_2 concentrations. These extracted frequencies were used to calculate the three parameters of area, width and average concentration (more details explained below). Also, this method helped to identify related frequencies to a specific constant difference pattern. To identify the similar behavior frequencies a few steps were followed and the sections below explain the procedure related to this process.

3. II. C. 1. Intensity normalization (I_i^{norm})

All the VF/CO_2 scans collected with different CO_2 concentrations were opened with the Origin 8.1 program (Fig. 3.2).[9] Frequencies for the 1000 strongest lines were selected and the intensity normalization calculations were carried out. To get the 1000 strongest lines, all four spectra were peak picked and then for each peak, the strongest of the four scans were chosen. This gave one spectrum with all the peaks at the strongest intensity from the four scans. Then the frequencies of these 1000 strongest peaks were used.

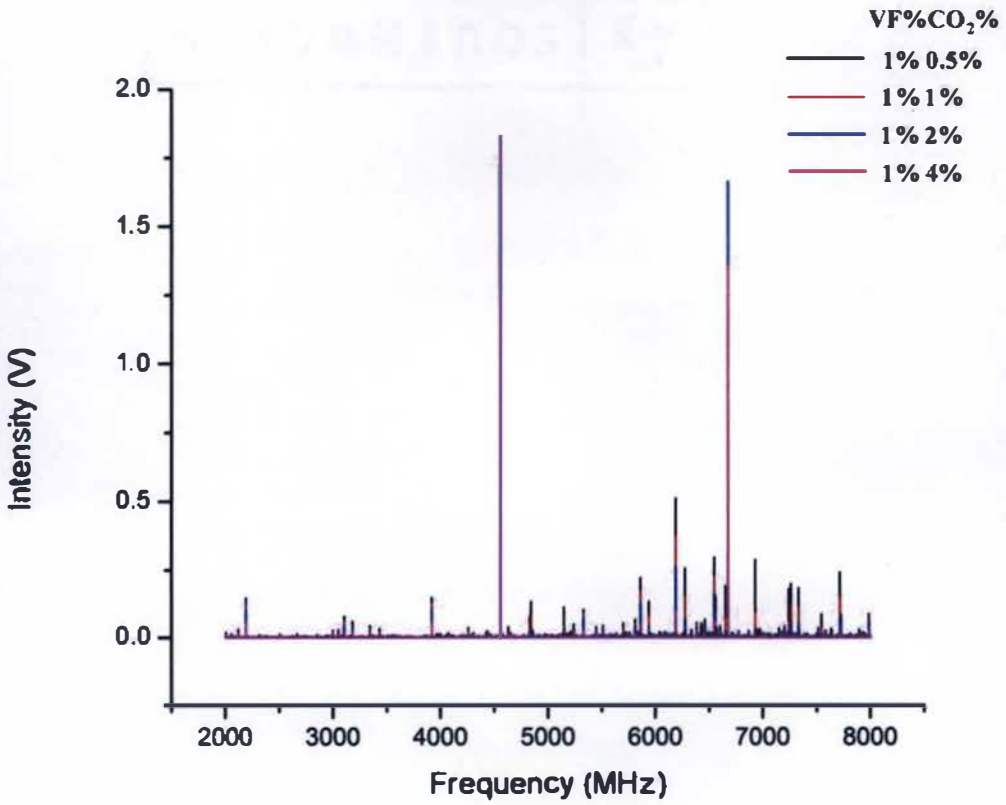

Figure 3.2: The Origin plot of four VF/CO_2 scans collected with different CO_2 concentrations[9]

Example calculations are shown in the Table 3.1, using a few frequencies which have higher intensities. This example uses "BS200" molecular cluster, (see 3.III for more details on this cluster spectrum). They were found from the 1% VF/CO_2 scan which was opened in the Origin plot with the intensity recorded at that frequency point from all four concentrations. All the intensities were divided by the largest intensity listed under each frequency (this will make the largest intensity=1 and other intensities between 0 and 1) (Table 3.2).

Table 3.1: Intensities at different CO_2 concentrations for selected frequencies in BS200 molecular cluster

Frequency (MHz)	Intensity at different CO_2 concentrations (mV)			
	0.5 %	1 %	2 %	4 %
7591.0875	3.45	3.43	1.65	0.15
6967.6375	4.97	4.68	2.24	0.25
6343.9000	3.73	3.51	1.51	0.09
5719.6500	3.37	3.31	1.30	0.21

e.g. for 7591.0875 MHz frequency,

$$I_i^{norm} \text{ at } 0.5\% = \frac{3.45}{3.45} = 1.0000$$

$$I_i^{norm} \text{at } 1\% = \frac{3.43}{3.45} = 0.9942$$

$$I_i^{norm} \text{at } 2\% = \frac{1.65}{3.45} = 0.4783$$

$$I_i^{norm} \text{at } 4\% = \frac{0.15}{3.45} = 0.0435$$

3. II. C. 2. Area calculation

Summation of all the normalized intensities under each frequency (Equation 3.2) gave the area corresponding to that frequency (Table 3.2).

$$Area = \sum_i I_i^{norm} \qquad \textit{Equation 3.2}$$

e.g. Area for 7591.0875 MHz frequency= 1.0000 + 0.9942 + 0.4783 + 0.0435 = 2.5160

3. II. C. 3. Average concentration calculation

The average concentration for each frequency was calculated using the normalized intensity, area and the corresponding CO_2 concentration. It was calculated using equation 3.3.

$$Average\ Concentration = \sum_i \left(\frac{I_i^{norm}}{Area}\right) conc_i \qquad \textit{Equation 3.3}$$

e. g. Average concentration for 7591.0875 MHz frequency=

$$= \left(\frac{1.0000}{2.5160} \times 0.5\right) + \left(\frac{0.9942}{2.5160} \times 1\right) + \left(\frac{0.4783}{2.5160} \times 2\right) + \left(\frac{0.0435}{2.5160} \times 4\right) = 1.0432\ \%$$

Table 3.2: Normalized intensities, area, average concentration and width at different CO_2 concentrations for selected frequencies in BS200 molecular cluster

Frequency (MHz)	Normalized intensity at different CO_2 concentrations				Area	Average concentration (%)	Width (%)
	0.5 %	1 %	2 %	4 %			
7591.0875	1.0000	0.9942	0.4783	0.0435	2.5160	1.0432	0.6657
6967.6375	1.0000	0.9416	0.4507	0.0503	2.4426	1.0416	0.6859
6343.9000	1.0000	0.9410	0.4048	0.0241	2.3699	0.9903	0.6064
5719.6500	1.0000	0.9822	0.3858	0.0623	2.4303	1:0299	0.7010

3. II. C. 4. Width calculation

The width for each frequency was calculated using the normalized intensity, area and the corresponding CO_2 concentration. It was calculated using equation 3.4.

$$Width = \left[\left(\sum_i \left(\frac{I_i^{norm}}{area}\right) conc_i^2\right) - \left(\sum_i \left(\frac{I_i^{norm}}{area}\right) \times conc_i\right)^2\right]^{\frac{1}{2}} \qquad \textit{Equation 3.4}$$

e. g. Width for 7591.0875 MHz frequency=

$$\left[\left(\left(\frac{1.0000}{2.5160} \times 0.5^2\right) + \left(\frac{0.9942}{2.5160} \times 1^2\right) + \left(\frac{0.4783}{2.5160} \times 2^2\right) + \left(\frac{0.0435}{2.5160} \times 4^2\right)\right) - \left(\left(\frac{1.0000}{2.5160} \times 0.5\right) + \left(\frac{0.9942}{2.5160} \times 1\right) + \left(\frac{0.4783}{2.5160} \times 2\right) + \left(\frac{0.0435}{2.5160} \times 4\right)\right)^2\right]^{\frac{1}{2}} = 0.6657\%$$

After calculating average concentration and the width for each frequency, the average concentration vs area and width vs area plots were created using Excel. On these plots the frequencies showing similar behavior were observed in certain clumps which were scattered over on the plot (Fig. 3.3 and 3.4). A MathCAD routine was developed to extract these frequencies which are having similar behaviors with different CO_2 concentrations from the clumps. Patterns were identified in the extracted frequencies and were assigned using the SPFIT program to give the rotational constants corresponding to these clusters.[10] Results from this analysis are given in section 3.III.C.

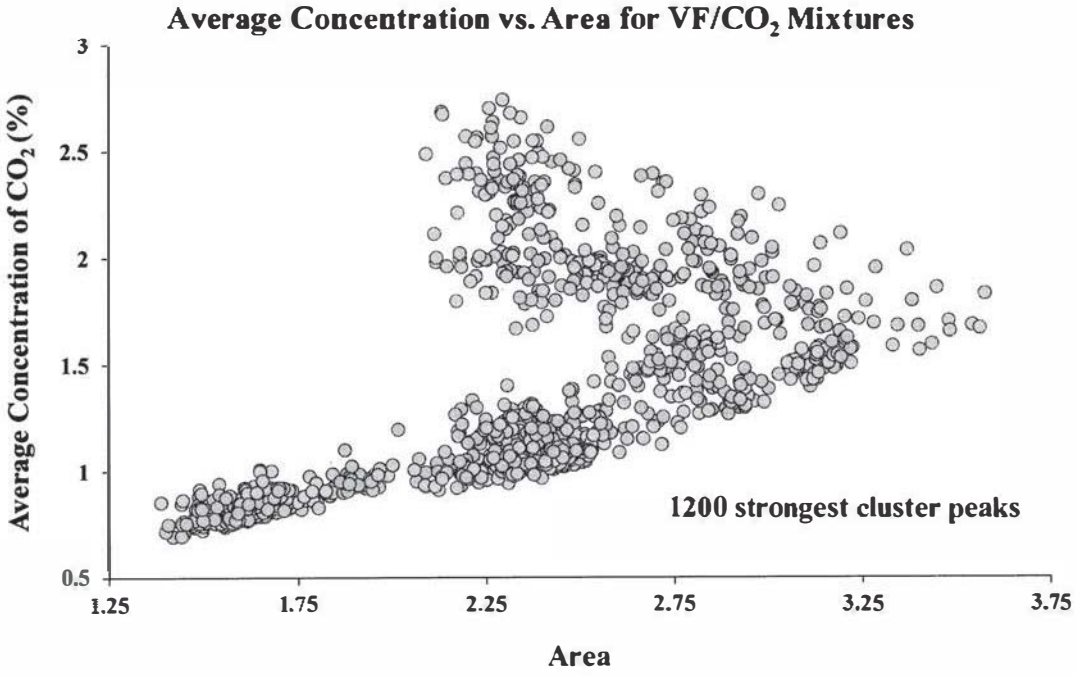

Figure 3.3: The plot of average concentration of CO_2 (%) vs. area

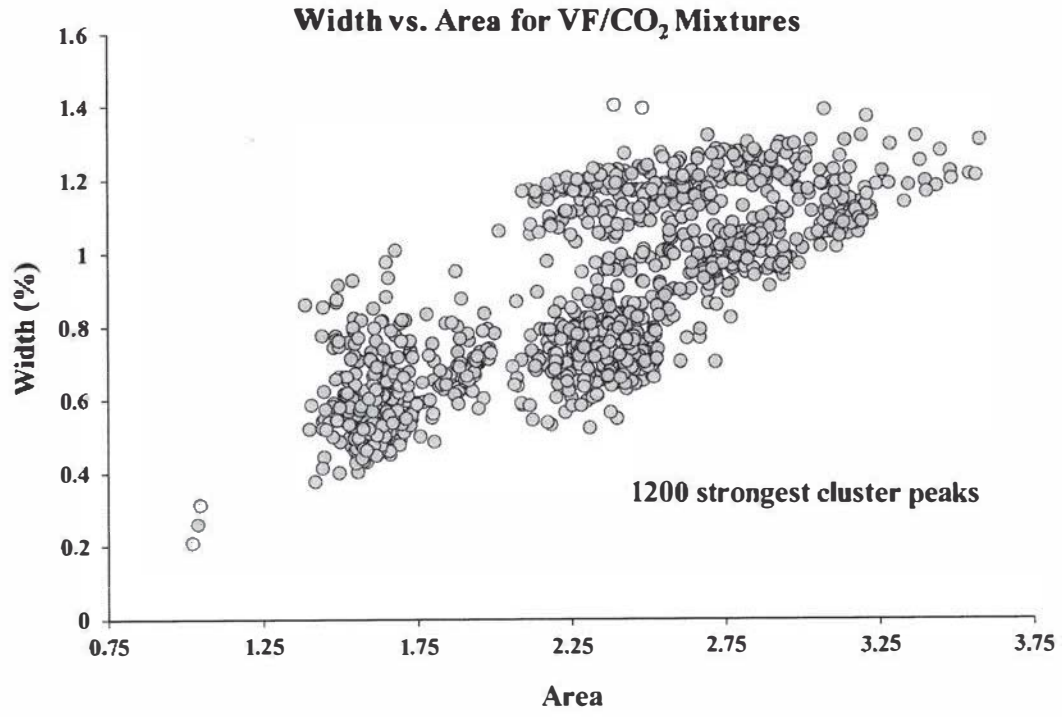

Figure 3.4: The plot of width (%) vs. area

3. II. D. Spectral assignment

After finding the mother pattern, and the related constant difference patterns, the quantum numbers were assigned. Calculating the frequency differences between adjacent patterns roughly provided the rotational constants. The SPCAT program was run and gave a predicted rotational spectrum by using the approximate rotational constants.[10] The SPFIT program was run to line up the predicted spectrum and the experimental spectrum related to the specific experimentally likely structure and to get the experimental rotational constants (See 2.II.C for more details).[10]

3. II. E. Predicting possible structures and rotational constants

To predict the initial structures of the unknown molecular clusters, a wide range of formulae were systematically tested using both the Gaussian 09 approach and the ABCluster force field approach. Traditional ideas of building each cluster from smaller clusters, such as using the VF...CO_2 dimer structures to build up the VF...CO_2...CO_2 trimer structures, did not work very well. All the structures guessed using the Gaussian 09 approach and resulting from the ABCluster force fields calculations were optimized at the DFT level with ωB97X-D and 6-31+G(d,p) basis set to obtain theoretical rotational constants.

3. III. Results and Discussion

3. III. A. Identification/Assignment of spectra

There were easily observable "mother" constant difference patterns in the region of 6000 MHz to 8000 MHz of the VF/CO_2 1% VF and 1% CO_2, 1 million spectra averaged scan (Fig. 3.1). The constant difference patterns that related to the mother pattern were distributed throughout in the scan within the 2-8 GHz region. The frequency

range of each constant difference pattern became wider as the transition frequency decreased. This is a general trend and when the quantum number of the transitions gets smaller the frequency range of the constant difference pattern will get wider.

Spectra that were identified by recognizing these constant difference patterns in the VF/CO_2 scan were labeled as BS100, BS200 and BS3 (Fig. 3.5). Also, two different constant difference patterns (BS400 and BS500) were extracted from the VF-only scan (Fig. 3.6).

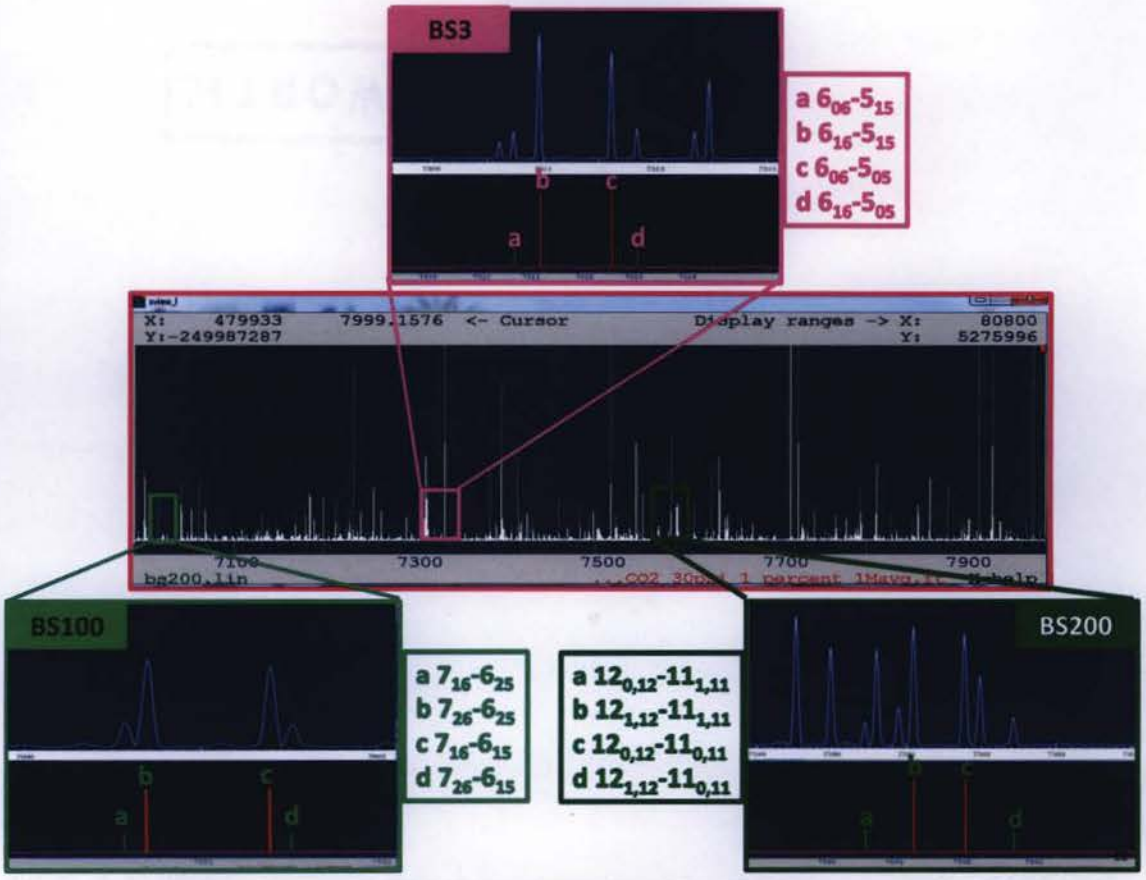

Figure 3.5: Mother constant difference patterns from VF/CO_2 scan; BS3, BS100 and BS200 molecular clusters. In each inset the a, b, c and d letters show the transitions with specific frequency and the numbers show the J, K_a and K_c quantum numbers in the order of $J_{K_aK_c}$

By looking at the width and the number of the constant difference patterns spread over the scan, the J values (used to denote the energy levels) were guessed. It was easy to guess the J values for BS3 and BS100 after finding 2 or 3 constant difference patterns that belong to the specific molecular cluster.

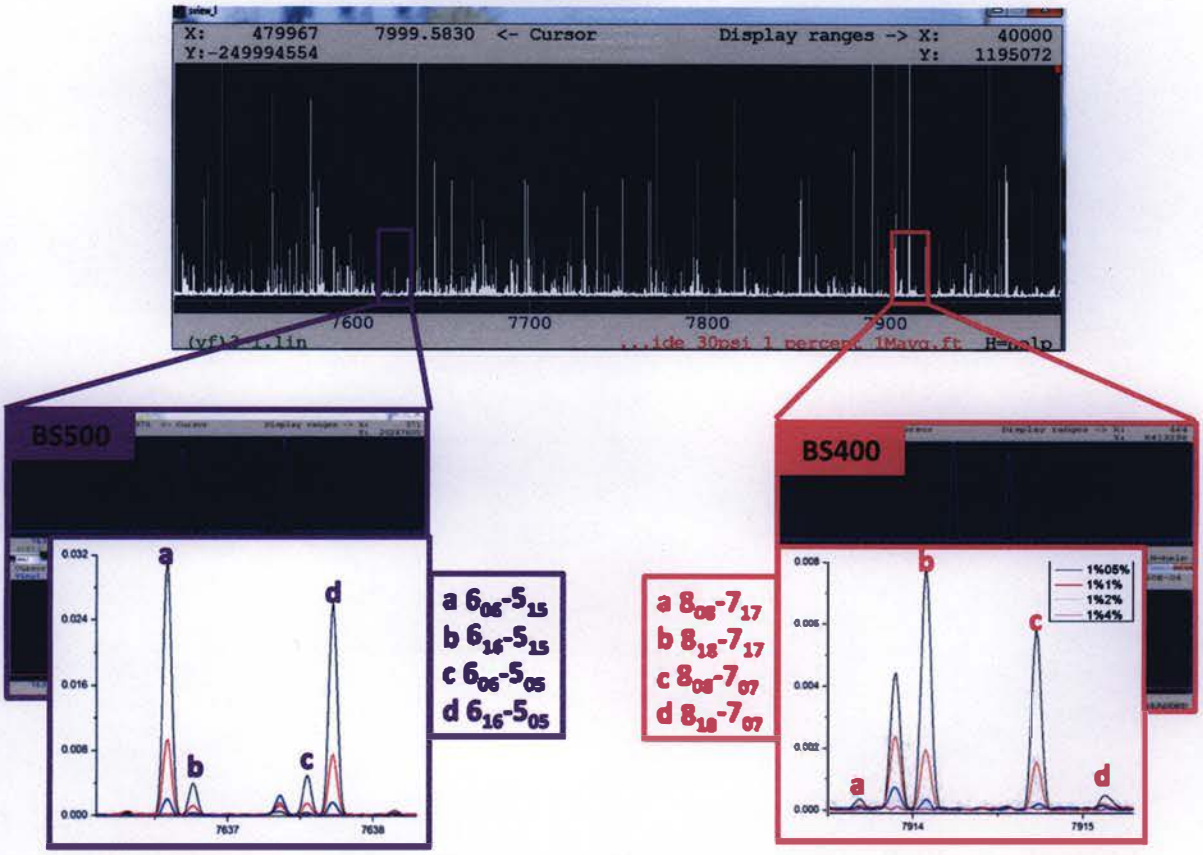

Figure 3.6: Mother constant difference patterns from VF-only scan; BS400 and BS500 molecular clusters. In each inset the a, b, c and d letters show the transitions with specific frequency and the numbers show the J, K_a and K_c quantum numbers in the order of $J_{K_aK_c}$

The rotational constants can roughly be calculated, and the frequencies or frequency range of the next pattern can be predicted, when 2 or 3 constant difference patterns are found in line. Hence, the SPCAT program can be run whenever 2 or 3 related constant difference patterns are available and can furnish the predicted/theoretical

rotational spectrum. Predicted rotational constants and the intensities need to be found to run the SPCAT program. These could be rough predictions which help to get the theoretical spectrum.

In the case of BS200, it was hard to guess the J values for the initial patterns, since it had a large J value. Different J values were applied by looking at the width of constant differences spread throughout the scan, but they did not fit exactly. Hence, more constant differences related to the BS200 were needed to get the correct J value for BS200 pattern. In the 2000 MHz to 5000 MHz region, since the frequency range of the constant difference patterns is large (making them harder to spot) (Fig. 3.7), the constant difference extraction method was developed by using the Excel program.

This can be observed in Fig. 3.7 where the numbers in the green color boxes are showing the frequency difference between the middle two transitions. The numbers in purple and orange color boxes show the constant differences in a specific pattern.

Each frequency recorded also was in a linear relationship with the pattern number (Fig. 3.8). It was easy to predict the next frequency in the series by using the equation from these linear plots, because, the "y" value which is corresponding to frequency was calculated by plugging the pattern number in the place of the "x" in the equation. This predicted frequency was not exactly the same as expected frequency; because the predicted frequencies did not show the constant difference patterns as expected (the difference between orange box and purple box was more than 4 kHz (Fig. 3.7.b), but the predicted frequency gave some idea about the location of exact frequency.

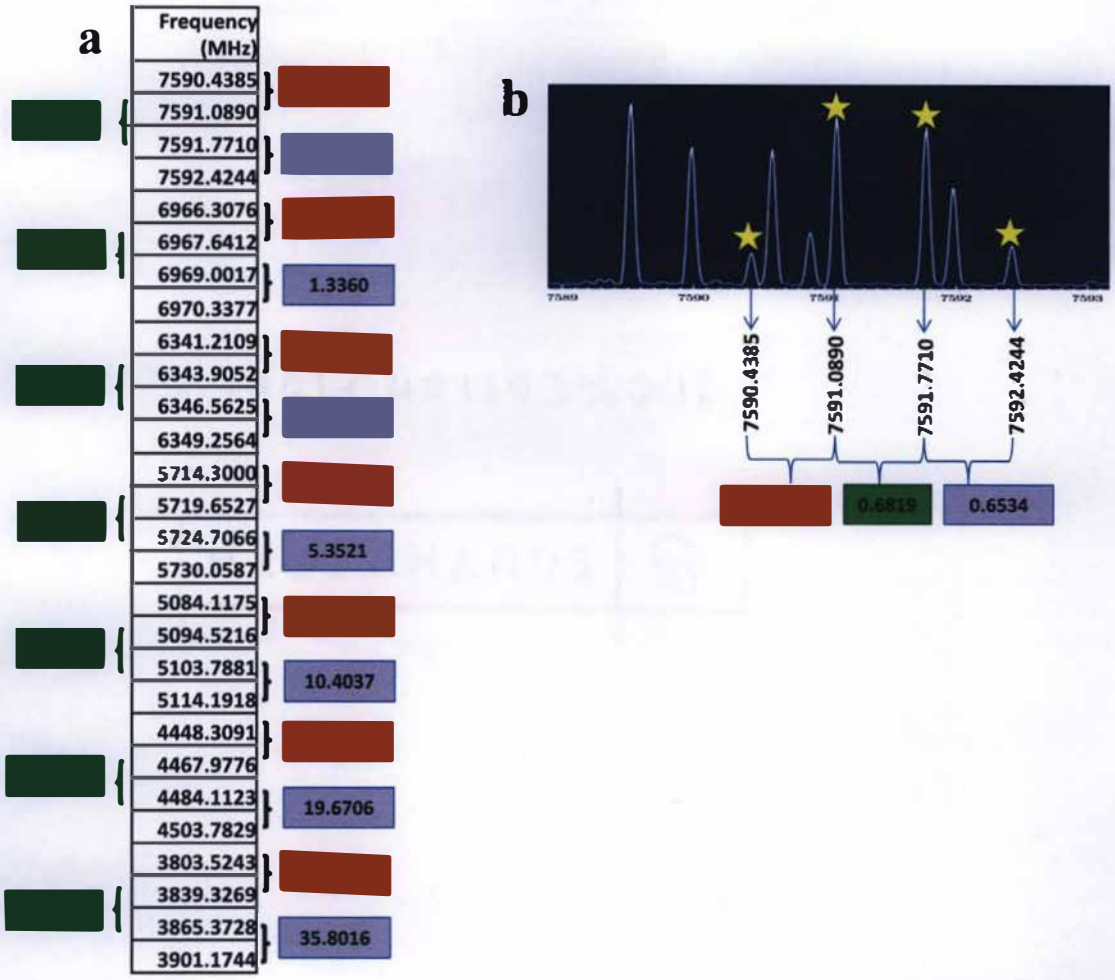

Figure 3.7: a). The constant differences between consecutive frequencies (MHz) (purple and orange) and frequency difference between two constant difference patterns (green) b). Identification of constant difference pattern

Relationships were observed not only between the frequencies and the pattern number, but also between the frequency differences and pattern number. There was a very important observation with the frequency differences getting larger when going down to the 2000 MHz region from 8000 MHz, because each consecutive frequency difference was increased by nearly the factor of two. Then these frequency differences were plotted against the pattern number, which gave a smooth curve type graph. The

order of polynomial was increased to give R^2 close to 1 to get the equation for each plot (Fig. 3.9). This equation was useful to predict the frequency difference related to the next pattern number. Also, the next frequency in the line was predicted using these plots.

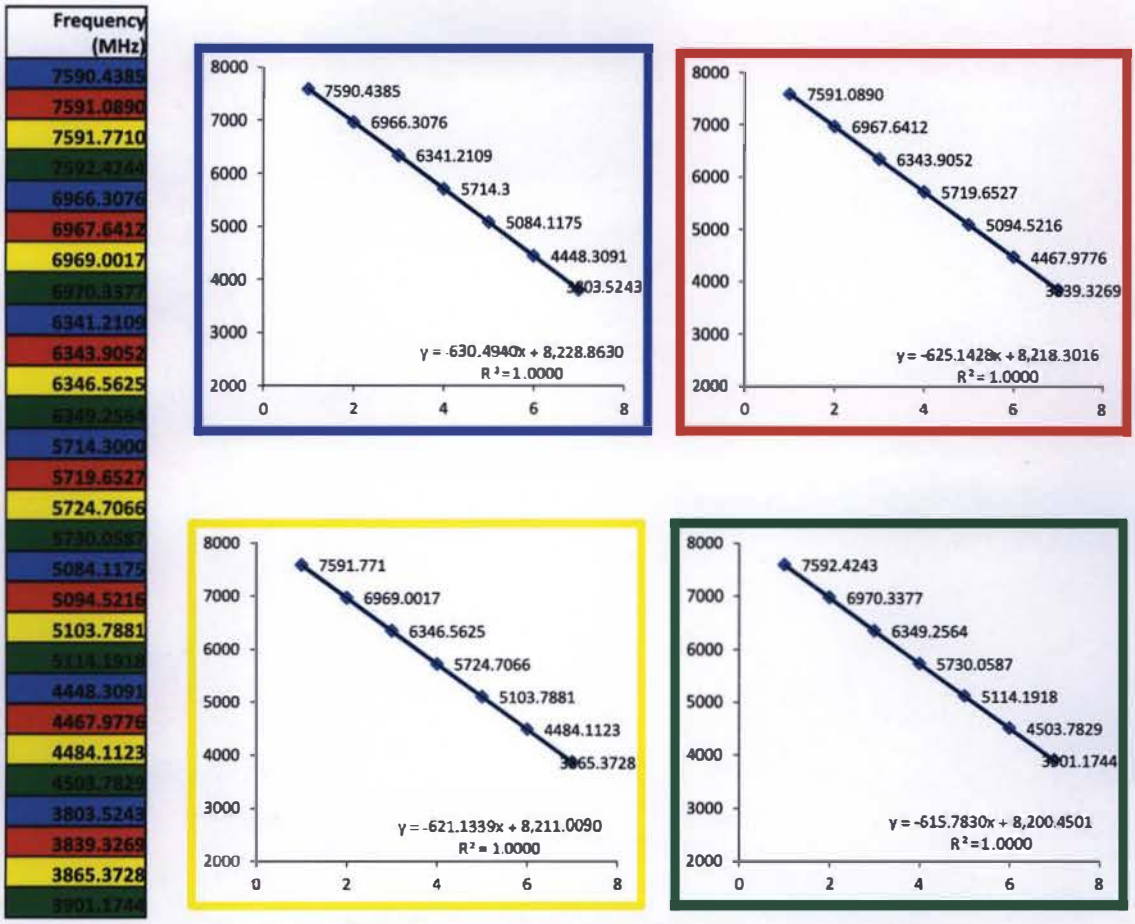

Figure 3.8: The plots of frequency vs the constant difference pattern number. Each of the plots has the colored frame and the color resembles the corresponding frequencies which are in the same color boxes in the table. The x axis of each plot shows the pattern number (the highest frequencies have pattern number 1) and the y axis shows the corresponding frequency (MHz)

The precision of the prediction was still sometimes not good enough to find the transition, because if the region in which the frequency is predicted particularly dense, there will be lots of options for each of the constant difference components that need to

be tested by hand. The predicted frequency gave the idea of the location of the exact frequency. For example, focusing on the red cells in Fig. 3.8, after the first four values were found, the next in line could be predicted. The four values were plotted in the graph and the next value predicted was 5096 MHz. The exact frequency was found at 5094.5216 MHz nearby the predicted frequency. The Excel sheets were used to get the exact frequency in the series by searching cells within a reasonable frequency range around the predicted frequency (Fig. 3.10) (Refer to Appendix I to see all the assigned frequencies).

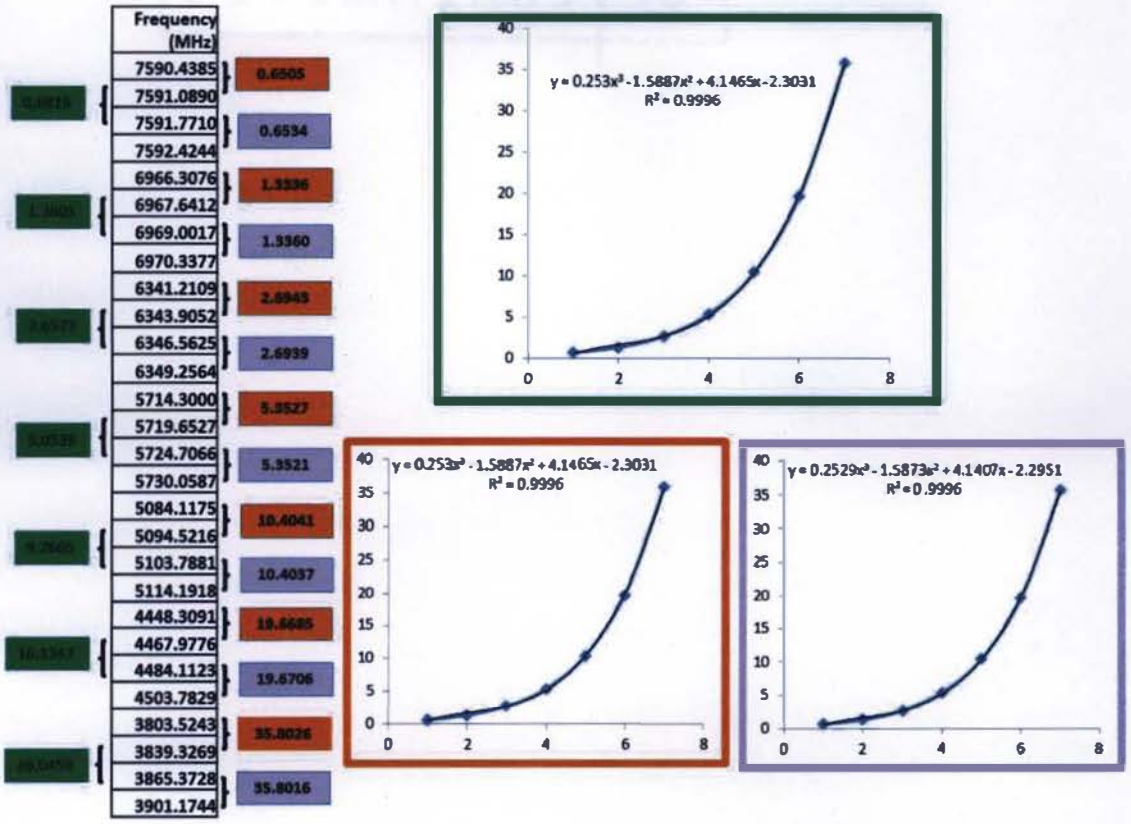

Figure 3.9: The plots of frequency difference vs constant difference pattern number. Each of the plots has the colored frame and the color resembles the corresponding frequency differences which are in the same color boxes around the table. The x axis of each plot shows the pattern number (the highest frequencies have pattern number 1) and they axis shows the corresponding frequency differences (MHz)

More and more frequencies that belong to spectra of specific molecular clusters were found and assigned by following this method. The experimental rotational constants related to these molecular clusters were obtained after running the SPFIT program as discussed in Chapter 2 (Table 3.3).

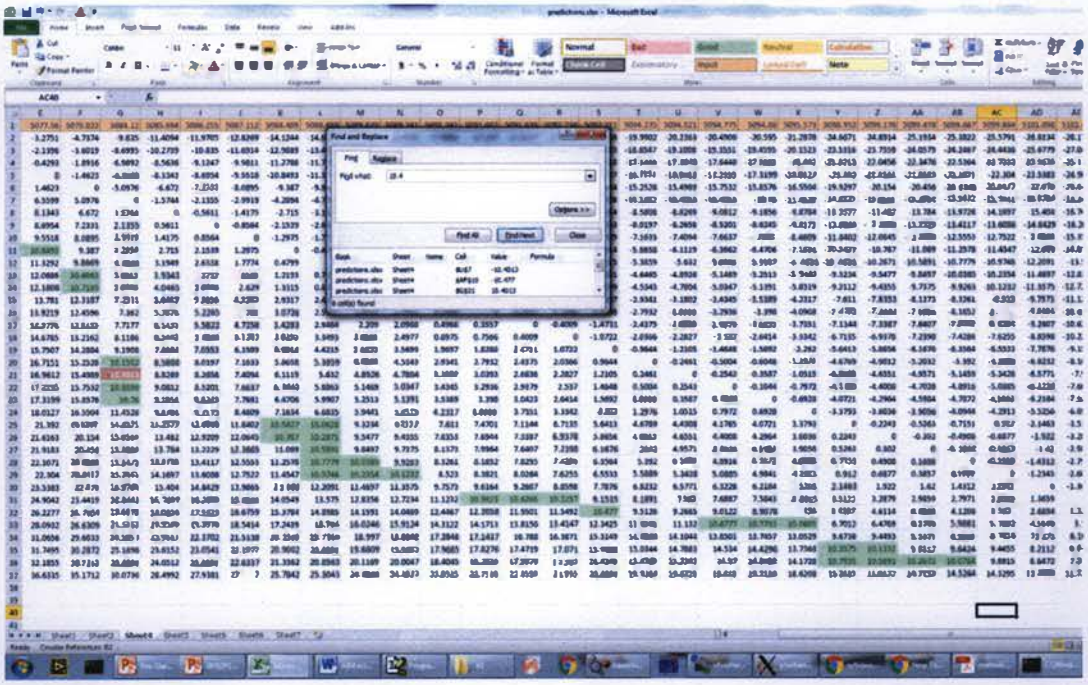

Figure 3.10: Spotting the constant difference in the excel sheet using the find tool

Table 3.3: The experimental rotational constants *A*, *B* and *C* for the molecular clusters which were found using constant difference patterns

Parameter	BS100	BS200	BS3	BS400	BS500
***A* / MHz**	698.1605(1)	590.2371(1)	786.9831(1)	602.5714(1)	1131.8623(1)
***B* / MHz**	621.6082(1)	356.7366(1)	683.6282(1)	523.0157(1)	906.6449(1)
***C* / MHz**	457.4325(1)	311.6427(1)	598.7616(1)	490.9273(1)	603.0449(1)

When close attention is paid to the rotational constants in Table 3.3, the *C* rotational constant of the BS200 molecular cluster is nearly a half of the slope of each

graph that is shown in Fig. 3.8. Therefore, these graphs can be used to predict the rotational constants for unassigned species as well.

3. III. B. Identification of molecular structures with the Gaussian 09 approach

After assigning these spectra, the next step was to find structures for these clusters. By looking at the rotational constants, it was possible to guess that these clusters are larger than trimers, because the trimers and the dimers had bigger rotational constants.

An initial Top-Side-Above structure for the VF...$(CO_2)_3$ tetramer which had one CO_2 in the top position, one CO_2 in the above position and the last CO_2 in the side position of the VF molecule was predicted (Fig. 3.11.a). The previously studied VF...CO_2 dimer and VF...CO_2...CO_2 trimer molecular cluster structures led to this prediction, and the predicted Top-Side-Above VF...$(CO_2)_3$ tetramer was a combination of the Top-Above and Side-Above VF...$(CO_2)_2$ trimers.[11] But the optimizations did not give rotational constants that matched any observed experimental rotational constants (Table 3.4). Also, the predicted dipole moments were quite far away from those expected based on the intensities of the peaks. Hence, the Top-Side-Above VF...$(CO_2)_3$ tetramer structure that was predicted using the knowledge and structures of VF...CO_2 dimer and VF...CO_2...CO_2 trimer studies was not observed.

The structure of the BS3 molecular cluster was guessed to be larger than a trimer, by looking at its rotational constants. Hence, when considering the tetramers that can form by using VF and CO_2 there are three different combinations such as, VF...CO_2...CO_2...CO_2, VF...VF...CO_2...CO_2 and VF...VF...VF...CO_2. Since the

molecular weights of VF (46 g/mol) and CO_2 (44 g/mol) are quite similar to each other, whatever combinations were tried for the tetramer always ended up with quite similar rotational constants. But one structure which had one VF molecule and three CO_2 molecules gave the most similar rotational constants to the BS3 experimental rotational constants. In that structure, the three CO_2 molecules were made like a pinwheel structure with VF molecule located in the middle of that pinwheel (Fig. 3.11.b).

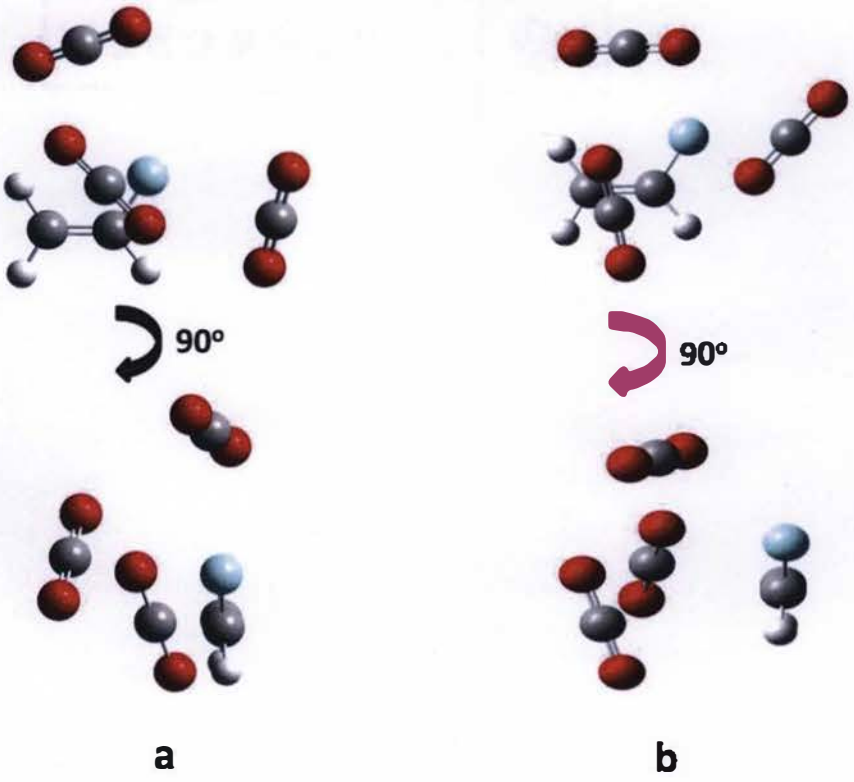

Figure 3.11: Predicted structures for a). Top-Side-Above VF...$(CO_2)_3$ tetramer, b). BS3 molecular cluster

The rotational constants of predicted VF...$(CO_2)_3$ pinwheel tetramer were nicely matched with the experimental rotational constants of BS3 and the dipole moments also

nicely matched with the peak intensities. To prove the experimental and theoretical rotational constants matched with each other nicely, the planar moments for each axis were calculated. The planar moments also proved that these theoretical rotational constants aligned with the experimental rotational constants (Table 3.4). This spectrum had strong *a*-type transitions and also observed comparatively weak *b* and *c*-type transitions. This observation was confirmed by the theoretical dipole moments.

Table 3.4: Experimental and predicted parameters for the BS3 molecular cluster

Parameter	Experimental constants for BS3	Top-Side-Above VF...$(CO_2)_3$ tetramer	Predicted VF...$(CO_2)_3$ tetramer
***A* / MHz**	786.9831(1)	962.5	781.4
***B* / MHz**	683.6282(1)	529.5	670.6
***C* / MHz**	598.7616(1)	498.9	576.1
P_{aa}/ amu Å^2	470.5640(2)	596.9	492.1
P_{bb}/ amu Å^2	373.4765(2)	507.8	385.2
P_{cc}/ amu Å^2	268.6961(2)	216.0	261.5
μ_a/ D	Strong	0.2	1.3
μ_b/ D	Medium	1.6	0.7
μ_c/ D	Weak	0.5	0.3
Int_{max}/ mV	12.6158		

Previously carried out research studies on the CO_2 clusters have found that CO_2 can form a trimer having a pinwheel like structure (Fig. 3.12).[12] A pinwheel like arrangement bearing a CO_2 trimer fragment was observed within the predicted VF...$(CO_2)_3$ tetramer structure. Hence, this observation suggests that within the VF...$(CO_2)_3$ tetramer structure the CO_2 molecules are trying to form the CO_2 trimer structure ($(CO_2)_3$) itself.

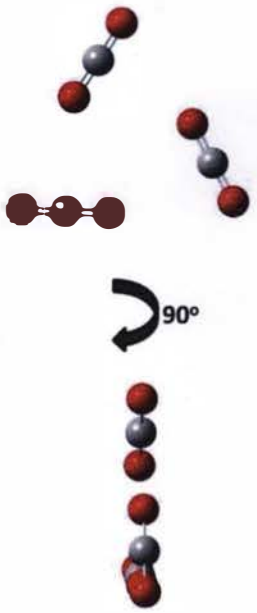

Figure 3.12: The CO_2 trimer ($(CO_2)_3$) structure[12]

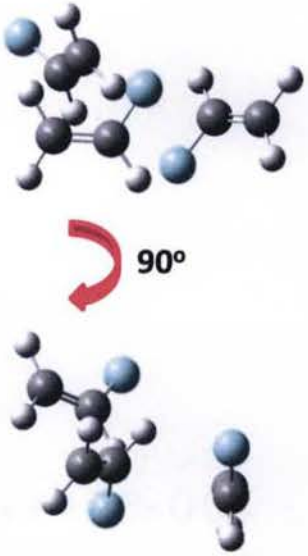

Figure 3.13: Predicted possible structure for BS500 molecular cluster by the Gaussian 09 program

The molecular cluster, BS500 which was found from the VF-only scan had lower rotational constants than VF…CO_2 dimers and also these rotational constants were quite

similar to the studied VF…CO_2…CO_2 trimer rotational constants. Hence, this BS500 VF-only cluster was suspected to be VF trimer. Then using the Gaussian 09 program VF trimer optimizations were carried out. One VF trimer optimization gave theoretical *B* and *C* rotational constants which nicely match the BS500 *B* and *C* rotational constants (Fig. 3.13), but the *A* rotational constant and dipole components were not matched with the experimental peak intensities (Table 3.5). Not only the dipole moments, but the predicted P_{cc} values were also quite off (% error = 53.02%) from the theoretical value. Hence, this prediction was rejected, but the rotational constants confirmed that this BS500 should be a trimer structure. However, a nicely matching structure for BS500 was found through a different approach and it will be discussed later on in this chapter.

Table 3.5: Experimental and predicted parameters for the BS500 molecular cluster

Parameter	Experimental constants for BS500	Predicted $(VF)_3$ trimer
***A* / MHz**	1131.8623(1)	1234.8
***B* / MHz**	906.6449(1)	921.9
***C* / MHz**	603.0449(1)	595.2
P_{aa}/ amu Å^2	474.4800(1)	493.9
P_{bb}/ amu Å^2	363.5655(1)	355.1
P_{cc}/ amu Å^2	82.9367(1)	54.2
μ_a/ D	Weak	1.3
μ_b/ D	Strong	0.6
μ_c/ D	Medium	0.5
Int_{max}/ mV	1.6371	

It was assumed that the structure of BS200 molecular cluster could be a VF/CO_2 pentamer since it has smaller rotational constants than the tetramer (Tables 3.3 and 3.4). The initial pentamer structures for all the combinations of VF and CO_2 were predicted

and two optimized structures had similar rotational constants to the BS200 molecular cluster (Table 3.6).

Table 3.6: Comparison of Experimental parameters for BS200 molecular cluster with the Gaussian predicted parameters for $(VF)_4...CO_2$ and $VF...(CO_2)_4$ pentamers

Parameter	Experimental constants for BS200	Predicted constants for $(VF)_4...CO_2$	Predicted constants for $VF...(CO_2)_4$
A / MHz	590.2371(1)	549.2	562.3
B / MHz	356.7366(1)	335.9	308.9
C / MHz	311.6427(1)	298.2	293.8
P_{aa}/ amu Å^2	1091.0519(3)	1139.5	1228.8
P_{bb}/ amu Å^2	530.6096(3)	555.1	491.5
P_{cc}/ amu Å^2	325.6209(3)	365.1	407.3
μ_a/ D	Strong	0.8	0.1
μ_b/ D	Medium	1.2	1.3
μ_c/ D	Weak	0.6	0.8
Int_{max}/ mV	1.6481		

Figure 3.14: Predicted structures for a). $(VF)_4...CO_2$ pentamer b). $VF...(CO_2)_4$ pentamer

Both structures were from the predictions of $(VF)_4...CO_2$ and $VF...(CO_2)_4$ pentamers (Figs. 3.14.a and 3.14.b). Even though the theoretical and experimental rotational constants were close enough to each other, the planar moments and the dipole components of these predicted structures were not close enough to the experimental parameters.

Both of the BS100 and BS400 molecular clusters were predicted to be tetramers by looking at the rotational constants (Table 3.3), because the experimental rotational constants of BS100 and BS400 were lower than the predicted $VF...CO_2...CO_2$ trimer rotational constants and also higher than the predicted pentamer rotational constants of BS200 cluster. The possible structures were guessed for both BS100 and BS400. Different VF tetramers structures were optimized for BS400 since it was found from the VF-only scan, but possible structural matches were not found for BS100 and BS400.

The Gaussian 09 approach provided some good structure candidates for observed spectra, but it also produced several unsatisfactory structures and there were some spectra with no good candidate structures, so other approaches to structure determination were needed. The coming sections will explain how other approaches were used for the further analysis.

3. III. C. Using concentration dependence studies to identify molecular formulas for the clusters

Both satisfactory and unsatisfactory structures were produced by the Gaussian 09 approach discussed in the previous section. The rotational constants of the unsatisfactory structures still gave an idea of how many molecules a certain cluster can contain. For instance, in the case of BS500 molecular structure, the theoretical rotational constants

were close enough to the predicted values to give the fact that it could be a trimer structure but the likely molecular arrangement was not determined. Hence, more data was needed to help predict structures for the unknown clusters.

Some possible experimental ideas were generated such as changing CO_2 concentration with constant VF concentration to get an idea of the composition of the unknown clusters, because larger clusters with large number of CO_2 seem to have better intensities at high concentrations of CO_2, while those with a lot of VF prefer low CO_2 concentration and drop off intensity quickly as the CO_2 concentration increases. The ideas that were implemented in this project are originally from Prof. Brooks Pate at the University of Virginia. He has experimented with some analysis techniques with temperature variations to identify spectra for changing conformer populations of molecules and in this experiment, we are using concentration variations to identify structures and compositions.

Some ideas were implemented from the extended cross correlation (XCC) technique which was developed by Prof. Robert W. Field to analyze big spectroscopic data sets.[13] The behavioral changes of the lines in the spectra (changes in the intensity of radiation absorbed, for instance) over the different conditions (such as systematically varying CO_2 concentrations, varying inert carrier gas, varying atomic masses) were observed similar to how they would be in the XCC technique. The CO_2 concentration was varied while keeping the VF concentration constant and the changes in peak intensity were observed, and to fully implement the XCC technique in this study, it would be necessary to plot the peak intensities from one spectrum vs. peak intensities from a second spectrum. In this case, the slightly different approach developed at UVa was

followed. Further developing innovative techniques such as XCC and the UVa approach will also help other researchers to analyze the components of complex mixtures.

The intensity differences over the different CO_2 concentrations were tested in this concentration dependent approach. The intensity of a peak which belongs to a cluster is directly related to the abundance of the specific molecular cluster. If the peak intensity is comparatively high at one concentration that means the cluster abundance is higher at that concentration. For instance, if one cluster's peak intensity is highest at 4% CO_2 concentration and gradually lowers the peak intensities at 2%, 1% and 0.5%, that means this specific cluster prefers to make highest number of molecular clusters at 4% CO_2 concentration and that is why it shows the highest peak intensity as well as if the peaks are strongest in 4% CO_2 scan, then the formula of the cluster is likely to have a higher ratio of CO_2:VF.

After recording all the scans, they were all opened in an Origin 8.1 plot (Fig. 3.1). All the plots together showed that there is a clear relationship between the concentration and the peak intensity. Fig. 3.15 can be used to explain how the peak intensity differs with the different CO_2 concentrations. In this figure, it shows the VF/CO_2 scans with the constant difference patterns. For instance when considering the BS200 inset in Fig. 3.16 to explain this phenomenon, the highest intensity peaks have tops that are black and red in color, representing the 0.5% and 1% CO_2 concentrations, respectively. This observation shows that the BS200 cluster prefers more VF molecules in the molecular cluster and whenever the VF concentration is higher in the system it tends to form higher number of BS200 clusters. In the previous section, possible molecular structures were optimized for BS200 using Gaussian 09. The optimizations suggested that BS200 could

be a pentamer with four VF molecules and one CO_2 molecule. Hence, these CO_2 concentration dependence plots are consistent with the Gaussian observations and confirm that BS200 molecular cluster should contain more VF molecules than CO_2 molecules.

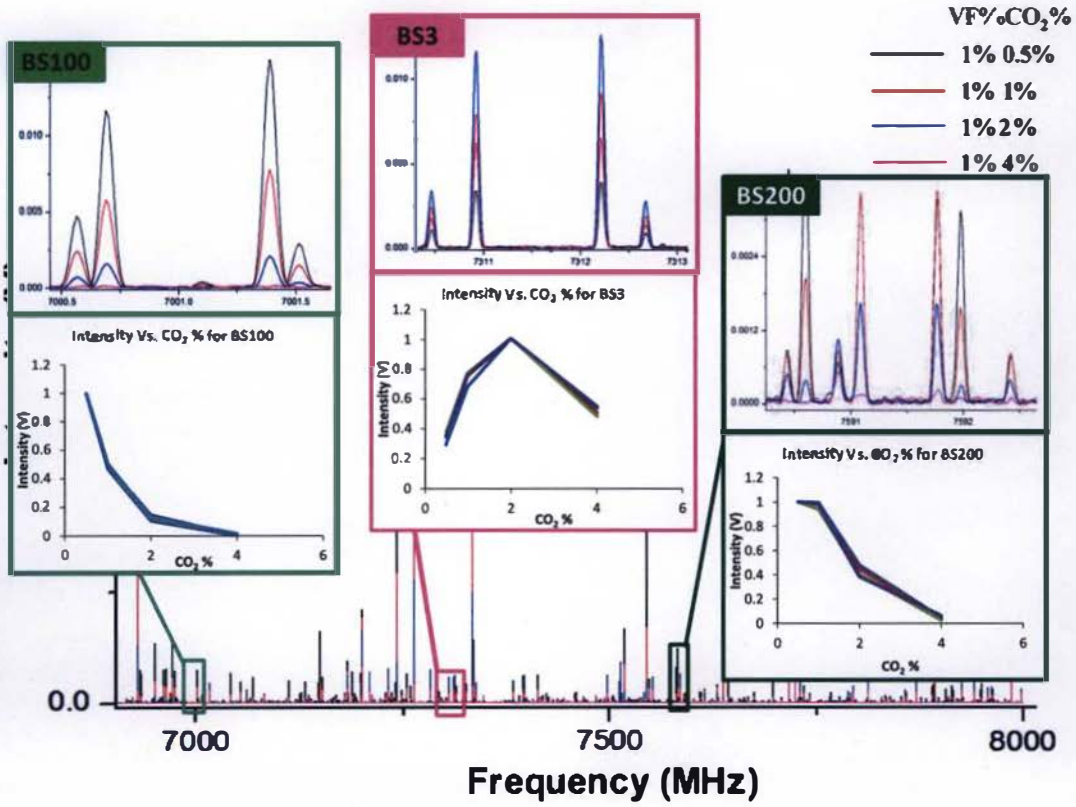

Figure 3.15: Intensity behavior over different CO_2 concentrations of the mother constant difference patterns of BS3, BS100 and BS200

This phenomenon can be confirmed using the already found BS3 cluster, the tetramer which had one VF molecule and three CO_2 molecules. Fig. 3.17 shows the inset from Fig. 3.15 belonging to BS3 molecule zoomed in with peak intensities of the mother constant difference pattern, which has the highest intensity peaks with blue color tops. The blue color plot is produced with the 2% CO_2 concentration, and the graph of intensity

vs CO_2 concentration (Fig. 3.15) shows that whenever the CO_2 concentration is lower, peak intensity is lower. Hence, that can conclude the BS3 molecular cluster prefers more CO_2 molecules in the molecular cluster.

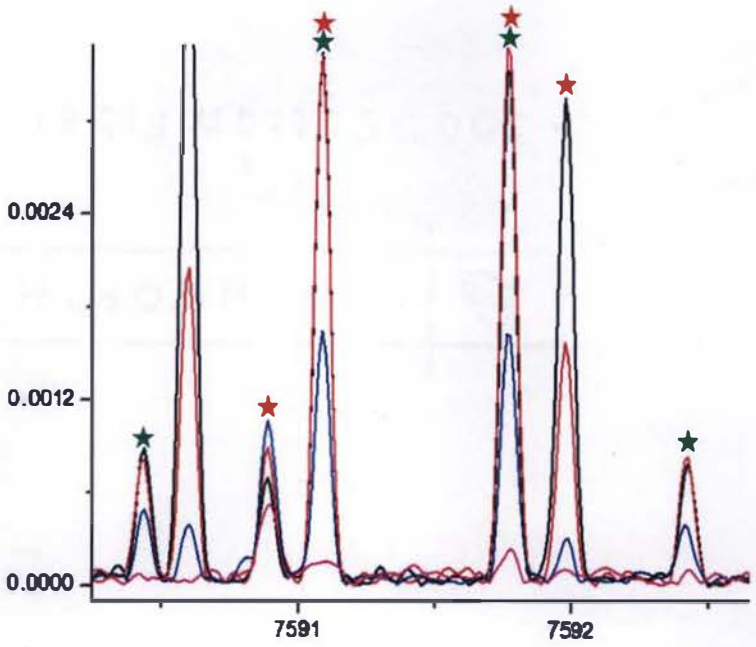

Figure 3.16: Spotting constant differences using the peaks with same color tops

These CO_2 concentration dependent plots helped to find constant difference patterns more easily, for example, in the Fig. 3.15 inset of BS200 (Fig. 3.16) having the mother constant difference pattern of the BS200 molecular cluster. In this figure green color stars mark peaks related to the constant difference pattern. If close attention is paid to the peaks in this figure, peaks assigned red stars also seem to be in a constant difference pattern, but in the CO_2 concentration dependent plots, the green starred peaks have red color tops, while the red starred peaks that do not belong to the constant difference pattern have blue and black color tops. So, the behavior of these peaks with the CO_2 concentration is different from other peaks. Therefore, these CO_2 concentration dependent plots are useful to identify patterns easily.

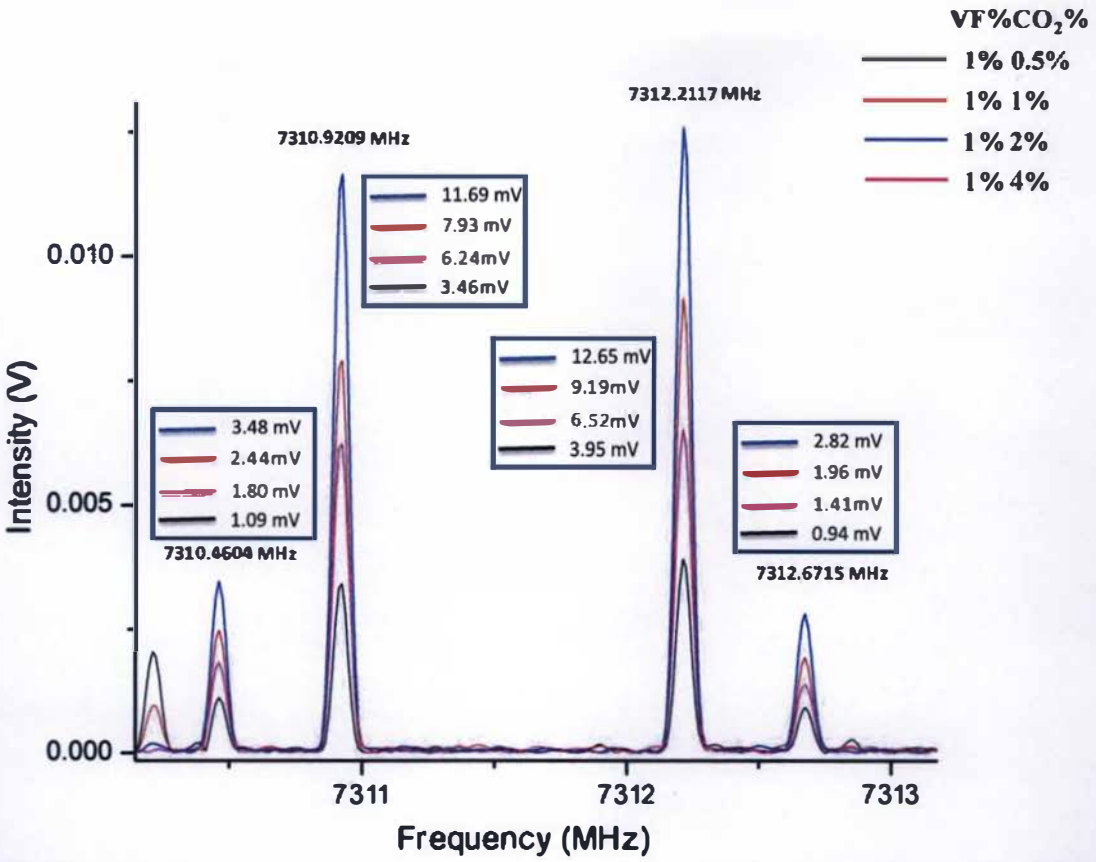

Figure 3.17: Peak intensities of the mother pattern frequencies of the BS3 molecular cluster over different CO_2 concentrations

After observing these intensity behaviors over different CO_2 concentrations, the MathCAD approach that has been explained in the experimental section was developed. After doing all the steps mentioned in the experimental section (section 3.II.C), average concentration vs area and width vs area plots were constructed (Fig. 3.3 and 3.4). To plot these graphs the 1000 strongest cluster peaks were used and then the clumps of points located throughout the plot were observed. The MathCAD routine was followed to extract five new groups of related peaks, corresponding to spectra of five molecular clusters with the points all lying in the general region of the plots close to the points for

the previously identified BS100 spectrum: BP100, BP200, BP300, BP400 and BP500. After the groups of related peaks were selected, patterns were identified from within these subsets of peaks from the whole data set, and these were then assigned and fitted by the SPFIT program and the experimental rotational constants were obtained (Table 3.7).

Table 3.7: The experimental rotational constants *A*, *B* and *C* for the molecular clusters (BP100, BP200, BP300, BP400 and BP500), which were found using MathCAD approach

Parameters	BP100	BP200	BP300	BP400	BP500
***A* / MHz**	1286.3844(12)	779.4479(8)	492.7755(35)	828.4558(35)	804.7719(16)
***B* / MHz**	1179.7087(9)	541.4087(1)	357.0756(3)	772.8230(7)	752.6993(13)
***C* / MHz**	720.7153(5)	488.8201(1)	321.3115(3)	721.9246(7)	719.8689(9)

All five spectra were found from the purple circled area of the average concentration vs area and width vs area plots (Fig. 3.18 and 3.19). The five different clusters extracted from this area showed similar intensity behavior over different CO_2 concentrations (Fig. 3.20).

This fact can be explained more by using the already known clusters: Top-Above and Side-Above VF...CO_2...CO_2 trimers. The plots for these species are in the same region in Fig. 3.18 since they have the same composition and therefore similar intensity behavior over the different CO_2 concentrations. Likewise, the BS200 and BS3 cluster peaks are located at different places in Fig. 3.18 since the cluster peaks have different intensity behavior (Fig. 3.15) over the different CO_2 concentrations. Finding clusters at different locations indicates that they have different compositions depending on their intensity behaviors over different CO_2 concentrations.

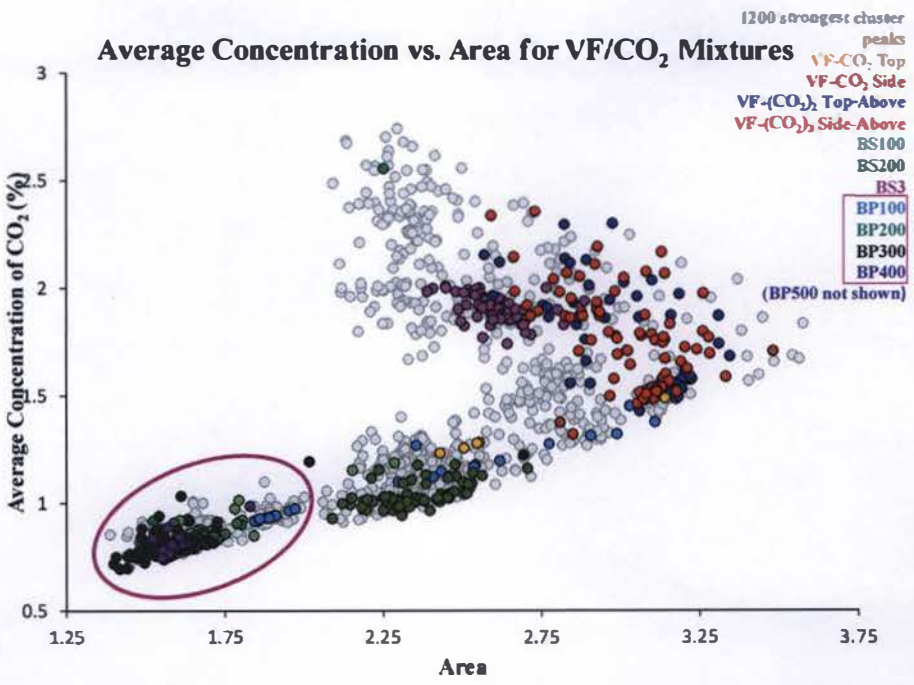

Figure 3.18: The MathCAD plot of the average concentration of CO_2 (%) vs area. The circled area in the plot shows the cluster peaks for BS100, BP100, BP200, BP300 and BP400

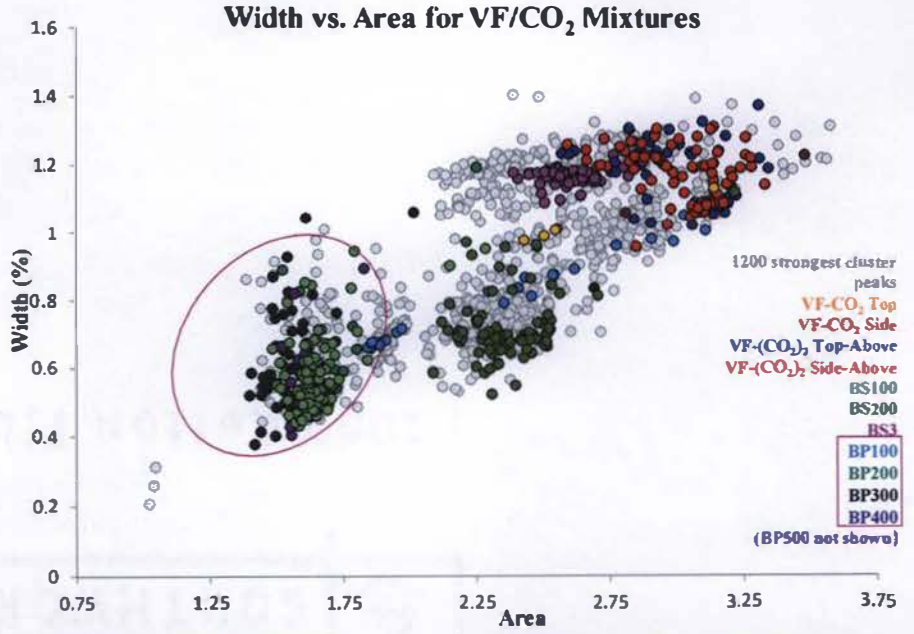

Figure 3.19: The MathCAD plot of the width (%) vs area. The circled area in the plot shows the cluster peaks for BS100, BP100, BP200, BP300 and BP400

The purple color circled area in both plots (Fig. 3.18 and 3.19) contains peaks which belong to all five different identified unknown clusters (BP500 is not shown in the plots). According to the intensity vs CO_2 concentration plot (Fig. 3.20), the clusters in this region show highest intensity with the lower CO_2 concentration. That shows these clusters prefer more VF molecules than CO_2 molecules in their molecular formulas, which was helpful to guess the formulas for these BP molecular clusters. The challenging part was to find the structures for these molecular clusters, which will be discussed further in Section 3.III D.

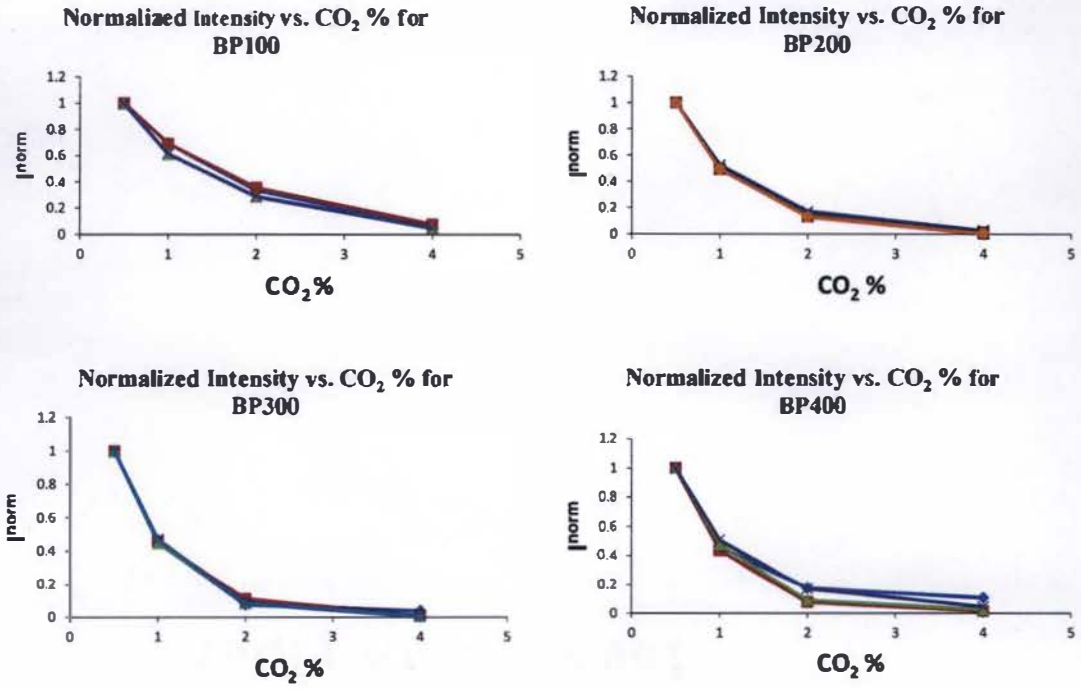

Figure 3.20: Normalized intensity (I^{norm}) vs. CO_2 concentration plots for BP100, BP200, BP300 and BP400 molecular clusters (The different colors are used to represent four different transitions that show how all the transitions of a given cluster follow the same intensity behavior as the CO_2 concentration is varied.)

Figure 3.21: Predicted structure for the BP100 molecular cluster

The BP100 molecular cluster has the rotational constants which are nearly the same to the rotational constants of the studied VF...CO_2...CO_2 trimer structure. And also the intensity behavior plots (Fig. 3.20) showed that these BP clusters prefer more VF molecules inside the cluster structures. Hence, initial structural guesses for BP100 which had two VF molecules and one CO_2 molecule were carried out using the Gaussian 09 approach (Fig. 3.21). One optimized VF...VF...CO_2 trimer structure showed the theoretical rotational constants which are quite similar to the experimental rotational constants of the BP100 molecular cluster (Table 3.8).

The predicted *A* value is quite off from the experimental value (% error = 5.92%). But when compared with the *B* (% error = 2.89%) and *C* (% error = 0.75%) constants, the *A* constant is not too way off. Further calculations were carried out to calculate the experimental and theoretical planar moments to show the guessed structure was nicely matching with the experimental parameters. The planar moments are not matching 100%,

but this is the best structural match obtained for BP100. The dipole moments were nicely matched with the peak intensities of *a*, *b* and *c* type transitions.

Table 3.8: Experimental and predicted parameters for the BP100 molecular cluster

Parameter	Experimental constants for BP100	Predicted constants for $(VF)_2...CO_2$ trimer
A **/ MHz**	1286.3844(12)	1367.3
B **/ MHz**	1179.7087(9)	1146.6
C **/ MHz**	720.7153(5)	726.1
P_{aa} **/ amu Å^2**	368.3719(7)	383.6
P_{bb} **/ amu Å^2**	332.8467(7)	312.4
P_{cc} **/ amu Å^2**	60.02115(7)	57.2
μ_a **/ D**	Strong	2.0
μ_b **/ D**	Weak	1.1
μ_c **/ D**	Weak	1.6
Int_{max} **/ mV**	69.8278	

The BP200 molecular cluster had rotational constants nearly the same as the rotational constants of BS3, which was predicted to be the the $VF...CO_2...CO_2...CO_2$ tetramer. Also, from the intensity behavior plots it was found that BP200 prefers more VF molecules than CO_2 molecules in it. Following this observation, structures with the $VF...VF...VF...CO_2$ formula were optimized using the Gaussian 09 approach, but any of the theoretical rotational constants and dipole moments belonging to those structures did not match with experimental rotational constants for the unknown molecular clusters. Hence, Gaussian 09 calculations for another tetramer, $VF...VF...CO_2...CO_2$, were carried out.

One $VF...VF...CO_2...CO_2$ tetramer structure (Fig. 3.22) gave theoretical rotational constants which are similar to the BP200 experimental rotational constants (Table 3.9). To confirm the rotational constants are matching with the experimental

rotational constants the planar moments were calculated for each axis. The planar moments also nicely matched with the experimental planar moments.

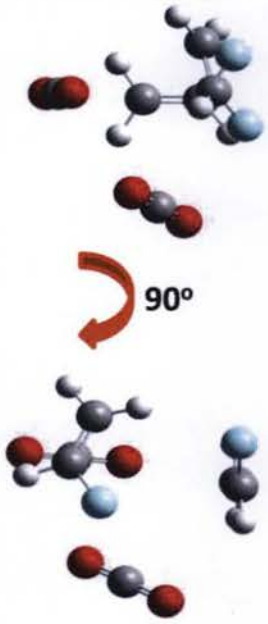

Figure 3.22: Predicted structure for the BP200 molecular cluster

Table 3.9: Experimental and predicted parameters for the BP200 molecular cluster

Parameter	Experimental constants for BP200	Predicted constants for $(VF)_2...(CO_2)_2$ tetramer
A / MHz	779.4479(8)	792.5
B / MHz	541.4087(1)	562.8
C / MHz	488.8201(1)	524.4
P_{aa}/ amu Å^2	659.4732(7)	594.2
P_{bb}/ amu Å^2	374.4021(7)	380.6
P_{cc}/ amu Å^2	273.9787(7)	246.8
μ_a/ D	Strong	1.7
μ_b/ D	Weak	1.4
μ_c/ D	Weak	1.0
Int_{max}/ mV	1.1158	

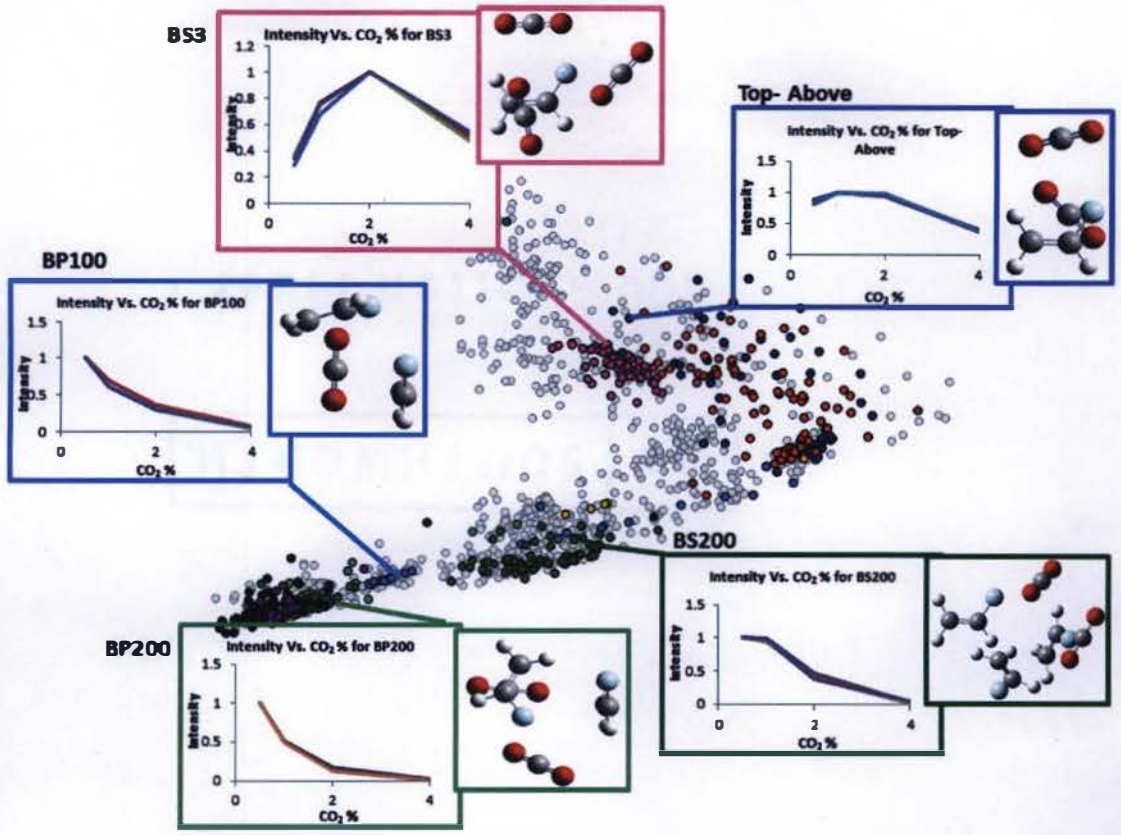

Figure 3.23: Comparison of the proposed structures for the molecular clusters and the intensity behaviors with different CO_2 concentrations

All the structures predicted using the Gaussian 09 approach for the clusters with unknown structures were matched with the intensity behaviors over the CO_2 concentrations. It can be clearly observed in Fig. 3.23, because the suggested numbers of VF and CO_2 molecules correspond to the intensity variation in these graphs. After finding these two likely structures for BP100 and BP200, the next task was to find structures for the other remaining unknown molecular clusters which are BP300, BP400 and BP500. This was a big challenge since the structures were getting larger, so the number of possible permutations of VF+CO_2 increases. As the number of molecules increases in the molecular cluster, the number of possible orientations for the molecules within the cluster

also increases. Hence, it was difficult to ensure the most stable conformations were considered in the Gaussian 09 structural optimizations.

The high cost of optimizing larger clusters was the other challenge. Usually for these VF/CO_2 cluster studies MP2 level calculations were used. MP2 level calculations are usually used to calculate energies of loosely bound complexes and are very reliable. Fast DFT methods usually cannot perform calculations for molecules which have weak interactions, but DFT methods such as M06-2X or ωB97X-D are capable of doing calculations for molecular clusters with weak interactions. MP2 optimizations take much longer to do than the DFT level optimizations, because some of the more involved parts of the calculation in an MP2 calculation are approximated in a DFT calculation rather than being calculated explicitly. In this approach, DFT level calculations were tested using the ωB97X-D/6-31+G(d,p) basis set. The DFT level calculations with the ωB97X-D/6-31+G(d,p) basis set is relatively reliable and almost as accurate as the MP2 calculations, that were used in the previous experiments.

Table 3.10: Comparison of DFT and MP2 level theoretical constants with experimental constants of BS3 molecular cluster

Parameter	Experimental constants for BS3	DFT level theoretical constants	MP2 level theoretical constants
A **/ MHz**	786.9831(1)	781.4	804.4
B **/ MHz**	683.6282(1)	670.6	690.9
C **/ MHz**	598.7616(1)	576.1	586.1
P_{aa} **/ amu Å^2**	470.5640(2)	492.0	482.7
P_{bb} **/ amu Å^2**	373.4765(2)	385.2	379.5
P_{cc} **/ amu Å^2**	268.6961(2)	261.5	248.8
μ_a **/ D**	Strong	1.3	1.3
μ_b **/ D**	Medium	0.7	0.7
μ_c **/ D**	Weak	0.3	0.4

Table 3.10 compares the DFT and MP2 level theoretical spectroscopic parameters with the experimental constants of the BS3 molecular cluster. The experimental *A* and *B* rotational constants are located in between the DFT and MP2 level constant values. Also, the planar moments and dipole moments of both levels were consistent with the observed transition intensities.

3. III. D. Identification of the molecular structures with ABCluster approach

To find the structures of the unknown molecular clusters the ABCluster program was used, which helps find the minimum energy structures. The force field approach in the ABCluster program which calculates energy of the structure by using charges of the atoms and Lennard-Jones potential of the molecules was used to find the minimum energy structures (see section 3.I for details). The ABCluster program is a way to probe a lot of possible cluster arrangements rapidly.

First ABCluster was tested with known molecular clusters (VF...CO_2 dimers and VF...CO_2...CO_2 trimers). Fig. 3.24 shows the first 30 lowest energy structures identified from the ABCluster force field approach for VF...CO_2...CO_2. Low energy experimentally observed Top-Above and Side-Above trimer structures were found within these 30 structures (Fig. 3.24). Same structures with slight changes in distances, angles and dihedrals were able to be observed multiple times among these 30 structures and the experimentally observed structures were corresponding to those structures. Other than the experimentally observed structures it produced different arrangements which had higher energies, and because of the high energy, they would be less likely to exist experimentally. Testing the known molecular cluster which is VF...CO_2...CO_2 trimer

with ABCluster force field approach proves that it is reliable and accurate in predicting possible structures for different molecular combinations for larger clusters.

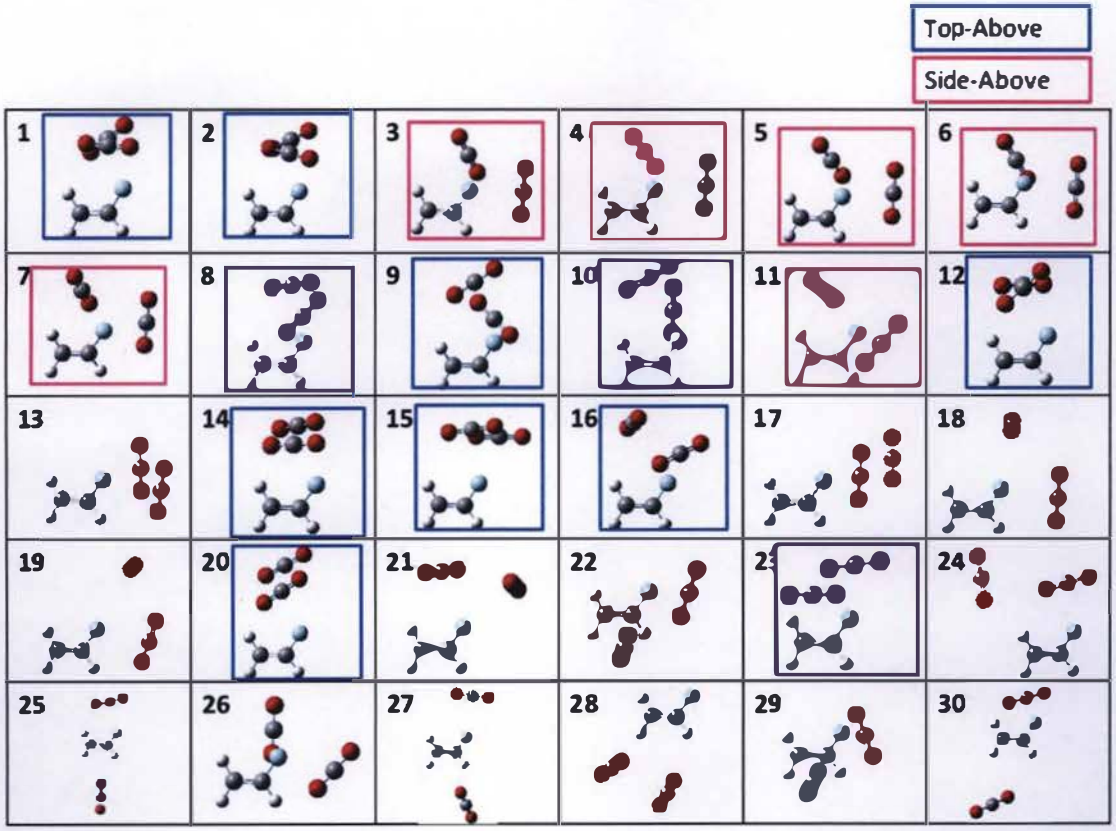

Figure 3.24: Top 30 hits for the VF...CO_2...CO_2 trimers obtained using the ABCluster force field approach[6,7,8]

The ABCluster force field approach was used to find minimum energy structures for VF/CO_2 tetramers and pentamers with different permutations of VF+CO_2. Then, more accurate structural matches for BS200 and BP300 were found. Also, the possible minimum energy structures were predicted by the ABCluster program for BS500 which was previously found as a VF trimer using the Gaussian 09 approach.

Table 3.11: Spectroscopic parameters for BS200, BP300 molecular clusters and minimum energy structures of all the possible pentamer permutations obtained by ABCluster program (see Table 3.6 for predictions from Gaussian approach)

Parameters	Experimental constants for BS200	Experimental constants for BP300	$VF(CO_2)_4$	$(VF)_2(CO_2)_3$	$(VF)_3(CO_2)_2$	$(VF)_4CO_2$
A / MHz	590.2371(1)	492.7755(35)	574.4	535.8	539.9	496.3
B / MHz	356.7366(1)	357.0756(3)	405.1	424.4	366.8	366.2
C / MHz	311.6427(1)	321.3115(3)	395.1	347.1	311.3	321.0
P_{aa}/ amu Å^2	1091.0519(3)	981.3070(7)	823.5	851.9	1032.5	968.1
P_{bb}/ amu Å^2	530.6096(3)	591.5560(7)	455.7	604.2	590.8	606.2
P_{cc}/ amu Å^2	325.6209(3)	434.0206(7)	424.1	338.9	345.2	412.0
μ_a/ D	Strong	Strong	0.8	0.0	0.7	1.3
μ_b/ D	Medium	Weak	0.3	0.3	0.3	0.4
μ_c/ D	Weak	Weak	1.3	0.7	0.03	0.1
Int_{max}/ mV	1.6481	0.3034				

The Gaussian approach was used to find the possible structures for the BS200 molecular cluster and this attempt was not successful, because the predicted spectroscopic parameters did not match with the experimental values (Table 3.6). Also, the concentration dependence study helped to eliminate the $VF...(CO_2)_4$ pentamer structure since the BS200 prefers more VF molecules than CO_2 molecules within the clusters (Fig. 3.15). The ABCluster program was used to predict low energy structures for BS200 with all the possible permutations with more VF molecules in it (Table 3.11). Finally, a possible structure for BS200 was found by using the ABCluster program.

The proposed structure for the BS200 cluster had all the rotational constants, planar moments and the dipole components, match the experimental parameters (Table 3.11). The proposed structure had three VF molecules and two CO_2 molecules which explains the fact that BS200 prefers more VF molecules than CO_2 molecules within the cluster (Fig. 3.25). In this case, the B and C rotational constants are quite nicely matching

with the predicted value, but the percentage difference of 9.3% was observed when comparing the predicted and the experimental *A* rotational constants.

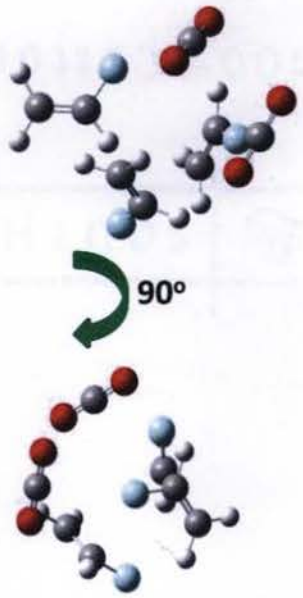

Figure 3.25: Predicted structure for the BS200 molecular cluster

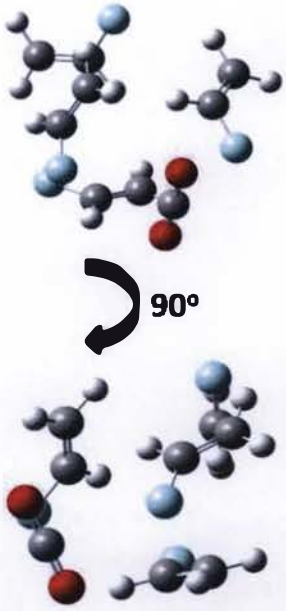

Figure 3.26: Predicted structure for the BP300 molecular cluster

A possible structural match for BP300 was also found by using the ABCluster program (Fig. 3.26). The experimental structural parameters were nicely matched with the predicted structural parameters (Table 3.11). This proposed structure was composed of four VF molecules and one CO_2 molecule and this nicely agreed with the intensity plots that were studied previously (Fig. 3.20), because the BP300 molecular cluster intensity plot shows highest intensity at low CO_2 concentrations and that suggests the BP300 cluster prefers more VF molecules than CO_2 molecules in the molecular cluster.

A possible structure for BS500 (which was found to be a VF trimer) with the Gaussian 09 approach was predicted (Fig. 3.13), but it was not the best structural fit. Hence, possible lower energy structures were predicted with the ABCluster program and one optimized structure was shown to be the best match for the BS500 molecular cluster (Fig. 3.27).

Figure 3.27: Predicted structure for the BS500 molecular cluster by the ABCluster program

All the parameters for the predicted structure were nicely matched with the experimental parameters (Table 3.12). The root-mean-square percent differences between observed and predicted rotational constants were calculated, as discussed in Chapter 2 in detail, to prove the improved match. The structure obtained from Gaussian gave the value 4.96%, and the structure obtained through the ABCluster force field method and then optimized by Gaussian gave 1.31%. When comparing the root-mean-square percent differences between observed and calculated rotational constants obtained through the Gaussian approach and the ABCluster approach it was obvious that the ABCluster approach (including optimization using Gaussian of the structures obtained by ABCluster) predicted more precise and accurate structure for the BS500 molecular cluster.

Table 3.12: Comparison of experimental parameters of the BS500 molecular cluster with the predicted structural parameters by the ABCluster and Gaussian programs

Parameter	Experimental constants for BS500	Predicted constants by ABCluster force field approach and optimized by Gaussian	Predicted constants for best structure from Gaussian 09 approach
A / MHz	1131.8623(1)	1153.08	1234.8087
B / MHz	906.6449(1)	894.9487	921.8830
C / MHz	603.0449(1)	602.2217	595.2387
P_{aa}/ amu Å^2	474.4800(2)	482.8034	493.9809
P_{bb}/ amu Å^2	363.5655(2)	356.3879	355.0550
P_{cc}/ amu Å^2	82.9367(2)	81.8984	54.2221
μ_a/ D	Weak	0.2809	1.3425
μ_b/ D	Strong	1.3757	0.6114
μ_c/ D	Medium	0.612	0.5515
Int_{max}/ mV	1.6371		

At this point structures for five unknown molecular clusters (BS3, BS200, BS500, BP100, and BP300) were found, and five unknown molecular clusters still remain (BS100, BS400, BP200, BP400 and BP500). BS400 was found from the VF only scan and by looking at the rotational constants it can be predicted that this molecular cluster could be a tetramer of VF ($(VF)_4$), because the rotational constants of the BS400 molecular cluster were smaller than the rotational constants of BS500 which was VF trimer. The rotational constants of the BS400 molecular cluster were in the range of VF+CO_2 tetramer clusters that was found through this study.

By looking at the rotational constants and the intensity behavior as a function of the CO_2 concentration helps predict the composition of the unknown clusters. Structures that contain H_2O molecules were not optimized since originally the peaks corresponding to any H_2O transitions were not observed in the scans, but there could be some H_2O molecules trapped inside the samples which would like to form complexes with VF and CO_2. So for the further studies structures with the H_2O molecules should be optimized. Also, a spectrum which is a dimer that contains VF and Ne was able to be assigned from the VF-only scan (ongoing study (see Appendix II for more details)); therefore, the unidentified molecular clusters might also contain Ne. Hence, for further studies, molecular clusters which contain Ne in the formulae should be optimized.

Both BP400 and BP500 molecular clusters have nearly the same rotational constants and also the numbers of transitions corresponding to these two molecules is smaller compared to other assignments. BP500 was suspected as isotopic substituent of the BP400 molecular cluster. Then the peak intensities were examined to confirm this assumption and the peak intensity of the BP500 was about 1/3 of that of BP400. Ne has

two isotopes ^{20}Ne and ^{22}Ne which have the relative abundance ratio of 9:1 but the intensity ratio of ^{20}Ne:^{22}Ne is usually less than 9:1 due to quantum mechanical isotope effects. Hence, for BP400:BP500 the peak intensity ratio should be observed less than 9:1 if they correspond to ^{20}Ne and ^{22}Ne isotopologues of the same species. To confirm this hypothesis experiments are ongoing.

As a summary, the development of new techniques to find more molecular clusters is very helpful to reduce the number of unassigned transitions from a specific scan. Even though it is possible to find many molecular clusters from a scan, it is not an easy task to find the structures of the molecular clusters. But the approaches such as concentration dependence plots will help to determine the composition of the molecular clusters. Moreover, programs like ABCluster help to predict the lower energy structures and ensure that the most favorable structures are being considered. Therefore, using combinations of different techniques will help to assign spectra for molecular clusters and find structures for them. Up to now, using the integrated techniques possible structures were found for BS200 ($(VF)_3...(CO_2)_2$), BS3 ($VF...(CO_2)_3$), BS500 ($(VF)_3$), BP100 ($(VF)_2...CO_2$), BP200 ($(VF)_2...(CO_2)_2$, and BP300 ($(VF)_4...CO_2$) molecular clusters and still need to find structures for BS100, BS400, BP400 and BP500 molecular clusters.

3. IV. References

[1]G. G. Brown, B. C. Dian, K. O. Douglass, S. M. Geyer, S. T. Shipman, B. H. Pate, A broadband Fourier transform microwave spectrometer based on chirped pulse excitation. *Rev. Sci. Instrum.* **2008**, 79, 053103.

[2]PTC Mathcad Prime 5.0.0.0, PTC Inc., Needham MA, 2018

[3]Gaussian 09, Revision A.02, M. J. Frisch, G. W. Trucks, H. B. Schlegel, G. E. Scuseria, M. A. Robb, J. R. Cheeseman, G. Scalmani, V. Barone, G. A. Petersson, H. Nakatsuji, X. Li, M. Caricato, A. Marenich, J. Bloino, B. G. Janesko, R. Gomperts, B. Mennucci, H. P. Hratchian, J. V. Ortiz, A. F. Izmaylov, J. L. Sonnenberg, D. Williams-Young, F. Ding, F. Lipparini, F. Egidi, J. Goings, B. Peng, A. Petrone, T. Henderson, D. Ranasinghe, V. G. Zakrzewski, J. Gao, N. Rega, G. Zheng, W. Liang, M. Hada, M. Ehara, K. Toyota, R. Fukuda, J. Hasegawa, M. Ishida, T. Nakajima, Y. Honda, O. Kitao, H. Nakai, T. Vreven, K. Throssell, J. A. Montgomery, Jr., J. E. Peralta, F. Ogliaro, M. Bearpark, J. J. Heyd, E. Brothers, K. N. Kudin, V. N. Staroverov, T. Keith, R. Kobayashi, J. Normand, K. Raghavachari, A. Rendell, J. C. Burant, S. S. Iyengar, J. Tomasi, M. Cossi, J. M. Millam, M. Klene, C. Adamo, R. Cammi, J. W. Ochterski, R. L. Martin, K. Morokuma, O. Farkas, J. B. Foresman, and D. J. Fox, Gaussian, Inc., Wallingford CT, 2016.

[4]J. Zhang, M. Dolg, ABCluster: The Artificial Bee Colony Algorithm for Cluster Global Optimization. *Phys. Chem. Chem. Phys.* **2015**, 17, 24173-24181.

[5]J. Zhang, M. Dolg, Global Optimization of Rigid Molecular Clusters by the Artificial Bee Colony Algorithm. *Phys. Chem. Chem. Phys.* **2016**, 18, 3003-3010.

[6]J. Zhang, ABCluster manual. Version 1.3, Institute for Theoretical Chemistry, University of Cologne, **2016**.

[7]K. Vanommeslaeghe, E. Hatcher, C. Acharya, S. Kundu, S. Zhong, J. Shim, E. Darian, O. Guvench, P. Lopes, I. Vorobyov, A. D. Mackerell Jr, CHARMM general force field: A force field for drug-like molecules compatible with the CHARMM all-atom additive biological force fields. *J. Comput. Chem.* **2010**, 31, 671-690.

[8] W. Yu, X. He, K. Vanommeslaeghe, A. D. MacKerell Jr. Extension of the CHARMM General Force Field to sulfonyl-containing compounds and its utility in biomolecular simulations. *J. Comput. Chem.* **2012**, 33, 2451-2468.

[9]Origin 8.1 SR1, v8.1.13.88 (Academic), OriginLab Corporation, Northampton MA, 1991-2009

[10]H. M. Pickett, The Fitting and Prediction of Vibration-Rotation Spectra with Spin Interactions, *J. Mol. Spectros.* **1991**, 148, 371-377.

[11] P. B. Kannangara, C. T. West, S. A. Peebles, R. A. Peebles, Towards microsolvation of fluorocarbons by CO_2: Two isomers of fluoroethylene-$(CO_2)_2$ observed using chirped-pulse Fourier-transform microwave spectroscopy. *Chem. Phys. Lett.* **2018,** 706, 538-542.

[12]M.J. Weida, D.J. Nesbitt, Geometric isomerism in clusters: High resolution infrared spectroscopy of a noncyclic CO_2 trimer. *J. Chem. Phys.* **1996**, 105, 10210-10223.

[13]M. P. Jacobson, S. L. Coy, R. W. Field, Extended cross correlation: A technique for spectroscopic pattern recognition. *J. Chem. Phys.* **1997**, 107, 8349.

CHAPTER 4

Conclusions

4. I. $VF...CO_2...CO_2$ trimer study

Chapter 2 describes the two experimentally observable isomers of the $VF...CO_2...CO_2$ trimer which are Side-Above and Top-Above structures. Both Side-Above and Top-Above trimers are combinations of previously studied $VF...CO_2$ dimers.[1] The Above form of the $VF...CO_2$ dimer which was not observed experimentally in the dimer studies was also observed as part of the $VF...CO_2...CO_2$ trimer structures. Within the $VF...CO_2...CO_2$ trimer structures it can be observed that the CO_2 molecules are arranged similarly to CO_2 dimers.[2] These dimers are more close to the T shaped CO_2 dimer structure, which is energetically less favorable than the slipped parallel form of $(CO_2)_2$. The higher energy T shaped CO_2 dimer can be stabilized within the $VF...CO_2...CO_2$ trimers in the presence of the VF molecule.

When comparing the atom...atom distances of the previously studied $VF...CO_2$ and $CO_2...CO_2$ dimers and the $VF...CO_2...CO_2$ trimers, the atom...atom distances within trimers are generally less than within dimers. Hence, the trimers can form more compact structures than the dimers, because of increased attractive interactions as a result of additional interacting monomers.

4. II. Developing new approaches to decode rotational spectra and to find the structures of unknown molecular clusters

Chapter 3 collectively describes how the unknown molecular clusters and their structures were found by using different analytical tools. Looking at the constant difference patterns in the original VF/CO_2 scan (Excel approach) identified the BS molecular clusters (BS100, BS200, BS3, BS400 and BS500) and the MathCAD approach found the BP molecular clusters (BP100, BP200, BP300, BP400 and BP500). All

identified cluster spectra were satisfactorily fitted to obtain experimental rotational constants (Table 4.1 and 4.2).

A matching structure was found for BS3 (Fig. 4.1.a) by the Gaussian approach. Also, possible structures for BS200 ($(VF)_3...(CO_2)_2$) (Fig. 4.1.b) and BS500 ($(VF)_3$) (Fig. 4.1.c) were found by the ABCluster force field approach. For the BP molecular clusters, identified by the MathCAD approach, matching structures were found for BP100 ($(VF)_2...CO_2$) (Fig. 4.2.a) and BP200 ($(VF)_2...(CO_2)_2$) (Fig. 4.2.b) from the Gaussian approach. Also, a possible structure for BP300 ($(VF)_4...CO_2$) (Fig. 4.2.c) was found by the ABCluster force field approach.

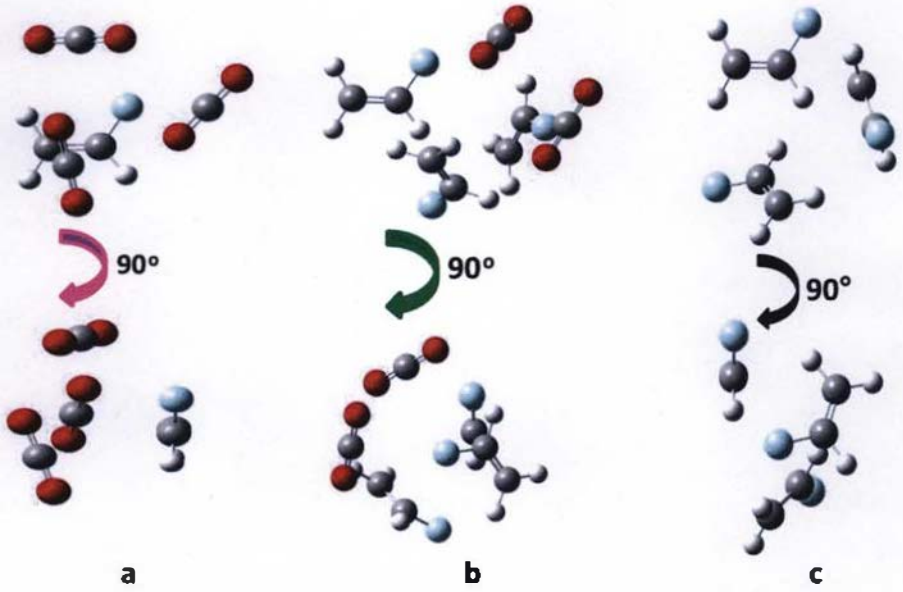

Figure 4.1: Predicted structure for a). BS3 ($VF...(CO_2)_3$), b). BS200 ($(VF)_3...(CO_2)_2$), c). BS500 ($(VF)_3$) molecular clusters

Atom...atom distances of $VF...CO_2$ dimers and $VF...CO_2...CO_2$ trimers were compared in Chapter 2 and shortening of atom...atom distances from $VF...CO_2$ dimers was observed when it came to the $VF...CO_2...CO_2$ distances (Figs. 4.3 and 4.4).

Table 4.1: Experimental rotational parameters for the BS molecular clusters

Parameter	BS100	BS200	BS3	BS400	BS500
A / MHz	698.16045(11)	590.23708(9)	786.98310(9)	602.57143(7)	1131.862317(48)
B / MHz	621.60821(8)	356.736570(38)	683.62819(8)	523.01568(5)	906.644889(44)
C / MHz	457.43250(8)	311.642724(33)	598.76157(8)	490.92731(5)	603.044894(48)
Δ_J / kHz	0.3243(15)	0.07124(13)	0.2399(13)	0.2257(5)	0.9609(8)
Δ_{JK}/ kHz	- 0.3178(6)	0.0680(6)	0.864(5)	0.0349(22)	1.841(1)
Δ_K / kHz	0.513(5)	0.0800(29)	-0.629(5)	0.2080(31)	-0.544(1)
δ_J / kHz	0.0797(7)	0.00760(9)	0.0194(7)	0.00934(28)	0.25335(11)
δ_K / kHz	0.0673(30)		-0.564(5)	-0.3560(31)	0.84761(7)
κ	0.364	-0.676	-0.098	-0.425	0.148
P_{aa}/ amu Å^2	596.98141(24)	1091.05190(27)	470.56395(16)	578.50627(17)	474.47996(7)
P_{bb}/ amu Å^2	507.83515(24)	530.60960(27)	373.47654(16)	450.93128(17)	363.56545(7)
P_{cc}/ amu Å^2	216.03714(24)	325.62093(27)	268.69609(16)	387.77261(17)	82.93674(7)
RMS/ kHz	1.6	1.5	1.2	1.2	1.2
# of lines	113	144	88	119	144

Table 4.2: Experimental rotational parameters for the BP molecular clusters

Parameters	BP100	BP200	BP300	BP400	BP500
A / MHz	1286.3844(12)	779.4479(8)	492.7743(35)	828.4558(35)	804.7719(15)
B / MHz	1179.7087(9)	541.40873(11)	357.07584(32)	772.8230 (7)	752.6993(12)
C / MHz	720.71527(47)	488.82010(12)	321.31155(25)	721.9246(7)	719.8689(9)
Δ_J / kHz	20.948(24)	0.3663(12)	0.0800(10)	1.514(11)	1.508(16)
Δ_{JK} / kHz	-70.28(10)	-0.439(6)	-0.087(6)	3.61(5)	3.75(8)
Δ_K / kHz	50.72(9)	-3.814(38)	3.40(42)		
δ_J / kHz	-7.081(13)		0.0158(15)	0.139(8)	0.108(11)
δ_K/ kHz	155.90(37)		0.239(35)	-4.95(7)	-4.47(8)
Φ_{JJK}/ Hz[a]	-78.61(40)				
Φ_{JKK}/ Hz[a]	242.2(11)				
Φ_K/ Hz[a]	-164.4(9)		-156(15)		
ϕ_{JJ}/ mHz[b]			-12(6)		
ϕ_{kk}/ mHz[b]			-141(13)		
κ	0.623	-0.638	-0.583	-0.044	-0.227
P_{aa}/ amu Å^2	368.3720(7)	659.4732(7)	981.305(7)	371.9788(27)	372.7437(18)
P_{bb}/ amu Å^2	332.8467(7)	374.4021(7)	591.558(7)	328.0653(27)	329.2994(18)
P_{cc}/ amu Å^2	60.0211(7)	273.9787(7)	434.022(7)	281.9600(27)	298.6786(18)
RMS/ kHz	2.9	2.6	2.9	2.9	2.9
# of lines	30	48	84	23	16

[a, b]The Φ and ϕ are additional distortion constants that depend on higher powers of the angular momentum (i.e. J^6 rather than J^4)

The T-shaped CO_2 dimer structure was observed Within the $VF...CO_2...CO_2$ trimers (Fig. 4.5.a) (See Chapter 2 for more details). Then the atom...atom distances were compared to the newly found BS and BP molecular clusters.

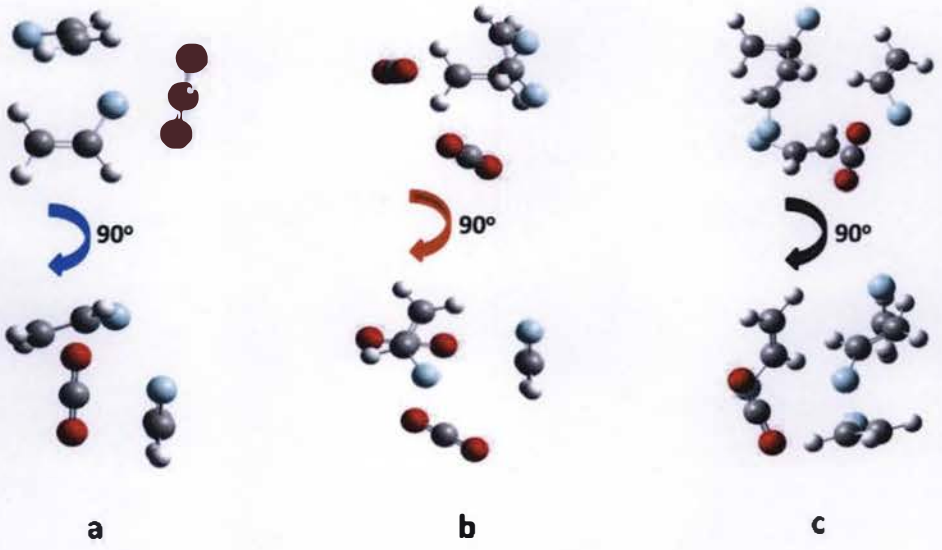

Figure 4.2: Predicted structure for a). BP100 ($(VF)_2...CO_2$), b). BP200 ($(VF)_2...(CO_2)_2$), c). BP300 ($(VF)_4...CO_2$) molecular clusters

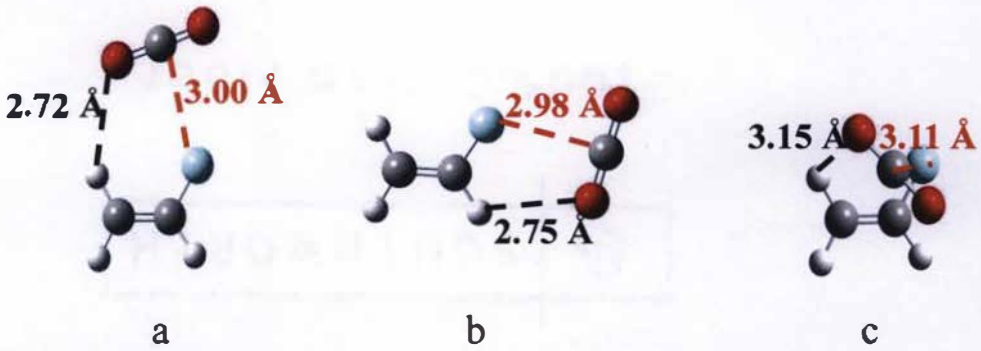

Figure 4.3: Comparison of atom...atom interaction distances in $VF...CO_2$ dimer structures a). Top b). Side c). Above (the distances shown are theoretical and the optimizations were carried out at the MP2/6-311++G(2d,2p) level)[1]

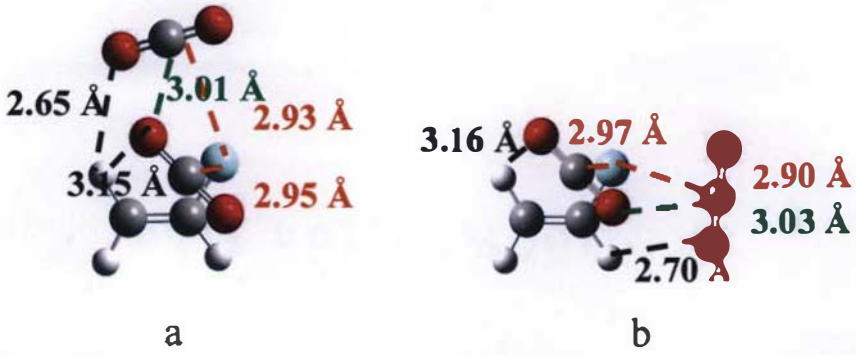

Figure 4.4: Comparison of atom...atom interaction distances in VF...CO_2...CO_2 trimer structures a). Top-Above b). Side-Above (the distances shown are theoretical and the optimizations were carried out at the MP2/6-311++G(2d,2p) level)

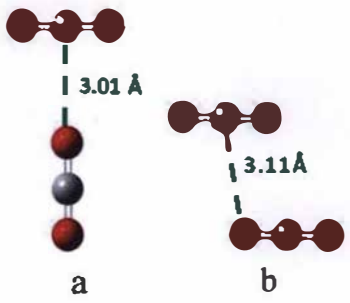

Figure 4.5: Comparison of atom...atom interaction distances in CO_2...CO_2 dimer structures a). T-Shaped b). Slipped parallel (the distances shown are theoretical and the optimizations were carried out at the MP2/6-311++G(2d,2p) level)[2]

Atom...atom distances for BS3 molecular cluster which was found to be VF...$(CO_2)_3$ tetramer, was compared with previously assigned VF...CO_2 dimers, VF...CO_2...CO_2 trimers and theoretical CO_2 trimer distances.[3] C...F and O...H distances were larger within BS3 compared to the VF...CO_2 dimers and VF...CO_2...CO_2 trimers (Fig. 4.6.a). The average increase of the C...F distance was ~ 0.5 Å and the O...H distance was ~0.3 Å. Even though the C...F and O...H distances increased, distinctive C...O interactions were observed between CO_2 molecules in the BS3 molecular cluster (Fig. 4.6.b), because, CO_2 molecules are trying to form $(CO_2)_3$ pinwheel structure (Fig.

4.6.c) within BS3 rather than forming C...F and O...H interactions. Hence, VF...CO_2...CO_2 trimers are trying to form more compact structures than BS3 cluster (VF...$(CO_2)_3$). The C...O distances within BS3 (Fig. 4.6.b) were compared with the theoretical values of the CO_2 trimer (Fig. 4.6.c). These distances were nicely matched with each other and it can be concluded that CO_2 trimer is contained within the BS3 molecular cluster.

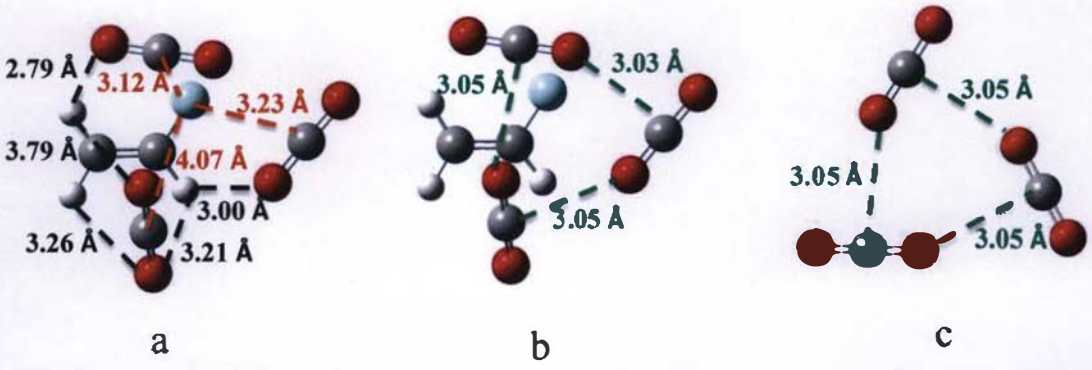

Figure 4.6: Comparison of atom...atom interaction distances in BS3 (VF...$(CO_2)_3$) with CO_2 trimer a). C...F and O...H within BS3 b). C...O within BS3 c). C...O within CO_2 trimer (the distances shown are theoretical and the optimizations were carried out at the ωB97X-D/6-31+G(d,p) level)[3]

Atom...Atom distances within BS200 molecular cluster which was found to be a pentamer with three VF and two CO_2 molecules were compared. A T-shaped CO_2 dimer fragment was observed within the BS200 molecular cluster because the atom...atom distance between C...O is 3.03 Å and it is much closer to the distance in Fig. 4.5.a (3.01 Å). Also, within the BS200 molecular cluster VF trimer structure was observed. Hence, H...F distances in BS200 were compared with the BS500 which was found to be VF trimer (Figs. 4.7.b and 4.7.c). Shortening of H...F distances in BS500 were observed within BS200. That suggests when the larger molecular clusters form the atom...atom

distances get shorter and they form more compact structures with stronger interactions between the molecules.

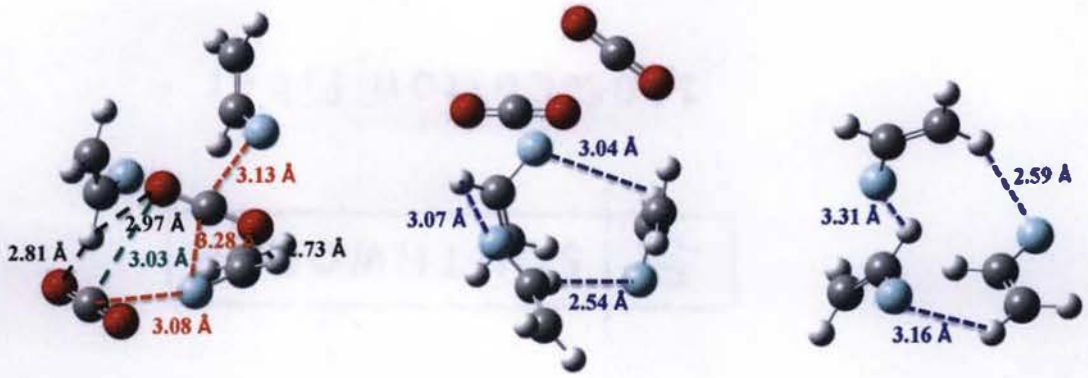

Figure 4.7: Comparison of atom...atom interaction distances in BS200 ($(VF)_3...(CO_2)_2$) with BS500 (VF trimer) a). C...F, O...H and C...O within BS200 b). H...F within BS200 c). H...F within BS500 (the distances shown are theoretical and the optimizations were carried out at the ωB97X-D/6-31+G(d,p) level)

The atom...atom distances in BP molecular clusters were compared with known structures (Fig. 4.8). The shortening of interaction distances were observed for all the structures, collectively. The major difference between BP100 and BP200 is the BP200 has one more CO_2 molecule than BP100. Hence, the overall atom...atom distances are shorter in BP200 compared to BP100 (Fig. 4.8.a and 4.8.b). The C...O distance (3.08 Å) in BP200 molecular cluster (Fig. 4.8.b) is closer to the value of slipped parallel CO_2 dimer structure (3.11 Å) (Fig. 4.5.b), but it does look more like the T-shaped structure. BP100 and BP200 molecular clusters both contain VF dimer itself. VF dimer in BP200 has shorter H...F distances compared to BP100 ($(VF)_2...(CO_2)_2$), because the cluster size is smaller in BP100, and BP200 can form strong interactions within the cluster. The

H...F distances in BP300 are lower than the values in the VF dimer and trimer (Fig. 4.8.c).

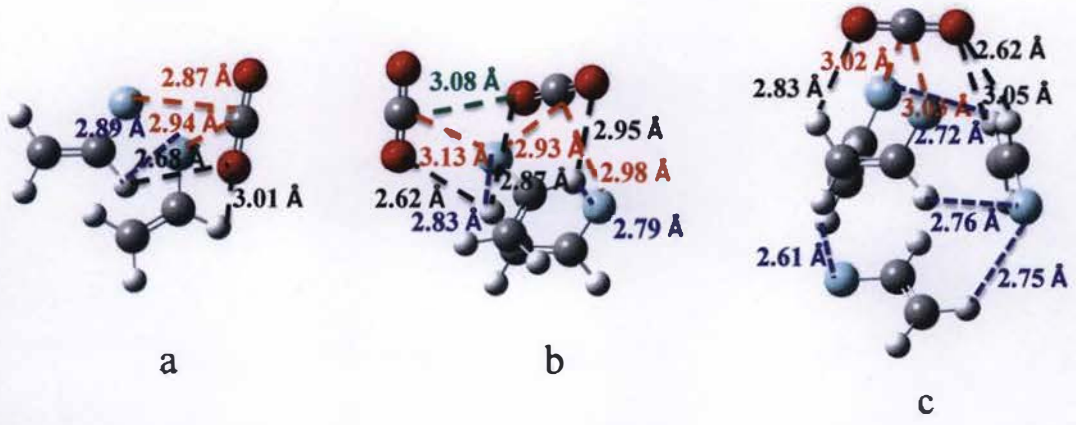

Figure 4.8: Comparison of atom...atom interaction distances in BP molecular clusters a). BP100 ($(VF)_2...CO_2$) b). BP200 ($(VF)_2...(CO_2)_2$) c). BP300 ($(VF)_4...CO_2$) (the distances shown are theoretical and the optimizations were carried out at the ωB97X-D/6-31+G(d,p) level)

When the cluster size becomes larger, they tend to form more compact structures which have stronger interactions. Average interaction distances in pentamers (BS200 ($(VF)_3...(CO_2)_2$) and BP300 ($(VF)_4...CO_2$)) are lower than the tetramers (BS3 ($VF...(CO_2)_3$) and BP200 ($(VF)_2...(CO_2)_2$) and trimers (Top-Above and Side-Above $VF...CO_2...CO_2$ and BP100($(VF)_2...CO_2$)). Hence, the interactions in pentamers are stronger than tetramers and trimers, because of that the pentamers can form more compact structures. Also, when the smaller cluster fragments combined with each other, they can form more compact structures. For instance, BS200 pentamer (Fig. 4.7.a) has three VF molecules and two CO_2 molecules. When the BS200 break down into fragments, VF trimer and CO_2 dimer fragments can be observed. When comparing average interaction distances within VF trimer fragment in BS200 and BS500 (VF trimer), shortening of distance (~ 0.14 Å) within VF trimer fragment was observed.

Fig. 4.9 shows the normalized intensity behavior over different CO_2 concentrations for the VF...CO_2 dimers, VF...CO_2...CO_2 trimers, BS and BP molecular clusters. Studied VF...CO_2 dimers (Figs. 4.3.a and 4.3.b) steep negative slopes, and this observation suggests VF...CO_2 dimers are preferred to have lower CO_2 concentration in order to form clusters. Normalized intensities are higher at the both 1% and 2% CO_2 concentrations for studied VF...CO_2...CO_2 trimers (Figs. 4.4.a and 4.4.b), and this observation suggests that trimer clusters favor more CO_2 molecules. The observation and structure of VF...CO_2...CO_2 are compatible with each other, because structures of trimers are preferred to have more CO_2 than VF in the clusters.

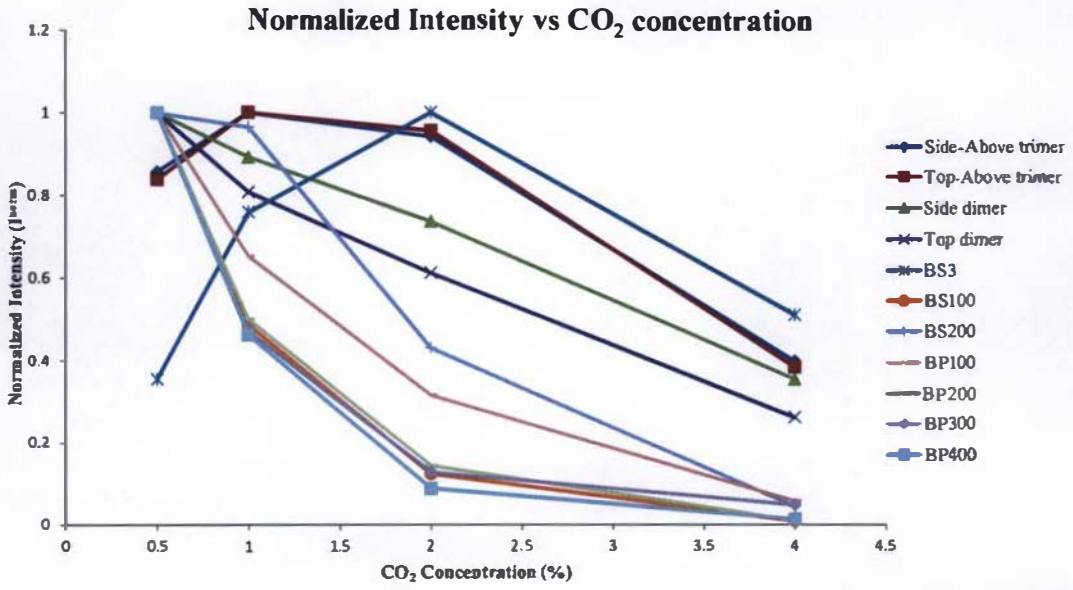

Figure 4.9: The plot of normalized intensity vs CO_2 concentration (%) for the VF...CO_2 dimers, VF...CO_2...CO_2 trimers, BS and BP molecular clusters

The behavior of BS3 and BS200 is quite unique when compared to the other clusters, and the plot in Fig. 4.9, suggests that BS3 cluster should have more CO_2 molecules in it and the predicted structure which is VF...$(CO_2)_3$ (Fig. 4.6.a) proves that.

BS200 should have more VF than CO_2 in the structure, since the normalized intensity is higher at the both 0.5% and 1% CO_2 concentrations, and this observation proves the predicted structure which is $((VF)_3...(CO_2)_2)$ (4.7.a). The normalized intensity variation is quite similar for BS100 and BP clusters which is normalized intensity is higher at the 0.5% concentrations. This observation suggests BP molecular clusters should have more number of VF than CO_2 in molecular formulas, and the above observation was proved by predicted structures for BP100 $((VF)_2...CO_2)$ (Fig. 4.8.a) and BP300 $((VF)_4...CO_2)$ (Fig. 4.8.b), since all the molecular formulas have higher ratio of $VF:CO_2$.

Table 4.3: Possible molecular formulas of BS and BP molecular clusters and their confidence scores

	Formula $VF_n(CO_2)_m$		Confidence Limit[a]
	n	m	
BS3	1	3	9
BS100	3	1	5
BS200	3	2	7
BS400	4	0	3
BS500	3	0	9
BP100	2	1	7
BP200	2	2	7
BP300	4	1	7
BP400[b]	-	-	1
BP500[b]	-	-	1

[a]Confidence limit ranging - 10=has a definite structure, 1=no clue about the structure
[b]Isotopic species which may contain Ne in the molecular cluster

Table 4.3 summarizes the guessed structural composition of the BS and BP molecular clusters and their confidence scores (these confidence scores attempt to give a numerical ranking to the confidence of the assignment). The theoretical parameters of the structures of BS3 and BS500 closely matched with the experimental parameters. Hence, the BS3 and BS500 have higher confidence score compared to other predicted structures.

More structural predictions and optimizations are needed for the structures which have confidence limit lower than 5. In this case, more possible structural guesses are needed to be sure that there are no better matches than the assigned structures. According to the rotational constant values the BS400 could be a VF tetramer and more structural predictions are needed for this molecular cluster.

BP400 could be a structure containing a Ne atom and BP500 would be the ^{22}Ne isotopologue of it. BP400 and BP500 could be tetramers, because the rotational constants are in the range BS3 ($VF...(CO_2)_3$) and BP200 ($(VF)_2...(CO_2)_2$) which were predicted to be tetramer structures (Tables 4.1 and 4.2). For instance, the *A* rotational constant of BP200 ($(VF)_2...(CO_2)_2$) (779.4479 MHz) is closer to the BP400 (828.4558 MHz) and BP500 (804.7719 MHz) values. There are a few possible structural combinations for BP400 and BP500 such as, $VF...(CO_2)_2...Ne$, $(VF)_2...CO_2...Ne$ and $VF...CO_2...Ne_2$.

Fig. 4.10 shows the MathCAD plot of the average concentration (%) vs area with black circled area in the plot. These black circles show the other regions that should be looked at to identify additional molecular clusters. Hence, there are many more clusters remaining in the original scan to be extracted and assigned.

A spectrum for VF...VF dimer was also extracted from the VF-only scan and it was completely analyzed to determine the structure of $(VF)_2$.[4] Also the microwave spectrum for the VF...Ne dimer was identified and we found a matching theoretical structure for this cluster (for more details see Appendix II).

This study shows how chirped-pulse Fourier-transform microwave spectroscopy was used as an analytical tool to find molecular clusters and the structures for them. Furthermore, continual development and refinement methods to find good structural

matches for the assigned spectra are needed. Also, there is a need to set threshold values for the theoretical structural parameters. Developing some statistical measures of the "goodness" or "quality" of agreement between a predicted structure's properties and experimental observations is needed, since there are lots of possible predicted structural matches for the unknown molecular clusters.

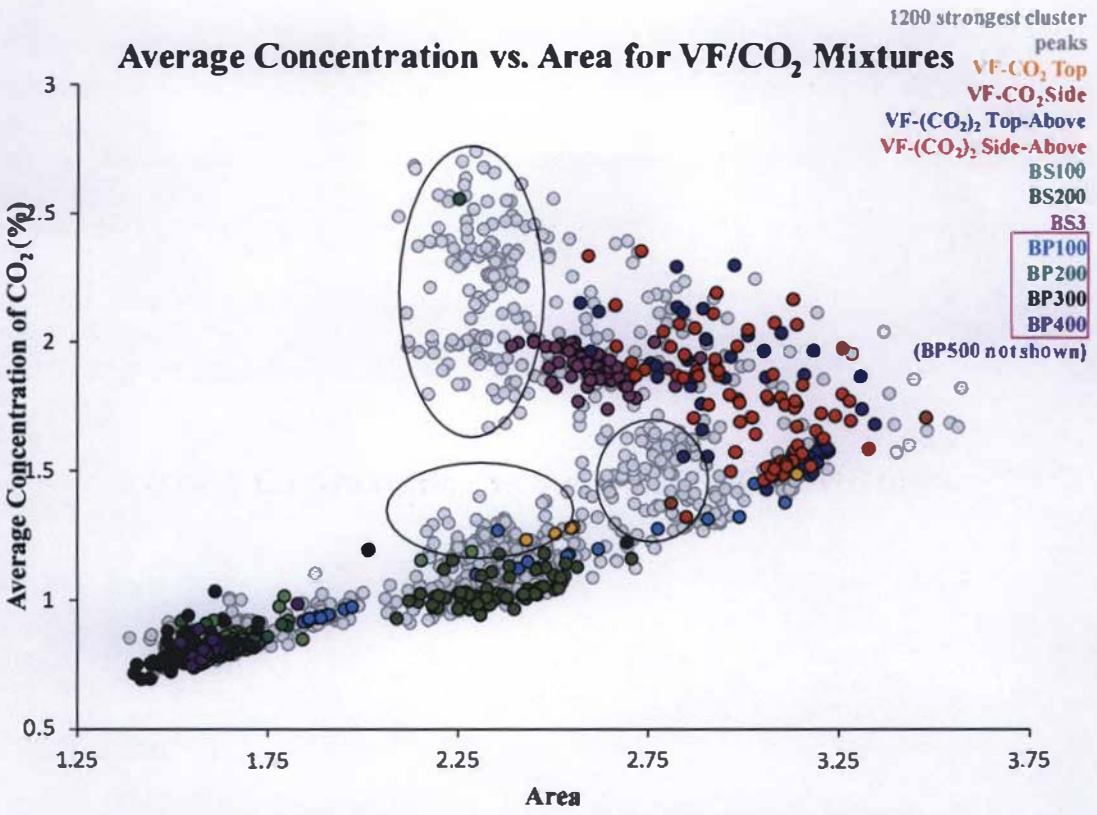

Figure 4.10: The MathCAD plot of the average concentration (%) vs area. The black circled area in the plot shows the other regions that should be paid attention to, to identify additional molecular clusters

4. III. References

[1] C. L. Christenholz, R. E. Dorris, R. A. Peebles, S. A. Peebles, Characterization of Two isomers of the Vinyl Fluoride—Carbon Dioxide complex. *J. Phys. Chem. A* **2016**, 120, 247-253.

[2] K. W. Jucks, Z. S. Huang, D. Dayton, R. E. Miller, The structure of the carbon dioxide dimer from near infrared spectroscopy. *J. Chem. Phys.* **1987**, 86, 4341.

[3] M. J. Weida, D. J. Nesbitt, Geometric isomerism in clusters: High resolution infrared spectroscopy of a noncyclic CO_2 trimer. *J. Chem. Phys.* **1996**, 105, 10210-10223.

[4] M. A. Martinez, P. B. Kannangara, S. A. Peebles, R. A. Peebles, in preparation for *J. Mol. Spectrosc.*(**2019**)

Appendix I

Measured frequencies for $VF+CO_2$ and VF-only molecular clusters

Table I.1: Side-Above VF...CO_2...CO_2 trimer

Quantum numbers						ν_{obs} (MHz)	ν_{calc} (MHz)	ν_{obs}- ν_{calc} (MHz)
J'	K_a'	K_c'	J''	K_a''	K_c''			
5	3	3	5	2	3	2075.6095	2075.6097	-0.0002
3	1	2	3	0	3	2076.2784	2076.2753	0.0031
5	2	3	5	2	4	2215.1346	2215.1366	-0.0020
1	1	1	0	0	0	2446.1229	2446.1233	-0.0004
5	3	2	5	2	3	2601.8679	2601.8683	-0.0004
2	2	1	2	1	2	2623.6427	2623.643	-0.0003
5	2	3	5	1	4	2644.2555	2644.2566	-0.0012
6	3	3	6	2	4	2674.0346	2674.0334	0.0011
4	3	2	4	2	2	2684.2436	2684.2437	-0.0001
2	2	0	2	1	2	2730.1342	2730.1326	0.0016
1	1	0	0	0	0	2770.1011	2770.1018	-0.0007
4	3	1	4	2	2	2836.2673	2836.2681	-0.0008
7	4	4	7	3	4	3027.2950	3027.2953	-0.0003
4	1	3	4	1	4	3087.4889	3087.4922	-0.0034
2	0	2	1	1	1	3133.9584	3133.9577	0.0007
3	3	1	3	2	1	3147.5034	3147.5036	-0.0002
4	1	3	4	0	4	3147.9866	3147.9864	0.0002
3	2	2	3	1	3	3168.0478	3168.0468	0.0011
3	3	0	3	2	1	3170.8455	3170.8453	0.0002
7	3	4	7	2	5	3177.0375	3177.0378	-0.0003
3	2	2	3	0	3	3323.8792	3323.8821	-0.0029
8	4	4	8	3	5	3409.6868	3409.6897	-0.0030
2	1	2	1	1	1	3467.0650	3467.0665	-0.0015
6	2	4	6	2	5	3487.4949	3487.4926	0.0023
7	4	3	7	3	4	3549.2272	3549.2282	-0.0009
3	3	1	3	2	2	3621.1147	3621.1153	-0.0006
3	2	1	3	1	3	3641.6546	3641.6585	-0.0039
3	3	0	3	2	2	3644.4584	3644.4571	0.0013
6	2	4	6	1	5	3679.9291	3679.9311	-0.0019
2	0	2	1	0	1	3684.5443	3684.5451	-0.0008
6	4	3	6	3	3	3797.6160	3797.6178	-0.0018
4	3	2	4	2	3	3866.9103	3866.9114	-0.0011
4	2	3	4	1	4	3891.6142	3891.6140	0.0001
4	2	3	4	0	4	3952.1068	3952.1082	-0.0013
6	4	2	6	3	3	3963.1614	3963.1622	-0.0008
3	0	3	2	1	1	4014.3130	4014.3111	0.0019
2	1	2	1	0	1	4017.6540	4017.6539	0.0001

Quantum numbers						ν_{obs} (MHz)	ν_{calc} (MHz)	ν_{obs}- ν_{calc} (MHz)
J'	K_a'	K_c'	J''	K_a''	K_c''			
4	3	1	4	2	3	4018.9353	4018.9358	-0.0005
2	1	1	1	1	0	4115.0057	4115.0057	-0.0004
8	3	5	8	2	6	4129.5341	4129.5342	-0.0001
5	3	3	5	2	4	4290.7459	4290.7464	-0.0005
5	1	4	5	1	5	4332.1101	4332.1095	0.0006
3	1	2	2	2	0	4332.3715	4332.3717	-0.0001
5	1	4	5	0	5	4353.0879	4353.0879	-0.0000
5	4	2	5	3	2	4371.7495	4371.7486	0.0009
5	4	1	5	3	2	4407.8617	4407.8611	0.0007
3	1	2	2	2	1	4438.8615	4438.8613	0.0002
5	1	5	4	2	3	4481.4359	4481.4347	0.0012
4	3	2	4	1	3	4671.0347	4671.0332	0.0015
4	4	1	4	3	1	4701.1953	4701.1954	-0.0001
4	4	0	4	3	1	4705.4001	4705.4000	0.0001
5	3	3	5	1	4	4719.8681	4719.8664	0.0017
5	2	4	5	1	5	4761.2288	4761.2295	-0.0007
5	2	4	5	0	5	4782.2080	4782.2079	0.0001
4	0	4	3	1	2	4792.2345	4792.2384	-0.0039
5	3	2	5	2	4	4817.0040	4817.0049	-0.0009
4	4	1	4	3	2	4853.2186	4853.2198	-0.0012
4	4	0	4	3	2	4857.4256	4857.4244	0.0012
7	2	5	7	2	6	4860.8808	4860.8807	0.0001
5	4	2	5	3	3	4898.0079	4898.0071	0.0008
6	3	4	6	2	5	4904.6871	4904.6875	-0.0004
5	4	1	5	3	3	4934.1202	4934.1196	0.0006
7	2	5	7	1	6	4936.9598	4936.959	0.0008
8	5	4	8	4	4	4978.8671	4978.8643	0.0028
3	0	3	2	1	2	4986.2287	4986.2289	-0.0002
2	1	1	1	0	1	4989.5716	4989.5717	-0.0001
4	2	2	3	3	0	5034.9529	5034.9504	0.0024
6	4	3	6	3	4	5054.4563	5054.4563	0.0000
4	2	2	3	3	1	5058.2935	5058.2922	0.0013
4	2	2	4	1	4	5074.2826	5074.2817	0.0009
6	3	4	6	1	5	5097.1272	5097.1261	0.0012
3	1	3	2	1	2	5142.0643	5142.0643	0.0000
6	1	6	5	2	4	5194.6140	5194.6130	0.0010
6	4	2	6	3	4	5220.0026	5220.0007	0.0019
5	0	5	4	1	3	5264.5787	5264.578	0.0007
3	0	3	2	0	2	5319.3379	5319.3377	0.0002

Quantum numbers						ν_{obs} (MHz)	ν_{calc} (MHz)	$\nu_{obs}-\nu_{calc}$ (MHz)
J'	K_a'	K_c'	J''	K_a''	K_c''			
7	4	4	7	3	5	5374.7331	5374.7327	0.0004
5	2	4	4	3	2	5375.7565	5375.7527	0.0037
3	1	3	2	0	2	5475.1731	5475.1731	0.0000
6	1	5	6	1	6	5538.2122	5538.2146	-0.0023
6	1	5	6	0	6	5545.0048	5545.0036	0.0012
7	5	2	7	4	3	5657.8480	5657.8482	-0.0002
3	2	2	2	2	1	5686.4678	5686.4681	-0.0002
7	3	5	7	2	6	5690.4810	5690.4811	-0.0001
6	2	5	6	1	6	5730.6529	5730.6531	-0.0002
6	2	5	6	0	6	5737.4448	5737.4421	0.0027
7	3	5	7	1	6	5766.5612	5766.5594	0.0018
2	2	1	1	1	0	5766.7310	5766.7309	0.0001
2	2	0	1	1	0	5873.2208	5873.2205	0.0003
7	4	3	7	3	5	5896.6650	5896.6656	-0.0006
6	5	2	6	4	2	5985.0774	5985.0776	-0.0002
6	5	1	6	4	2	5992.3192	5992.3184	0.0009
3	2	1	2	2	0	6053.5894	6053.5902	-0.0008
3	1	2	2	1	1	6090.5861	6090.5865	-0.0004
2	2	1	1	1	1	6090.7098	6090.7095	0.0004
6	2	5	5	3	2	6108.2627	6108.2612	0.0016
7	5	3	7	4	4	6138.8498	6138.8506	-0.0008
6	5	2	6	4	3	6150.6228	6150.6220	0.0008
6	5	1	6	4	3	6157.8651	6157.8628	0.0023
5	5	1	5	4	1	6160.9243	6160.9233	0.0010
5	5	1	5	4	2	6197.0356	6197.0358	-0.0003
2	2	0	1	1	1	6197.1994	6197.1991	0.0003
5	5	0	5	4	2	6197.7197	6197.7183	0.0014
4	1	3	3	2	1	6219.0057	6219.0063	-0.0005
6	3	4	5	4	1	6605.0878	6605.0876	0.0002
6	2	5	5	3	3	6634.5182	6634.5197	-0.0015
6	3	4	5	4	2	6641.2012	6641.2001	0.0011
7	1	6	7	1	7	6680.7528	6680.7557	-0.0029
7	1	6	7	0	7	6682.8547	6682.8538	0.0009
4	1	3	3	2	2	6692.6176	6692.6180	-0.0005
4	0	4	3	1	3	6712.6776	6712.6784	-0.0008
2	2	0	1	0	1	6747.7900	6747.7865	0.0035
7	2	6	7	1	7	6756.8328	6756.8340	-0.0012
7	2	6	7	0	7	6758.9331	6758.9321	0.0010
4	1	4	3	1	3	6773.1725	6773.1726	-0.0000

Quantum numbers						ν_{obs} (MHz)	ν_{calc} (MHz)	$\nu_{obs}-\nu_{calc}$ (MHz)
J'	K_a'	K_c'	J''	K_a''	K_c''			
4	0	4	3	0	3	6868.5131	6868.5138	-0.0006
4	1	4	3	0	3	6929.0071	6929.0079	-0.0008
5	2	3	5	1	5	6976.3677	6976.3661	0.0015
3	2	2	2	1	1	7338.1931	7338.1932	-0.0001
3	1	2	2	0	2	7395.6124	7395.6131	-0.0007
7	6	2	7	5	2	7464.3627	7464.3651	-0.0024
7	6	1	7	5	2	7465.6732	7465.6744	-0.0012
4	2	3	3	2	2	7496.7391	7496.7398	-0.0007
7	6	2	7	5	3	7505.2950	7505.2956	-0.0005
7	6	1	7	5	3	7506.6039	7506.6049	-0.0010
6	6	1	6	5	2	7576.9196	7576.9205	-0.0010
6	6	0	6	5	2	7577.0271	7577.0244	0.0027
5	2	3	4	3	2	7590.8888	7590.8894	-0.0006
5	1	4	4	2	2	7630.8758	7630.8765	-0.0007
7	2	6	6	3	4	7652.5028	7652.5050	-0.0022
4	3	2	3	3	1	7742.5351	7742.5359	-0.0008
3	2	1	2	1	1	7811.8047	7811.8050	-0.0003
6	3	3	5	4	1	7861.9276	7861.9261	0.0015
4	3	1	3	3	0	7871.2179	7871.2185	-0.0006
6	3	3	5	4	2	7898.0379	7898.0386	-0.0007
4	1	3	3	1	2	7940.2234	7940.2248	-0.0014

Table 1.2: Top-Above VF...CO_2...CO_2 trimer

Quantum numbers						ν_{obs} (MHz)	ν_{calc} (MHz)	$\nu_{obs}-\nu_{calc}$ (MHz)
J'	K_a'	K_c'	J''	K_a''	K_c''			
1	0	1	0	0	0	2016.7101	2016.7083	0.0018
3	3	0	3	2	1	2262.2083	2262.2095	-0.0012
6	3	3	6	2	4	2311.9083	2311.9085	-0.0002
5	2	3	5	2	4	2398.8181	2398.8197	-0.0016
1	1	1	0	0	0	2399.3584	2399.3573	0.0011
5	2	3	5	1	4	2572.2345	2572.2340	0.0005
3	2	2	3	1	3	2670.0270	2670.0251	0.0019
6	4	2	6	3	3	2678.4890	2678.4877	0.0013
1	1	0	0	0	0	2721.5501	2721.5544	-0.0044
3	3	1	3	2	2	2790.7219	2790.7194	0.0025
8	4	4	8	3	5	2840.9714	2840.9710	0.0004
4	1	3	4	1	4	2980.1975	2980.1969	0.0006

Quantum numbers						ν_{obs} (MHz)	ν_{calc} (MHz)	ν_{obs}- ν_{calc} (MHz)
J'	K_a'	K_c'	J''	K_a''	K_c''			
4	1	3	4	0	4	3002.4305	3002.4306	-0.0001
5	4	1	5	3	2	3063.4017	3063.4006	0.0011
4	3	2	4	2	3	3090.7982	3090.7995	-0.0012
7	3	4	7	2	5	3128.2077	3128.2091	-0.0014
8	5	3	8	4	4	3361.4890	3361.4940	-0.0050
4	2	3	4	1	4	3395.2761	3395.2754	0.0008
4	4	0	4	3	1	3420.3193	3420.3212	-0.0019
2	0	2	1	1	1	3515.8931	3515.8933	-0.0002
5	3	3	5	2	4	3584.4424	3584.4432	-0.0008
6	2	4	6	2	5	3599.6416	3599.6424	-0.0009
9	4	5	9	3	6	3644.4584	3644.4579	0.0005
4	4	1	4	3	2	3652.3376	3652.3412	-0.0036
6	2	4	6	1	5	3659.8609	3659.8619	-0.0010
2	1	2	1	1	1	3711.1991	3711.1988	0.0004
5	4	2	5	3	3	3748.8173	3748.8174	-0.0001
5	3	3	5	1	4	3757.8588	3757.8575	0.0013
2	0	2	1	0	1	3898.5408	3898.5424	-0.0015
6	4	3	6	3	4	4000.4495	4000.4488	0.0007
2	1	2	1	0	1	4093.8471	4093.8478	-0.0007
5	2	4	5	1	5	4240.8501	4240.8520	-0.0019
5	2	4	5	0	5	4246.9510	4246.9494	0.0015
6	3	4	6	2	5	4261.3225	4261.3227	-0.0002
8	3	5	8	2	6	4263.0070	4263.0049	0.0021
6	5	1	6	4	2	4292.1270	4292.1237	0.0033
6	3	4	6	1	5	4321.5424	4321.5422	0.0002
2	1	1	1	1	0	4355.5641	4355.5641	-0.0000
7	4	4	7	3	5	4446.7286	4446.7281	0.0005
5	5	0	5	4	1	4549.0484	4549.0514	-0.0029
6	5	2	6	4	3	4599.8193	4599.8188	0.0005
5	5	1	5	4	2	4624.1494	4624.1503	-0.0008
7	5	3	7	4	4	4658.5347	4658.5315	0.0032
7	2	5	7	2	6	4779.4693	4779.4692	0.0001
7	2	5	7	1	6	4798.0766	4798.0774	-0.0008
8	5	4	8	4	5	4867.9463	4867.9459	0.0004
2	1	1	1	0	1	5060.4119	5060.4103	0.0016
7	3	5	7	2	6	5077.5570	5077.5575	-0.0005
6	1	5	6	1	6	5093.3117	5093.3119	-0.0002
6	1	5	6	0	6	5094.8791	5094.8770	0.0021
7	3	5	7	1	6	5096.1649	5096.1657	-0.0008

Quantum numbers						ν_{obs} (MHz)	ν_{calc} (MHz)	ν_{obs}- ν_{calc} (MHz)
J'	K_a'	K_c'	J''	K_a''	K_c''			
8	6	2	8	5	3	5145.2688	5145.2665	0.0022
6	2	5	6	1	6	5153.5317	5153.5314	0.0003
6	2	5	6	0	6	5155.0962	5155.0965	-0.0002
3	1	2	2	2	1	5273.8841	5273.8845	-0.0004
3	0	3	2	1	2	5421.7810	5421.7808	0.0002
7	6	1	7	5	2	5462.9030	5462.9027	0.0003
3	1	3	2	1	2	5494.4740	5494.4743	-0.0003
2	2	1	1	1	0	5503.4850	5503.4838	0.0012
8	6	3	8	5	4	5512.5799	5512.5805	-0.0006
7	6	2	7	5	3	5568.5787	5568.5791	-0.0004
3	0	3	2	0	2	5617.0864	5617.0863	0.0001
2	2	0	1	1	0	5638.3076	5638.3066	0.0011
3	1	3	2	0	2	5689.7792	5689.7797	-0.0005
2	2	1	1	1	1	5825.6813	5825.6810	0.0003
2	2	0	1	1	1	5960.5050	5960.5037	0.0013
8	3	6	8	1	7	5983.4739	5983.4773	-0.0033
3	2	2	2	2	1	6050.0171	6050.0172	-0.0001
7	1	6	7	0	7	6077.4592	6077.4569	0.0022
7	2	6	7	1	7	6095.6805	6095.6808	-0.0004
3	1	2	2	1	1	6421.8038	6421.8043	-0.0005
5	2	4	4	3	1	6455.7226	6455.7222	0.0004
3	2	1	2	2	0	6482.8510	6482.8499	0.0011
4	2	2	3	3	1	6508.7253	6508.7254	-0.0001
3	2	2	2	1	1	7197.9363	7197.9369	-0.0006
4	0	4	3	1	3	7209.4587	7209.4586	0.0001
4	1	4	3	1	3	7231.6929	7231.6923	0.0005
4	0	4	3	0	3	7282.1522	7282.1521	0.0001
4	1	4	3	0	3	7304.3861	7304.3858	0.0004
4	1	3	3	2	2	7541.8634	7541.8642	-0.0008
3	1	2	2	0	2	7583.6725	7583.6722	0.0003
3	2	1	2	1	1	7765.5911	7765.5924	-0.0012
4	2	3	3	2	2	7956.9419	7956.9426	-0.0007

Table I.3: BS100 molecular cluster

Quantum numbers						ν_{obs} (MHz)	ν_{calc} (MHz)	ν_{obs}- ν_{calc} (MHz)
J'	K_a'	K_c'	J''	K_a''	K_c''			
2	0	2	1	0	1	2049.2912	2049.2933	-0.0021

Quantum numbers						ν_{obs} (MHz)	ν_{calc} (MHz)	ν_{obs}- ν_{calc} (MHz)
J'	K_a'	K_c'	J''	K_a''	K_c''			
2	1	2	1	0	1	2070.4491	2070.4523	-0.0032
2	1	1	1	1	0	2322.2458	2322.2452	0.0006
2	1	1	1	0	1	2562.9762	2562.9728	0.0034
2	2	0	1	1	0	2660.6811	2660.681	0.0001
3	0	3	2	1	2	2931.3877	2931.3896	-0.0019
3	1	3	2	1	2	2935.2172	2935.2173	-0.0001
3	0	3	2	0	2	2952.5480	2952.5485	-0.0005
3	1	3	2	0	2	2956.3768	2956.3763	0.0005
3	2	2	2	2	1	3237.0954	3237.0948	0.0006
3	1	2	2	1	1	3369.7997	3369.7997	0.0000
3	2	2	2	1	1	3466.7519	3466.7528	-0.0009
3	2	1	2	2	0	3521.6341	3521.6333	0.0008
4	0	4	3	1	3	3856.3295	3856.3322	-0.0027
4	1	4	3	1	3	3856.9020	3856.9026	-0.0006
3	2	1	2	1	1	3860.0686	3860.0691	-0.0005
4	0	4	3	0	3	3860.1573	3860.1599	-0.0026
4	1	4	3	0	3	3860.7304	3860.7303	0.0001
3	1	2	2	0	2	3883.4796	3883.4792	0.0004
3	2	2	2	1	2	3959.2725	3959.2734	-0.0009
3	3	1	2	2	0	3977.1223	3977.1204	0.0019
3	3	0	2	2	0	4035.0477	4035.0471	0.0006
3	3	1	2	2	1	4085.9019	4085.8981	0.0038
3	3	0	2	2	1	4143.8263	4143.8248	0.0015
4	1	3	3	2	2	4196.1474	4196.1469	0.0005
4	2	3	3	2	2	4221.6712	4221.6707	0.0005
4	1	3	3	1	2	4293.1003	4293.1000	0.0003
4	2	3	3	1	2	4318.6252	4318.6238	0.0014
4	3	2	3	3	1	4446.9495	4446.9521	-0.0026
4	2	2	3	2	1	4651.6770	4651.6770	0.0000
4	3	1	3	3	0	4667.4164	4667.4156	0.0008
5	1	5	4	1	4	4772.9502	4772.9474	0.0028
5	0	5	4	0	4	4773.4409	4773.4411	-0.0002
4	3	2	3	2	1	4902.4406	4902.4391	0.0015
4	2	2	3	1	2	5141.9479	5141.9464	0.0015
5	1	4	4	2	3	5158.1976	5158.1982	-0.0006
5	2	4	4	2	3	5163.1734	5163.1734	0.0000

Quantum numbers						ν_{obs} (MHz)	ν_{calc} (MHz)	ν_{obs}- ν_{calc} (MHz)
J'	K_a'	K_c'	J''	K_a''	K_c''			
4	3	1	3	2	1	5180.8314	5180.8294	0.0020
5	1	4	4	1	3	5183.7222	5183.7221	0.0001
5	2	4	4	1	3	5188.6969	5188.6972	-0.0003
4	1	3	3	0	3	5224.0311	5224.0306	0.0005
4	2	3	3	1	3	5245.7250	5245.7268	-0.0018
4	3	2	3	2	2	5295.7561	5295.7554	0.0007
5	2	3	4	3	2	5390.2350	5390.2359	-0.0009
4	4	1	3	3	0	5407.4152	5407.4135	0.0017
4	4	0	3	3	0	5433.3284	5433.3272	0.0012
4	4	1	3	3	1	5465.3421	5465.3402	0.0019
5	3	3	4	3	2	5482.6661	5482.6668	-0.0007
4	4	0	3	3	1	5491.2549	5491.2539	0.0010
4	3	1	3	2	2	5574.1450	5574.1457	-0.0007
5	4	2	4	4	1	5626.9753	5626.9731	0.0022
5	2	3	4	2	2	5640.9982	5640.998	0.0002
4	3	1	3	1	2	5671.0978	5671.0988	-0.0010
5	3	3	4	2	2	5733.4297	5733.4289	0.0008
5	4	1	4	4	0	5770.7497	5770.7488	0.0009
5	3	2	4	3	1	5882.3423	5882.3427	-0.0004
4	2	2	3	0	3	6072.8733	6072.8771	-0.0038
6	1	5	5	2	4	6083.9878	6083.9887	-0.0009
6	2	5	5	2	4	6084.8124	6084.8122	0.0002
6	1	5	5	1	4	6088.9629	6088.9638	-0.0009
6	2	5	5	1	4	6089.7876	6089.7873	0.0003
4	4	1	3	2	2	6314.1349	6314.1436	-0.0087
5	4	2	4	3	1	6366.9714	6366.9710	0.0004
5	3	2	4	2	2	6411.4962	6411.4951	0.0011
6	2	4	5	3	3	6434.8342	6434.8353	-0.0011
6	3	4	5	3	3	6458.3273	6458.3282	-0.0009
5	2	3	4	1	3	6489.8443	6489.8445	-0.0002
6	2	4	5	2	3	6527.2653	6527.2661	-0.0008
5	4	1	4	3	1	6536.6615	6536.6604	0.0011
5	1	4	4	0	4	6547.5947	6547.5928	0.0019
6	3	4	5	2	3	6550.7590		-0.0001
5	2	4	4	1	4	6551.9951	6551.9975	-0.0024
5	3	3	4	2	3	6556.7516	6556.7515	0.0001

Quantum numbers						ν_{obs} (MHz)	ν_{calc} (MHz)	ν_{obs}- ν_{calc} (MHz)
J'	K_a'	K_c'	J''	K_a''	K_c''			
5	4	2	4	3	2	6645.3621	6645.3613	0.0008
6	4	3	5	4	2	6713.6854	6713.6861	-0.0007
6	5	2	5	5	1	6783.3414	6783.3420	-0.0006
5	4	1	4	3	2	6815.0507	6815.0507	0.0000
5	5	1	4	4	0	6826.5175	6826.5185	-0.0010
5	5	0	4	4	0	6836.8654	6836.8654	0.0000
5	5	1	4	4	1	6852.4325	6852.4321	0.0004
6	5	1	5	5	0	6861.6349	6861.6355	-0.0006
5	5	0	4	4	1	6862.7792	6862.7791	0.0001
6	3	3	5	3	2	6963.8852	6963.8841	0.0011
7	1	6	6	2	5	7000.5700	7000.5701	-0.0001
7	2	6	6	2	5	7000.6953	7000.6934	0.0019
7	1	6	6	1	5	7001.3931	7001.3936	-0.0005
7	2	6	6	1	5	7001.5184	7001.5169	0.0015
5	4	1	4	2	2	7065.8128	7065.8128	0.0000
6	4	3	5	3	2	7198.3147	7198.3144	0.0003
5	3	2	4	2	3	7234.8177	7234.8177	0.0000
5	3	2	4	1	3	7260.3411	7260.3415	-0.0004
7	2	5	6	3	4	7389.7048	7389.7069	-0.0021
7	3	5	6	3	4	7394.4546	7394.4560	-0.0014
7	2	5	6	2	4	7413.1983	7413.1999	-0.0016
7	3	5	6	2	4	7417.9496	7417.949	0.0006
7	3	4	6	4	3	7656.4148	7656.4113	0.0035
6	4	2	5	3	2	7707.7014	7707.7015	-0.0001
5	4	2	4	2	3	7719.4471	7719.4460	0.0011
6	3	3	5	2	3	7734.3788	7734.3812	-0.0024
7	4	4	6	4	3	7734.4644	7734.4650	-0.0006
6	2	4	5	1	4	7833.3881	7833.3885	-0.0004
6	5	2	5	4	1	7839.1116	7839.1117	-0.0001
6	3	4	5	2	4	7851.9087	7851.9063	0.0024
6	1	5	5	0	5	7863.1193	7863.1155	0.0038
6	2	5	5	1	5	7863.8626	7863.8623	0.0003
6	4	3	5	3	3	7876.3812	7876.3806	0.0006
7	3	4	6	3	3	7890.8407	7890.8416	-0.0009
7	5	3	6	5	2	7913.8976	7913.8982	-0.0006
7	6	2	6	6	1	7923.6108	7923.6113	-0.0005

Quantum numbers						ν_{obs} (MHz)	ν_{calc} (MHz)	ν_{obs}- ν_{calc} (MHz)
J'	K_a'	K_c'	J''	K_a''	K_c''			
6	5	1	5	4	1	7927.7531	7927.7521	0.0010
5	3	3	4	1	4	7945.5736	7945.5757	-0.0021
7	6	1	6	6	0	7960.5560	7960.5556	0.0004
7	4	4	6	3	3	7968.8950	7968.8953	-0.0003

Table I.4: BS200 molecular cluster

Quantum numbers						ν_{obs} (MHz)	ν_{calc} (MHz)	ν_{obs}- ν_{calc} (MHz)
J'	K_a'	K_c'	J''	K_a''	K_c''			
3	1	2	2	1	1	2068.7937	2068.7921	0.0016
4	0	4	3	1	3	2473.3110	2473.3124	-0.0014
4	1	4	3	1	3	2572.8000	2572.8006	-0.0006
4	0	4	3	0	3	2619.5561	2619.5542	0.0019
4	2	3	3	2	2	2668.8705	2668.8711	-0.0006
4	2	2	3	2	1	2722.7804	2722.7822	-0.0018
4	1	3	3	1	2	2750.2608	2750.2591	0.0017
5	1	5	4	1	4	3207.8143	3207.8139	0.0004
5	0	5	4	0	4	3245.4473	3245.4515	-0.0042
3	3	1	2	2	0	3282.9242	3282.9209	0.0033
5	2	4	4	2	3	3328.7173	3328.7181	-0.0008
5	3	3	4	3	2	3357.5751	3357.5759	-0.0008
5	3	2	4	3	1	3367.5191	3367.5200	-0.0009
5	1	4	4	1	3	3423.3291	3423.3294	-0.0003
5	2	3	4	2	2	3424.8607	3424.8596	0.0011
6	0	6	5	1	5	3803.5238	3803.5220	0.0018
6	1	6	5	1	5	3839.3272	3839.3276	-0.0004
6	0	6	5	0	5	3865.3728	3865.3726	0.0002
4	3	1	3	2	2	3971.1253	3971.1246	0.0007
6	2	5	5	2	4	3983.8805	3983.8806	-0.0001
6	4	3	5	4	2	4029.9674	4029.9667	0.0007
6	3	4	5	3	3	4030.9035	4030.9026	0.0009
6	4	2	5	4	1	4031.1540	4031.1559	-0.0019
6	3	3	5	3	2	4056.1896	4056.1910	-0.0014
6	1	5	5	1	4	4084.5677	4084.5684	-0.0007
6	2	4	5	2	3	4127.5317	4127.5329	-0.0012
7	1	6	6	2	5	4370.9250	4370.9267	-0.0017
6	2	5	5	1	4	4444.7146	4444.7172	-0.0026

Quantum numbers						ν_{obs} (MHz)	ν_{calc} (MHz)	ν_{obs}- ν_{calc} (MHz)
J'	K_a'	K_c'	J''	K_a''	K_c''			
7	0	7	6	1	6	4448.3100	4448.3074	0.0026
7	1	7	6	1	6	4467.9779	4467.9776	0.0003
7	0	7	6	0	6	4484.1127	4484.1130	-0.0003
7	1	7	6	0	6	4503.7835	4503.7831	0.0004
5	3	3	4	2	2	4573.5507	4573.5521	-0.0014
5	3	2	4	2	2	4586.9004	4586.9003	0.0001
7	2	6	6	2	5	4633.8100	4633.8092	0.0008
5	3	2	4	2	3	4669.7735	4669.7734	0.0001
7	3	5	6	3	4	4702.6135	4702.6143	-0.0008
7	4	4	6	4	3	4706.5743	4706.5739	0.0004
7	4	3	6	4	2	4710.4468	4710.4491	-0.0023
7	1	6	6	1	5	4731.0752	4731.0754	-0.0002
7	3	4	6	3	3	4755.0385	4755.0391	-0.0006
7	2	5	6	2	4	4824.3768	4824.3768	0.0000
7	2	6	6	1	5	4993.9587	4993.9580	0.0007
8	0	8	7	1	7	5084.1175	5084.1174	0.0001
8	1	8	7	1	7	5094.5216	5094.5216	0.0000
8	1	7	7	2	6	5099.6623	5099.6640	-0.0017
8	0	8	7	0	7	5103.7881	5103.7875	0.0006
8	1	8	7	0	7	5114.1918	5114.1918	0.0000
5	4	2	4	3	1	5134.5228	5134.5215	0.0013
5	4	1	4	3	2	5138.2256	5138.2273	-0.0017
6	3	4	5	2	3	5179.5944	5179.5951	-0.0007
8	2	7	7	2	6	5278.3002	5278.3006	-0.0004
6	3	4	5	2	4	5358.6108	5358.6097	0.0011
8	1	7	7	1	6	5362.5477	5362.5465	0.0012
8	3	6	7	3	5	5371.2520	5371.2518	0.0002
8	5	4	7	5	3	5375.9273	5375.9256	0.0017
8	5	3	7	5	2	5376.3724	5376.3727	-0.0003
8	4	5	7	4	4	5384.4094	5384.4088	0.0006
8	4	4	7	4	3	5394.6878	5394.6883	-0.0005
6	3	3	5	2	4	5397.2437	5397.2463	-0.0026
8	3	5	7	3	4	5463.5013	5463.4994	0.0019
8	2	6	7	2	5	5511.1132	5511.1127	0.0005
8	2	7	7	1	6	5541.1847	5541.1831	0.0016
9	0	9	8	1	8	5714.3010	5714.3014	-0.0004
9	1	9	8	1	8	5719.6525	5719.6526	-0.0001

Quantum numbers						ν_{obs} (MHz)	ν_{calc} (MHz)	ν_{obs}- ν_{calc} (MHz)
J'	K_a'	K_c'	J''	K_a''	K_c''			
9	0	9	8	0	8	5724.7059	5724.7057	0.0002
9	1	9	8	0	8	5730.058	5730.0569	0.0011
6	4	3	5	3	2	5796.9675	5796.9682	-0.0007
9	1	8	8	2	7	5804.0455	5804.0449	0.0006
6	4	3	5	3	3	5810.3172	5810.3164	0.0008
6	4	2	5	3	3	5811.8095	5811.8073	0.0022
7	3	4	6	2	4	5845.7388	5845.7379	0.0009
7	2	6	6	1	6	5902.2399	5902.2424	-0.0025
9	2	8	8	2	7	5917.5608	5917.5604	0.0004
9	1	8	8	1	7	5982.6814	5982.6815	-0.0001
9	3	7	8	3	6	6035.5003	6035.5006	-0.0003
9	5	5	8	5	4	6053.9444	6053.9422	0.0022
9	5	4	8	5	3	6055.3656	6055.3647	0.0009
9	4	6	8	4	5	6062.6580	6062.6576	0.0004
7	3	5	6	2	5	6077.3409	6077.3434	-0.0025
9	4	5	8	4	4	6085.9946	6085.9943	0.0003
9	2	8	8	1	7	6096.1953	6096.197	-0.0017
9	3	6	8	3	5	6176.8494	6176.8487	0.0007
9	2	7	8	2	6	6184.6826	6184.6806	0.002
8	2	6	7	1	6	6287.2321	6287.2296	0.0025
10	0	10	9	1	9	6341.2109	6341.2107	0.0002
10	1	10	9	1	9	6343.9052	6343.9046	0.0006
10	0	10	9	0	9	6346.5625	6346.5619	0.0006
10	1	10	9	0	9	6349.2564	6349.2558	0.0006
7	4	4	6	3	3	6447.3507	6447.3511	-0.0004
7	4	3	6	3	3	6452.7199	6452.7172	0.0027
8	3	5	7	2	5	6484.8612	6484.8605	0.0007
7	4	4	6	3	4	6485.9856	6485.9877	-0.0021
7	4	3	6	3	4	6491.3551	6491.3538	0.0013
10	2	9	9	2	8	6552.1767	6552.1769	-0.0002
10	1	9	9	1	8	6597.5287	6597.5286	0.0001
10	2	9	9	1	8	6665.6924	6665.6924	0.0000
10	3	8	9	3	7	6694.3550	6694.3551	-0.0001
10	8	2	9	8	1	6709.1622	6709.1622	0.0000
10	6	5	9	6	4	6721.8991	6721.9050	-0.0059
10	6	4	9	6	3	6722.0614	6722.0652	-0.0038
10	5	6	9	5	5	6733.6965	6733.6953	0.0012

Quantum numbers						ν_{obs} (MHz)	ν_{calc} (MHz)	ν_{obs}- ν_{calc} (MHz)
J'	K_a'	K_c'	J''	K_a''	K_c''			
10	5	5	9	5	4	6737.5589	6737.5588	0.0001
10	4	7	9	4	6	6740.1266	6740.1263	0.0003
10	4	6	9	4	5	6786.6315	6786.6310	0.0005
9	3	7	8	2	6	6825.9375	6825.9395	-0.002
6	6	1	5	5	1	6827.6013	6827.6010	0.0003
10	2	8	9	2	7	6842.4578	6842.4580	-0.0002
10	3	7	9	3	6	6887.7426	6887.7414	0.0012
11	0	11	10	1	10	6966.3083	6966.3081	0.0002
11	1	11	10	1	10	6967.6415	6967.6415	0.0000
11	0	11	10	0	10	6969.0017	6969.0020	-0.0003
11	1	11	10	0	10	6970.3356	6970.3354	0.0002
7	5	3	6	4	2	6985.5429	6985.5450	-0.0021
7	5	2	6	4	3	6987.1748	6987.1721	0.0027
11	2	9	10	3	8	6989.8238	6989.8235	0.0003
8	4	5	7	3	4	7076.7208	7076.7209	-0.0001
8	4	4	7	3	4	7092.3674	7092.3664	0.0010
9	2	7	8	1	7	7109.3643	7109.3637	0.0006
8	4	5	7	3	5	7167.7807	7167.7822	-0.0015
11	2	10	10	2	9	7182.9984	7182.9994	-0.0010
8	4	4	7	3	5	7183.4273	7183.4278	-0.0005
11	1	10	10	1	9	7212.0202	7212.0210	-0.0008
11	2	10	10	1	9	7251.1634	7251.1633	0.0001
11	3	9	10	3	8	7347.2168	7347.2177	-0.0009
11	9	2	10	9	1	7379.1681	7379.1652	0.0029
11	6	6	10	6	5	7400.6272	7400.6268	0.0004
11	6	5	10	6	4	7401.1292	7401.1292	0.0000
11	5	7	10	5	6	7414.9004	7414.9007	-0.0003
11	4	8	10	4	7	7415.3818	7415.3775	0.0043
11	5	6	10	5	5	7424.1565	7424.1561	0.0004
11	2	9	10	2	8	7482.9800	7482.9795	0.0005
11	3	8	10	3	7	7589.5206	7589.5184	0.0022
12	0	12	11	1	11	7590.4385	7590.4379	0.0006
12	1	12	11	1	11	7591.0892	7591.0889	0.0003
12	0	12	11	0	11	7591.7715	7591.7714	0.0001
12	1	12	11	0	11	7592.4248	7592.4224	0.0024
8	5	4	7	4	3	7651.0196	7651.0215	-0.0019
12	2	10	11	3	9	7750.2870	7750.2898	-0.0028

Quantum numbers						ν_{obs} (MHz)	ν_{calc} (MHz)	ν_{obs}- ν_{calc} (MHz)
J'	K_a'	K_c'	J''	K_a''	K_c''			
12	2	11	11	2	10	7810.9626	7810.9642	-0.0016
12	1	11	11	1	10	7828.3901	7828.3927	-0.0026
11	3	9	10	2	8	7840.3737	7840.3736	0.0001
12	2	11	11	1	10	7850.1078	7850.1065	0.0013
12	3	10	11	3	9	7993.9436	7993.9471	-0.0035

Table 1.5: BS3 molecular cluster

Quantum numbers						ν_{obs} (MHz)	ν_{calc} (MHz)	ν_{obs}- ν_{calc} (MHz)
J'	K_a'	K_c'	J''	K_a''	K_c''			
2	1	2	1	1	1	2479.9012	2479.9001	0.0011
2	0	2	1	0	1	2529.8102	2529.8115	-0.0013
2	1	1	1	1	0	2649.6356	2649.6367	-0.0011
2	1	1	1	0	1	2837.8614	2837.8581	0.0033
2	2	1	1	1	0	2959.6914	2959.6926	-0.0012
2	2	0	1	1	1	3079.5236	3079.5217	0.0019
3	0	3	2	1	2	3680.8441	3680.8463	-0.0022
3	1	3	2	1	2	3701.0713	3701.0716	-0.0003
3	0	3	2	0	2	3734.2871	3734.2877	-0.0006
3	1	3	2	0	2	3754.5114	3754.5130	-0.0016
3	2	2	2	2	1	3847.1216	3847.1226	-0.0010
3	1	2	2	1	1	3945.7112	3945.7118	-0.0006
3	2	1	2	2	0	3959.9784	3959.9783	0.0001
3	1	2	2	0	2	4253.7601	4253.7584	0.0017
3	2	1	2	1	1	4304.9938	4304.9946	-0.0008
3	2	2	2	1	2	4411.7852	4411.7838	0.0014
3	3	0	2	2	0	4569.8208	4569.8201	0.0007
3	3	1	2	2	1	4594.8183	4594.8181	0.0002
3	3	0	2	2	1	4604.7807	4604.7804	0.0003
4	0	4	3	1	3	4903.8402	4903.8391	0.0011
4	1	4	3	1	3	4910.1291	4910.1288	0.0003
4	0	4	3	0	3	4924.0642	4924.0644	-0.0002
4	1	4	3	0	3	4930.3536	4930.3541	-0.0005
4	1	3	3	2	2	4986.3658	4986.3662	-0.0004
4	2	3	3	2	2	5101.0983	5101.0967	0.0016
4	3	2	3	3	1	5179.0655	5179.0646	0.0009
4	1	3	3	1	2	5197.8331	5197.8330	0.0001
4	3	1	3	3	0	5230.8253	5230.8259	-0.0006

Quantum numbers						ν_{obs} (MHz)	ν_{calc} (MHz)	ν_{obs}- ν_{calc} (MHz)
J'	K_a'	K_c'	J''	K_a''	K_c''			
4	2	2	3	2	1	5304.2029	5304.2015	0.0014
4	2	3	3	1	2	5312.5629	5312.5635	-0.0006
4	2	2	3	1	2	5663.4815	5663.4843	-0.0028
4	1	3	3	0	3	5717.3041	5717.3037	0.0004
4	3	2	3	2	1	5778.9442	5778.9440	0.0002
4	2	3	3	1	3	5811.8088	5811.8089	-0.0001
4	3	1	3	2	1	5840.6679	5840.6677	0.0002
4	3	2	3	2	2	5926.7596	5926.7601	-0.0005
4	3	1	3	2	2	5988.4837	5988.4837	0.0000
5	0	5	4	1	4	6110.3179	6110.3182	-0.0003
5	1	5	4	1	4	6112.0713	6112.0706	0.0007
5	0	5	4	0	4	6116.6074	6116.6080	-0.0006
5	1	5	4	0	4	6118.3610	6118.3604	0.0006
5	2	3	4	3	2	6138.713	6138.7133	-0.0003
4	4	1	3	3	0	6149.5864	6149.5878	-0.0014
4	4	0	3	3	0	6151.9176	6151.9162	0.0014
4	4	1	3	3	1	6159.5501	6159.5501	0.0000
4	4	0	3	3	1	6161.8804	6161.8785	0.0019
4	2	2	3	0	3	6182.9538	6182.9550	-0.0012
4	3	1	3	1	2	6199.9528	6199.9505	0.0023
5	1	4	4	2	3	6286.4607	6286.4607	0.0000
5	2	4	4	2	3	6335.2420	6335.2418	0.0002
5	1	4	4	1	3	6401.1912	6401.1911	0.0001
5	2	4	4	1	3	6449.9723	6449.9722	0.0001
5	3	3	4	3	2	6464.0088	6464.0075	0.0013
5	4	2	4	4	1	6488.2444	6488.2432	0.0012
5	4	1	4	4	0	6505.2493	6505.2500	-0.0007
5	3	2	4	3	1	6598.7230	6598.7226	0.0004
5	2	3	4	2	2	6613.4565	6613.4559	0.0006
5	3	3	4	2	2	6938.7499	6938.7501	-0.0002
5	2	3	4	1	3	7079.1051	7079.1071	-0.0020
5	3	2	4	2	2	7135.1883	7135.1888	-0.0005
5	1	4	4	0	4	7194.4285	7194.4304	-0.0019
5	2	4	4	1	4	7236.9218	7236.9218	0.0000
5	3	3	4	2	3	7289.6700	7289.6709	-0.0009
6	0	6	5	1	5	7310.4642	7310.4658	-0.0016
6	1	6	5	1	5	7310.9233	7310.9224	0.0009
6	0	6	5	0	5	7312.2166	7312.2182	-0.0016
6	1	6	5	0	5	7312.6767	7312.6749	0.0018

Quantum numbers						ν_{obs} (MHz)	ν_{calc} (MHz)	ν_{obs}- ν_{calc} (MHz)
J'	K_a'	K_c'	J''	K_a''	K_c''			
5	4	2	4	3	1	7407.0042	7407.0050	-0.0008
5	4	1	4	3	1	7426.3390	7426.3403	-0.0013
5	4	2	4	3	2	7468.7277	7468.7287	-0.0010
5	3	2	4	2	3	7486.1112	7486.1096	0.0016
5	4	1	4	3	2	7488.0648	7488.0639	0.0009
6	1	5	5	2	4	7535.0971	7535.0970	0.0001
6	2	4	5	3	3	7545.2798	7545.2790	0.0008
6	2	5	5	2	4	7552.3273	7552.3273	0.0000
6	1	5	5	1	4	7583.8776	7583.8781	-0.0005
5	3	2	4	1	3	7600.8389	7600.8401	-0.0012
6	2	5	5	1	4	7601.1089	7601.1085	0.0004
5	5	1	4	4	0	7728.4091	7728.4124	-0.0033
5	5	0	4	4	0	7728.9052	7728.9019	0.0033
6	3	4	5	3	3	7729.6566	7729.6569	-0.0003
5	5	0	4	4	1	7731.2303	7731.2303	0.0000
6	5	2	5	5	1	7786.8628	7786.8619	0.0009
6	5	1	5	5	0	7791.4369	7791.4371	-0.0002
6	4	3	5	4	2	7794.0348	7794.0349	-0.0001
6	4	2	5	4	1	7857.6056	7857.6056	0.0000
6	2	4	5	2	3	7870.5743	7870.5732	0.0011
6	3	3	5	3	2	7961.3059	7961.3058	0.0001

Table I.6: BS400 molecular cluster (VF-only scan)

Quantum numbers						ν_{obs} (MHz)	ν_{calc} (MHz)	ν_{obs}- ν_{calc} (MHz)
J'	K_a'	K_c'	J''	K_a''	K_c''			
3	0	3	2	1	2	2957.4955	2957.4936	0.0019
3	3	1	2	2	0	3516.3363	3516.3354	0.0009
3	3	0	2	2	0	3517.6023	3517.6015	0.0008
3	3	1	2	2	1	3524.2494	3524.2509	-0.0015
3	3	0	2	2	1	3525.5172	3525.5170	0.0002
4	1	3	3	2	1	3866.7662	3866.7694	-0.0032
4	0	4	3	1	3	3963.3713	3963.3746	-0.0033
4	1	4	3	1	3	3978.7843	3978.7852	-0.0009
4	0	4	3	0	3	3995.0880	3995.0886	-0.0006
4	1	4	3	0	3	4010.4980	4010.4992	-0.0012
4	2	3	3	2	2	4049.4579	4049.4587	-0.0008
4	3	2	3	3	1	4068.4631	4068.4632	-0.0001

Quantum numbers						ν_{obs} (MHz)	ν_{calc} (MHz)	ν_{obs}- ν_{calc} (MHz)
J'	K_a'	K_c'	J''	K_a''	K_c''			
4	3	1	3	3	0	4075.7326	4075.7310	0.0016
4	1	3	3	1	2	4099.8720	4099.8718	0.0002
4	2	2	3	2	1	4109.9169	4109.9172	-0.0003
4	2	3	3	1	2	4245.7164	4245.7153	0.0011
4	1	3	3	0	3	4322.8551	4322.8558	-0.0007
4	2	2	3	1	2	4343.0189	4343.0196	-0.0007
4	2	3	3	1	3	4436.9852	4436.9853	-0.0001
4	3	2	3	2	1	4514.0629	4514.0645	-0.0016
4	3	1	3	2	1	4522.5976	4522.5985	-0.0009
4	3	2	3	2	2	4550.9095	4550.9103	-0.0008
4	3	1	3	2	2	4559.4455	4559.4443	0.0012
4	4	1	3	3	0	4725.3994	4725.3951	0.0043
4	4	0	3	3	0	4725.5638	4725.5622	0.0016
4	4	1	3	3	1	4726.6599	4726.6612	-0.0013
4	4	0	3	3	1	4726.8296	4726.8282	0.0014
5	1	4	4	2	2	4859.3145	4859.3150	-0.0005
5	1	4	4	2	3	4956.6203	4956.6194	0.0009
5	0	5	4	1	4	4958.4076	4958.4069	0.0007
5	1	5	4	1	4	4965.0963	4965.0957	0.0006
5	0	5	4	0	4	4973.8171	4973.8175	-0.0004
5	1	5	4	0	4	4980.5085	4980.5062	0.0023
5	2	4	4	2	3	5052.0925	5052.0924	0.0001
5	3	3	4	3	2	5086.2544	5086.2538	0.0006
5	4	2	4	4	1	5087.1077	5087.1048	0.0029
5	4	1	4	4	0	5088.4057	5088.4047	0.0010
5	1	4	4	1	3	5102.4630	5102.4629	0.0001
5	3	2	4	3	1	5109.3070	5109.3063	0.0007
5	2	3	4	2	2	5146.5777	5146.5772	0.0005
5	2	4	4	1	3	5197.9364	5197.9360	0.0004
5	2	3	4	1	3	5389.7262	5389.7251	0.0011
5	1	4	4	0	4	5430.2312	5430.2300	0.0012
5	3	3	4	2	2	5490.4014	5490.4011	0.0003
5	2	4	4	1	4	5510.2932	5510.2925	0.0007
6	2	5	5	3	3	5513.6289	5513.6297	-0.0008
5	3	2	4	2	2	5521.9872	5521.9875	-0.0003
5	3	3	4	2	3	5587.7050	5587.7054	-0.0004
5	4	2	4	3	1	5736.7675	5736.7689	-0.0014
5	4	1	4	3	1	5738.2361	5738.2358	0.0003
5	4	2	4	3	2	5745.3016	5745.3029	-0.0013

Quantum numbers						ν_{obs} (MHz)	ν_{calc} (MHz)	ν_{obs}- ν_{calc} (MHz)
J'	K_a'	K_c'	J''	K_a''	K_c''			
6	2	4	5	3	2	5798.5863	5798.5876	-0.0013
6	2	4	5	3	3	5830.1729	5830.1740	-0.0011
6	0	6	5	1	5	5946.4651	5946.4661	-0.0010
6	1	6	5	1	5	5949.1667	5949.1667	0.0000
6	0	6	5	0	5	5953.1546	5953.1549	-0.0003
6	1	6	5	0	5	5955.8566	5955.8555	0.0011
6	1	5	5	2	4	5994.8173	5994.8153	0.0020
6	2	5	5	2	4	6049.2425	6049.2427	-0.0002
6	1	5	5	1	4	6090.2879	6090.2884	-0.0005
6	3	4	5	3	3	6101.1891	6101.1891	0.0000
6	5	2	5	5	1	6103.7552	6103.7571	-0.0019
6	5	1	5	5	0	6103.9503	6103.9519	-0.0016
6	4	3	5	4	2	6108.7051	6108.7040	0.0011
6	4	2	5	4	1	6114.2546	6114.2546	0.0000
6	2	5	5	1	4	6144.7166	6144.7157	0.0009
6	3	3	5	3	2	6152.3959	6152.3952	0.0007
6	2	4	5	2	3	6173.9981	6173.9979	0.0002
6	3	4	5	2	3	6445.0120	6445.0130	-0.0010
6	2	4	5	1	4	6461.2606	6461.2601	0.0005
6	3	3	5	2	3	6527.8053	6527.8055	-0.0002
6	1	5	5	0	5	6546.7016	6546.7010	0.0006
6	2	5	5	1	5	6594.4397	6594.4395	0.0002
6	3	4	5	2	4	6636.8023	6636.8021	0.0002
6	3	3	5	2	4	6719.5898	6719.5946	-0.0048
6	4	3	5	3	2	6736.1654	6736.1667	-0.0013
6	4	2	5	3	2	6743.1839	6743.1841	-0.0002
6	4	3	5	3	3	6767.7528	6767.7531	-0.0003
6	4	2	5	3	3	6774.7702	6774.7706	-0.0004
6	3	3	5	1	4	6815.0684	6815.0677	0.0007
7	2	5	6	3	3	6834.2041	6834.2039	0.0002
7	2	5	6	3	4	6916.9950	6916.9964	-0.0014
6	2	4	5	0	5	6917.6711	6917.6726	-0.0015
7	0	7	6	1	6	6930.9083	6930.9094	-0.0011
7	1	7	6	1	6	6931.9490	6931.9486	0.0004
7	0	7	6	0	6	6933.6097	6933.6100	-0.0003
7	1	7	6	0	6	6934.6494	6934.6492	0.0002
6	5	2	5	4	1	6946.4715	6946.4722	-0.0007
6	5	1	5	4	1	6946.6888	6946.6870	0.0018
6	5	2	5	4	2	6947.9378	6947.9391	-0.0013

Quantum numbers						ν_{obs} (MHz)	ν_{calc} (MHz)	ν_{obs}- ν_{calc} (MHz)
J'	K_a'	K_c'	J''	K_a''	K_c''			
6	5	1	5	4	2	6948.1544	6948.1539	0.0005
7	2	6	6	2	5	7041.2072	7041.2068	0.0004
7	1	6	6	1	5	7068.1953	7068.1962	-0.0009
7	2	6	6	1	5	7095.6337	7095.6341	-0.0004
7	3	5	6	3	4	7111.4621	7111.4618	0.0003
7	5	3	6	5	2	7125.8296	7125.8267	0.0029
7	5	2	6	5	1	7126.8618	7126.8610	0.0008
7	4	4	6	4	3	7130.5275	7130.5266	0.0009
7	4	3	6	4	2	7147.3772	7147.3769	0.0003
7	2	5	6	2	4	7188.0116	7188.0115	0.0001
7	3	4	6	3	3	7198.7833	7198.7826	0.0007
7	3	5	6	2	4	7382.4756	7382.4769	-0.0013
7	3	4	6	2	4	7552.5908	7552.5902	0.0006
7	2	5	6	1	5	7558.9844	7558.9832	0.0012
7	1	6	6	0	6	7661.7426	7661.7423	0.0003
7	2	6	6	1	6	7686.4797	7686.4796	0.0001
7	3	5	6	2	5	7699.0214	7699.0213	0.0001
7	4	4	6	3	3	7714.2966	7714.2981	-0.0015
7	4	3	6	3	3	7738.1645	7738.1658	-0.0013
7	4	4	6	3	4	7797.0913	7797.0906	0.0007
8	0	8	7	1	7	7913.6908	7913.6902	0.0006
8	1	8	7	1	7	7914.0767	7914.0767	0.0000
8	0	8	7	0	7	7914.7280	7914.7294	-0.0014
8	1	8	7	0	7	7915.1169	7915.1158	0.0011
7	3	4	6	1	5	7923.5622	7923.5619	0.0003
7	5	3	6	4	2	7958.0437	7958.0443	-0.0006
7	5	2	6	4	2	7959.2942	7959.2933	0.0009
7	5	3	6	4	3	7965.0614	7965.0618	-0.0004
7	5	2	6	4	3	7966.3114	7966.3108	0.0006

Table 1.7: BS500 molecular cluster (VF-only scan)

Quantum numbers						ν_{obs} (MHz)	ν_{calc} (MHz)	ν_{obs}- ν_{calc} (MHz)
J'	K_a'	K_c'	J''	K_a''	K_c''			
1	1	0	0	0	0	2038.4985	2038.4975	0.0010
8	5	3	8	4	4	2065.0730	2065.073	0.0000
3	2	2	3	1	3	2127.8665	2127.8658	0.0007
4	4	0	4	3	1	2130.0302	2130.0295	0.0007

Quantum numbers						ν_{obs} (MHz)	ν_{calc} (MHz)	ν_{obs}- ν_{calc} (MHz)
J'	K_a'	K_c'	J''	K_a''	K_c''			
6	3	3	6	2	4	2139.1934	2139.1932	0.0002
7	5	2	7	4	3	2173.2334	2173.2324	0.0010
4	3	2	4	2	3	2323.5217	2323.5207	0.0010
5	2	3	5	1	4	2433.1415	2433.1416	-0.0001
9	5	4	9	4	5	2447.7019	2447.7020	-0.0001
4	4	1	4	3	2	2477.0592	2477.0598	-0.0006
6	5	1	6	4	2	2560.1852	2560.1830	0.0022
2	0	2	1	1	1	2628.8897	2628.8899	-0.0002
5	4	2	5	3	3	2651.1729	2651.1719	0.0010
4	1	3	4	0	4	2671.3730	2671.3723	0.0007
4	3	1	4	2	3	2692.8571	2692.8581	-0.0010
2	1	2	1	1	1	2715.7519	2715.7530	-0.0011
8	4	4	8	3	5	2718.8864	2718.8877	-0.0013
4	2	3	4	1	4	2810.7307	2810.7313	-0.0006
2	0	2	1	0	1	2854.1062	2854.1069	-0.0007
5	3	3	5	2	4	2863.7284	2863.7275	0.0009
5	5	0	5	4	1	2911.4526	2911.4541	-0.0015
2	1	2	1	0	1	2940.9703	2940.9700	0.0003
11	6	5	11	5	6	2947.3415	2947.3427	-0.0012
6	4	3	6	3	4	3014.5596	3014.5593	0.0003
5	5	1	5	4	2	3073.7481	3073.748	0.0001
5	5	0	5	4	2	3080.4030	3080.4036	-0.0006
7	3	4	7	2	5	3086.3594	3086.3589	0.0005
6	5	2	6	4	3	3109.7757	3109.7757	0.0000
5	4	2	5	2	3	3123.3337	3123.3347	-0.0010
6	5	1	6	4	3	3174.0656	3174.0640	0.0016
10	7	3	10	6	4	3283.8832	3283.8816	0.0016
7	5	3	7	4	4	3295.2889	3295.2892	-0.0003
2	1	1	1	1	0	3322.9286	3322.9299	-0.0013
6	2	4	6	2	5	3364.5359	3364.5370	-0.0011
6	2	4	6	1	5	3374.5786	3374.579	-0.0004
7	6	1	7	5	2	3391.6314	3391.6322	-0.0008
5	1	4	5	0	5	3531.1842	3531.1835	0.0007
6	3	4	6	2	5	3547.1536	3547.1538	-0.0002
7	4	4	7	3	5	3567.3480	3567.3483	-0.0003
5	2	4	5	1	5	3571.7975	3571.7986	-0.0011
7	5	2	7	4	4	3600.2543	3600.2542	0.0001
6	4	2	6	3	4	3628.4401	3628.4403	-0.0002
6	6	0	6	5	1	3662.7222	3662.7241	-0.0019

Quantum numbers						ν_{obs} (MHz)	ν_{calc} (MHz)	ν_{obs}- ν_{calc} (MHz)
J'	K_a'	K_c'	J''	K_a''	K_c''			
7	6	2	7	5	3	3674.9238	3674.9228	0.0010
8	5	4	8	4	5	3678.0529	3678.0529	0.0000
8	6	3	8	5	4	3713.1767	3713.1754	0.0013
6	6	1	6	5	2	3725.1546	3725.1565	-0.0019
9	4	5	9	3	6	3740.8426	3740.8415	0.0011
9	7	2	9	6	3	3820.4871	3820.4867	0.0004
7	5	3	7	3	4	3831.4499	3831.4564	-0.0065
2	1	1	1	0	1	3851.7409	3851.7415	-0.0006
9	6	4	9	5	5	3916.1780	3916.1789	-0.0009
3	0	3	2	1	2	3964.5805	3964.5824	-0.0019
3	1	3	2	1	2	3987.4677	3987.4687	-0.0010
2	2	1	1	1	0	3998.5720	3998.5715	0.0005
3	0	3	2	0	2	4051.4441	4051.4455	-0.0014
3	1	3	2	0	2	4074.3311	4074.3318	-0.0007
3	1	2	2	2	1	4155.6533	4155.6517	0.0016
2	2	0	1	1	0	4163.8130	4163.8134	-0.0004
8	7	1	8	6	2	4190.1335	4190.1339	-0.0004
11	8	3	11	7	4	4204.5037	4204.5046	-0.0009
9	7	3	9	6	4	4249.7358	4249.7355	0.0003
9	5	5	9	4	6	4250.3104	4250.3105	-0.0001
7	2	5	7	1	6	4257.3573	4257.3564	0.0009
8	4	5	8	3	6	4261.0055	4261.0055	0.0000
10	7	4	10	6	5	4295.7828	4295.7818	0.0010
2	2	1	1	1	1	4302.1661	4302.1660	0.0001
7	3	5	7	2	6	4310.3543	4310.3543	0.0000
8	7	2	8	6	3	4310.6227	4310.6220	0.0007
10	6	5	10	5	6	4323.6294	4323.6325	-0.0031
11	7	5	11	6	6	4521.3025	4521.3029	-0.0004
3	2	2	2	2	1	4528.9207	4528.9214	-0.0007
10	8	2	10	7	3	4672.9496	4672.9490	0.0006
2	2	0	1	0	1	4692.6249	4692.6250	-0.0001
11	8	4	11	7	5	4804.1996	4804.1991	0.0005
3	1	2	2	1	1	4831.2929	4831.2932	-0.0003
10	8	3	10	7	4	4870.5400	4870.5374	0.0026
9	8	1	9	7	2	4939.2233	4939.2224	0.0009
10	5	6	10	4	7	4958.9869	4958.9858	0.0011
9	3	6	9	2	7	4970.9234	4970.9223	0.0011
9	8	2	9	7	3	4984.0901	4984.0904	-0.0003
3	2	1	2	2	0	5006.4414	5006.4415	-0.0001

Quantum numbers						ν_{obs} (MHz)	ν_{calc} (MHz)	ν_{obs}- ν_{calc} (MHz)
J'	K_a'	K_c'	J''	K_a''	K_c''			
9	4	6	9	3	7	5031.9234	5031.9225	0.0009
9	4	6	9	3	7	5031.9240	5031.9225	0.0015
8	2	6	8	1	7	5091.8369	5091.8354	0.0015
8	3	6	8	2	7	5105.6532	5105.6533	-0.0001
4	1	3	3	2	1	5113.0442	5113.0455	-0.0013
3	2	2	2	1	1	5204.5634	5204.5629	0.0005
4	0	4	3	1	3	5212.3009	5212.3011	-0.0002
4	1	4	3	1	3	5217.2470	5217.2474	-0.0004
5	3	3	4	4	0	5231.4665	5231.4648	0.0017
4	0	4	3	0	3	5235.1865	5235.1873	-0.0008
4	1	4	3	0	3	5240.1342	5240.1337	0.0005
12	5	7	12	4	8	5439.4555	5439.4531	0.0024
6	2	5	5	3	3	5565.0479	5565.0482	-0.0003
12	6	7	12	5	8	5645.3236	5645.3234	0.0002
10	9	1	10	8	2	5658.4490	5658.4511	-0.0021
11	4	7	11	3	8	5674.9255	5674.9259	-0.0004
11	5	7	11	4	8	5740.5036	5740.5043	-0.0007
4	1	3	3	2	2	5755.8074	5755.8075	-0.0001
10	3	7	10	2	8	5816.7511	5816.7506	0.0005
3	1	2	2	0	2	5828.9277	5828.9279	-0.0002
10	4	7	10	3	8	5833.4290	5833.4302	-0.0012
3	2	1	2	1	1	5847.3250	5847.3250	0.0000
4	2	3	3	2	2	5900.1122	5900.1129	-0.0007
3	2	2	2	1	2	6115.3342	6115.3345	-0.0003
4	1	3	3	1	2	6129.0768	6129.0772	-0.0004
4	3	2	3	3	1	6252.5038	6252.5032	0.0006
4	2	3	3	1	2	6273.3834	6273.3826	0.0008
6	3	4	5	4	1	6292.0803	6292.0805	-0.0002
3	3	1	2	2	0	6334.8104	6334.8098	0.0006
6	4	3	5	5	0	6395.1856	6395.1858	-0.0002
3	3	0	2	2	0	6401.7211	6401.7203	0.0008
5	0	5	4	1	4	6428.5953	6428.5958	-0.0005
5	1	5	4	1	4	6429.5600	6429.5576	0.0024
5	0	5	4	0	4	6433.5413	6433.5421	-0.0008
5	1	5	4	0	4	6434.5049	6434.5040	0.0009
3	3	1	2	2	1	6500.0524	6500.0517	0.0007
12	4	8	12	3	9	6531.2709	6531.2718	-0.0009
4	3	1	3	3	0	6554.9297	6554.9301	-0.0004
3	3	0	2	2	1	6566.9632	6566.9623	0.0009

Quantum numbers						ν_{obs} (MHz)	ν_{calc} (MHz)	ν_{obs}- ν_{calc} (MHz)
J'	K_a'	K_c'	J''	K_a''	K_c''			
4	2	2	3	2	1	6681.1315	6681.1316	-0.0001
3	2	1	2	1	2	6758.0970	6758.0965	0.0005
7	3	5	6	4	2	6778.3699	6778.3697	0.0002
3	2	1	2	0	2	6844.9617	6844.9596	0.0021
5	2	3	4	3	1	6889.3297	6889.3315	-0.0018
6	4	2	5	5	1	7015.7212	7015.7225	-0.0013
5	1	4	4	2	3	7149.0475	7149.0480	-0.0005
5	2	4	4	2	3	7190.6244	7190.6249	-0.0005
7	5	2	7	2	5	7222.7787	7222.7803	-0.0016
5	2	3	4	3	2	7258.6682	7258.6689	-0.0007
5	1	4	4	1	3	7293.3533	7293.3533	0.0000
5	2	4	4	1	3	7334.9306	7334.9303	0.0003
6	0	6	5	1	5	7636.5872	7636.5870	0.0002
6	1	6	5	1	5	7636.7649	7636.7622	0.0027
6	0	6	5	0	5	7637.5486	7637.5489	-0.0003
6	1	6	5	0	5	7637.7271	7637.7241	0.0030
4	2	2	3	1	2	7697.1631	7697.1633	-0.0002
5	3	3	4	3	2	7730.8320	7730.8317	0.0003
7	4	4	6	5	1	7785.5318	7785.5350	-0.0032
5	4	2	4	4	1	7904.9443	7904.9438	0.0005
4	1	3	3	0	3	7906.5598	7906.5596	0.0002
6	2	4	5	3	2	7912.9708	7912.9696	0.0012
4	3	1	3	2	1	7950.2089	7950.2090	-0.0001

Table I.8: BP100 molecular cluster

Quantum numbers						ν_{obs} (MHz)	ν_{calc} (MHz)	ν_{obs}- ν_{calc} (MHz)
J'	K_a'	K_c'	J''	K_a''	K_c''			
2	1	2	1	1	1	3341.6873	3341.6835	0.0038
2	0	2	1	0	1	3432.0659	3432.0647	0.0012
2	1	1	1	1	0	4258.8623	4258.8584	0.0039
3	1	3	2	1	2	4826.8299	4826.8301	-0.0002
3	0	3	2	0	2	4841.9809	4841.9812	-0.0003
3	2	2	2	2	1	5700.5122	5700.5071	0.0051
3	1	2	2	1	1	5940.3257	5940.3313	-0.0056
4	1	4	3	1	3	6274.5627	6274.5649	-0.0022
4	0	4	3	0	3	6276.1286	6276.1316	-0.003
3	2	1	2	2	0	6558.5906	6558.5875	0.0031

Quantum numbers						ν_{obs} (MHz)	ν_{calc} (MHz)	ν_{obs}- ν_{calc} (MHz)
J'	K_a'	K_c'	J''	K_a''	K_c''			
4	2	3	3	2	2	7263.0486	7263.0533	-0.0047
4	1	3	3	1	2	7332.8489	7332.8484	0.0005
4	2	2	4	2	3	2383.4898	2383.4955	-0.0057
9	6	4	9	4	5	4514.0293	4514.0229	0.0064
6	2	4	6	2	5	4553.2091	4553.2037	0.0054
6	3	3	6	3	4	3426.2487	3426.2436	0.0051
7	4	3	7	4	4	3280.2892	3280.2845	0.0047
8	5	3	8	5	4	3054.5512	3054.5511	1E-04
4	3	2	4	1	3	2624.2732	2624.2682	0.005
5	3	3	5	1	4	3554.712	3554.717	-0.005
6	3	4	6	1	5	4559.7206	4559.7265	-0.0059
7	3	5	7	1	6	5577.6544	5577.6576	-0.0032
8	3	6	8	1	7	6596.1742	6596.1731	0.0011
4	4	1	4	2	2	2322.1207	2322.1243	-0.0036
6	4	3	6	2	4	3561.3083	3561.3044	0.0039
7	4	4	7	2	5	4541.1534	4541.1619	-0.0085
8	4	5	8	2	6	5556.764	5556.7693	-0.0053
9	6	3	9	6	4	2749.3274	2749.3287	-0.0013
5	5	1	5	3	2	2857.9894	2857.9816	0.0078
8	5	4	8	3	5	4522.8907	4522.8966	-0.0059
9	5	5	9	3	6	5529.9452	5529.9496	-0.0044
10	5	6	10	3	7	6550.529	6550.5307	-0.0017
11	5	7	11	3	8	7570.3292	7570.3333	-0.0041
6	6	1	6	4	2	3554.5798	3554.5829	-0.0031
10	6	5	10	4	6	5498.4965	5498.497	-0.0005
11	6	6	11	4	7	6518.3635	6518.3545	0.009
12	6	7	12	4	8	7540.5531	7540.5563	-0.0032
5	2	3	5	2	4	3507.918	3507.9178	0.0002
4	1	3	4	1	4	3547.581	3547.5808	0.0002
4	2	3	4	0	4	3559.505	3559.5053	-0.0003
5	2	4	5	0	5	4574.4646	4574.4645	0.0001
6	2	5	6	0	6	5592.8624	5592.8586	0.0038
6	1	5	6	1	6	5592.7318	5592.7277	0.0041
7	2	6	7	0	7	6611.1586	6611.1592	-0.0006
5	1	5	4	1	4	7716.3417	7716.3396	0.0021
5	0	5	4	0	4	7716.4783	7716.476	0.0023
12	8	5	12	6	6	5442.3909	5442.3926	-0.0017

Quantum numbers						ν_{obs} (MHz)	ν_{calc} (MHz)	ν_{obs}- ν_{calc} (MHz)
J'	K_a'	K_c'	J''	K_a''	K_c''			
11	7	5	11	5	6	5466.5022	5466.5019	0.0003
7	2	5	7	2	6	5576.8878	5576.8861	0.0017
9	3	6	9	3	7	6575.8525	6575.8503	0.0022
9	3	7	9	1	8	7613.855	7613.8528	0.0022
8	1	7	8	1	8	7629.0843	7629.0867	-0.0024
11	4	7	11	4	8	7570.1293	7570.1249	0.0044
3	2	2	2	1	2	7397.6958	7397.6986	-0.0028

Table I.9: BP200 molecular cluster

Quantum numbers						ν_{obs} (MHz)	ν_{calc} (MHz)	ν_{obs}- ν_{calc} (MHz)
J'	K_a'	K_c'	J''	K_a''	K_c''			
2	1	2	1	1	1	2007.8521	2007.8591	-0.0070
2	0	2	1	0	1	2052.6603	2052.6571	0.0032
2	1	1	1	1	0	2113.0371	2113.0363	0.0008
3	1	3	2	1	2	3007.2121	3007.2127	-0.0006
3	0	3	2	0	2	3060.5620	3060.5615	0.0005
3	2	2	2	2	1	3090.6585	3090.6575	0.0010
3	2	1	2	2	0	3120.7410	3120.7430	-0.0020
3	1	2	2	1	1	3164.2500	3164.2481	0.0019
4	1	4	3	1	3	4002.0207	4002.0237	-0.0030
4	0	4	3	0	3	4051.4331	4051.4325	0.0006
4	2	3	3	2	2	4114.7452	4114.7462	-0.0010
4	3	2	3	3	1	4134.4769	4134.4773	-0.0004
4	3	1	3	3	0	4138.7942	4138.7955	-0.0013
4	2	2	3	2	1	4184.0762	4184.0786	-0.0024
4	1	3	3	1	2	4208.0627	4208.0601	0.0026
5	1	5	4	1	4	4992.1271	4992.1295	-0.0024
5	0	5	4	0	4	5029.4781	5029.4766	0.0015
5	2	4	4	2	3	5133.7085	5133.7076	0.0009
5	4	2	4	4	1	5168.2995	5168.3023	-0.0028
5	4	1	4	4	0	5168.7487	5168.7515	-0.0028
5	3	3	4	3	2	5170.9900	5170.9954	-0.0004
5	3	2	4	3	1	5185.6289	5185.6288	0.0001
5	1	4	4	1	3	5240.4396	5240.4353	0.0043
5	2	3	4	2	2	5254.7420	5254.7429	-0.0009
6	1	6	5	1	5	5978.0543	5978.0570	-0.0027
6	0	6	5	0	5	6002.1903	6002.1895	0.0008

Quantum numbers						ν_{obs} (MHz)	ν_{calc} (MHz)	ν_{obs}- ν_{calc} (MHz)
J'	K_a'	K_c'	J''	K_a''	K_c''			
6	2	5	5	2	4	6146.5686	6146.566	0.0026
6	3	4	5	3	3	6206.6970	6206.6972	-0.0002
6	4	3	5	4	2	6207.0079	6207.0062	0.0017
6	4	2	5	4	1	6208.9918	6208.9927	-0.0009
6	3	3	5	3	2	6243.3886	6243.3873	0.0013
6	1	5	5	1	4	6256.8653	6256.8592	0.0061
6	2	4	5	2	3	6323.4458	6323.4463	-0.0005
7	2	5	6	3	4	6344.1662	6344.1677	-0.0015
7	1	7	6	1	6	6960.7246	6960.7277	-0.0031
7	0	7	6	0	6	6974.7034	6974.7042	-0.0008
5	4	2	4	3	1	7002.2277	7002.2283	-0.0006
7	2	6	6	2	5	7152.7333	7152.7292	0.0041
7	5	2	6	5	1	7239.3190	7239.3192	-0.0002
7	3	5	6	3	4	7239.6880	7239.6892	-0.0012
7	4	4	6	4	3	7247.5801	7247.5802	-0.0001
7	4	3	6	4	2	7254.0127	7254.0104	0.0023
7	1	6	6	1	5	7254.3723	7254.3664	0.0059
7	3	4	6	3	3	7313.9602	7313.9566	0.0036
7	2	5	6	2	4	7382.6906	7382.6910	-0.0004
6	2	4	5	0	5	7814.5202	7814.5235	-0.0033
8	1	8	7	1	7	7941.1205	7941.1248	-0.0043
8	0	8	7	0	7	7948.6492	7948.6514	-0.0022

Table 1.10: BP300 molecular cluster

Quantum numbers						ν_{obs} (MHz)	ν_{calc} (MHz)	ν_{obs}- ν_{calc} (MHz)
J'	K_a'	K_c'	J''	K_a''	K_c''			
3	0	3	2	0	2	2011.5590	2011.5519	0.0071
4	1	4	3	1	3	2631.4150	2631.4182	-0.0032
4	0	4	3	0	3	2660.3581	2660.3558	0.0023
4	2	2	3	2	1	2761.7972	2761.7981	-0.0009
4	1	3	3	1	2	2770.4596	2770.4642	-0.0046
5	1	5	4	1	4	3281.5275	3281.5226	0.0049
5	0	5	4	0	4	3301.4891	3301.4875	0.0016
5	2	4	4	2	3	3378.1921	3378.1956	-0.0035
5	2	4	4	2	3	3378.1922	3378.1956	-0.0034
5	3	3	4	3	2	3407.0027	3407.0055	-0.0028
5	3	2	4	3	1	3420.3925	3420.3871	0.0054

Quantum numbers						ν_{obs} (MHz)	ν_{calc} (MHz)	$\nu_{obs}-\nu_{calc}$ (MHz)
J'	K_a'	K_c'	J''	K_a''	K_c''			
5	1	4	4	1	3	3446.9354	3446.9376	-0.0022
5	2	3	4	2	2	3468.1166	3468.1163	0.0003
6	1	6	5	1	5	3928.8208	3928.8169	0.0039
6	0	6	5	0	5	3940.5466	3940.5432	0.0034
6	2	5	5	2	4	4043.0028	4043.0028	0.0000
6	3	4	5	3	3	4088.7743	4088.7739	0.0004
6	4	3	5	4	2	4090.6368	4090.6346	0.0022
6	4	2	5	4	1	4092.7832	4092.7823	0.0009
6	1	5	5	1	4	4110.5854	4110.5885	-0.0031
6	3	3	5	3	2	4121.5073	4121.5061	0.0012
6	2	4	5	2	3	4170.5652	4170.5667	-0.0015
7	1	7	6	1	6	4574.0993	4574.0953	0.0040
7	0	7	6	0	6	4580.2904	4580.2902	0.0002
7	1	7	6	0	6	4585.9612	4585.9620	-0.0008
7	2	6	6	2	5	4702.8149	4702.8148	0.0001
7	1	6	6	1	5	4760.4524	4760.4535	-0.0011
7	3	5	6	3	4	4767.8888	4767.8881	0.0007
7	4	4	6	4	3	4776.8646	4776.8626	0.002
7	4	3	6	4	2	4783.7322	4783.7327	-0.0005
7	3	4	6	3	3	4831.5619	4831.5604	0.0015
7	2	5	6	2	4	4864.2518	4864.2518	0.0000
8	1	8	7	1	7	5218.0979	5218.0958	0.0021
8	0	8	7	0	7	5221.1487	5221.1527	-0.0040
8	2	7	7	2	6	5357.8260	5357.8271	-0.0011
8	1	7	7	1	6	5400.1348	5400.1351	-0.0003
8	3	6	7	3	5	5442.9524	5442.9504	0.0020
8	5	4	7	5	3	5457.2911	5457.2846	0.0065
8	5	3	7	5	2	5458.3457	5458.3461	-0.0004
8	4	4	7	4	3	5481.1315	5481.1290	0.0025
9	0	9	8	0	8	5862.8036	5862.8041	-0.0005
9	2	8	8	2	7	6008.6910	6008.6932	-0.0022
9	1	8	8	1	7	6035.8435	6035.8456	-0.0021
9	3	7	8	3	6	6112.9389	6112.9386	0.0003
9	3	7	8	3	6	6112.9389	6112.9386	0.0003
9	6	4	8	6	3	6136.4962	6136.5031	-0.0069
9	6	3	8	6	2	6136.6398	6136.6398	0.0000
9	5	5	8	5	4	6145.3513	6145.3520	-0.0007
9	5	5	8	5	4	6145.3513	6145.3520	-0.0007
9	5	4	8	5	3	6148.6723	6148.6713	0.0010

Quantum numbers						ν_{obs} (MHz)	ν_{calc} (MHz)	ν_{obs}- ν_{calc} (MHz)
J'	K_a'	K_c'	J''	K_a''	K_c''			
9	5	4	8	5	3	6148.6723	6148.6713	0.0010
9	4	6	8	4	5	6149.1607	6149.1624	-0.0017
9	4	6	8	4	5	6149.1607	6149.1624	-0.0017
9	4	5	8	4	4	6187.2565	6187.2533	0.0032
9	2	7	8	2	6	6212.9137	6212.9147	-0.0010
10	0	10	9	1	9	6503.7222	6503.7238	-0.0016
10	1	10	9	1	9	6504.2391	6504.2400	-0.0009
10	0	10	9	0	9	6504.8959	6504.8976	-0.0017
10	1	10	9	0	9	6505.4060	6505.4139	-0.0079
10	2	9	9	2	8	6656.3470	6656.3480	-0.0010
10	1	9	9	1	8	6672.0602	6672.0623	-0.0021
10	3	8	9	3	7	6777.3386	6777.3356	0.0030
10	6	5	9	6	4	6823.9443	6823.9477	-0.0034
10	6	4	9	6	3	6824.4467	6824.4469	-0.0002
10	4	7	9	4	6	6832.3984	6832.4041	-0.0057
10	5	6	9	5	5	6834.6226	6834.6258	-0.0032
10	5	5	9	5	4	6843.4138	6843.4096	0.0042
10	2	8	9	2	7	6864.3262	6864.3260	0.0002
11	1	11	10	1	10	7146.9179	7146.9182	-0.0003
11	0	11	10	0	10	7147.2104	7147.2110	-0.0006
11	2	10	10	2	9	7301.7679	7301.7651	0.0028
11	1	10	10	1	9	7310.2174	7310.2154	0.0020
11	3	9	10	3	8	7436.1836	7436.1800	0.0036
11	2	9	10	2	8	7503.1419	7503.1408	0.0011
11	4	8	10	4	7	7511.6765	7511.6832	-0.0067
11	6	6	10	6	5	7513.0404	7513.0406	-0.0002
11	6	5	10	6	4	7514.5827	7514.5802	0.0025
11	5	6	10	5	5	7544.5662	7544.5605	0.0057
11	4	7	10	4	6	7623.3833	7623.3906	-0.0073
12	1	12	11	1	11	7789.4976	7789.4953	0.0023
12	0	12	11	0	11	7789.6231	7789.6233	-0.0002
16	3	14	15	4	11	7851.5136	7851.5142	-0.0006
12	2	11	11	2	10	7945.7719	7945.7670	0.0049
12	1	11	11	1	10	7950.0854	7950.0811	0.0043

Table 1.11: BP400 molecular cluster

Quantum numbers						ν_{obs} (MHz)	ν_{calc} (MHz)	ν_{obs}- ν_{calc} (MHz)
J'	K_a'	K_c'	J''	K_a''	K_c''			
2	1	2	1	1	1	2938.5193	2938.5184	0.0009
2	0	2	1	0	1	2966.9985	2966.9972	0.0013
2	1	1	1	1	0	3040.3514	3040.3462	0.0052
3	1	3	2	1	2	4395.7024	4395.7027	-0.0003
3	0	3	2	0	2	4413.3032	4413.3039	-0.0007
3	2	2	2	2	1	4483.9923	4483.9926	-0.0003
3	1	2	2	1	1	4541.4716	4541.4700	0.0016
3	2	1	2	2	0	4554.7630	4554.7680	-0.0005
4	1	4	3	1	3	5845.4781	5845.4795	-0.0001
4	0	4	3	0	3	5852.2612	5852.2626	-0.0001
4	2	3	3	2	2	5960.0469	5960.0449	0.0002
4	3	2	3	3	1	6009.6328	6009.6360	-0.0003
4	1	3	3	1	2	6013.8518	6013.8499	0.0019
4	2	2	3	2	1	6084.6113	6084.6119	-0.0006
5	1	5	4	1	4	7291.1238	7291.1247	-0.0009
5	0	5	4	0	4	7293.1633	7293.1638	-0.0005
5	2	4	4	2	3	7423.5103	7423.5053	0.0005
5	1	4	4	1	3	7457.2498	7457.2476	0.0022
5	3	3	4	3	2	7504.0486	7504.0529	-0.0004
5	4	2	4	4	1	7521.7326	7521.7339	-0.0001
5	4	1	4	4	0	7534.4559	7534.4525	0.0034
5	2	3	4	2	2	7590.5979	7590.6038	-0.0006
5	3	2	4	3	1	7591.9790	7591.9750	0.0004

Table 1.12: BP500 molecular cluster

Quantum numbers						ν_{obs} (MHz)	ν_{calc} (MHz)	ν_{obs}- ν_{calc} (MHz)
J'	K_a'	K_c'	J''	K_a''	K_c''			
3	1	3	2	1	2	4362.0300	4362.0304	-0.0004
3	0	3	2	0	2	4378.8756	4378.8773	-0.0017
3	1	2	2	1	1	4457.9087	4457.9074	0.0013
4	1	4	3	1	3	5807.1944	5807.1971	-0.0027
4	0	4	3	0	3	5815.8162	5815.8150	0.0012
4	3	1	3	3	0	5921.0400	5921.0363	0.0037
4	1	3	3	1	2	5924.1084	5924.1062	0.0022
4	2	2	3	2	1	5954.1458	5954.1480	-0.0022
4	3	1	3	2	1	6222.0972	6222.0984	-0.0012

Quantum numbers						ν_{obs} (MHz)	ν_{calc} (MHz)	ν_{obs}- ν_{calc} (MHz)
J'	K_a'	K_c'	J''	K_a''	K_c''			
5	1	5	4	1	4	7249.1210	7249.1228	-0.0018
5	0	5	4	0	4	7252.5268	7252.5233	0.0035
5	2	4	4	2	3	7336.7271	7336.7340	-0.0069
5	1	4	4	1	3	7372.0818	7372.0780	0.0038
5	3	3	4	3	2	7381.1999	7381.1977	0.0022
5	3	2	4	3	1	7422.2840	7422.2875	-0.0035
5	2	3	4	2	2	7442.4726	7442.4703	0.0023

Appendix II

VF…Ne dimer study

II. I). VF...Ne dimer

Initially several high intensity frequencies that were not assigned from VF+CO_2 and VF-only scans were found. Then the Stark effect measurements were collected for them and predicted related frequencies in line and assigned them (Table II.1).[1,2] A spectrum related to the VF...Ne dimer molecular cluster was extracted from the VF-only scan (see 3. II. A for more details) obtained from the CP-FTMW spectrometer at the University of Virginia and also with the help of Balle-Flygare FTMW spectrometer at the Eastern Illinois University.[3,4,5]

Table II.1: Experimental and Calculated rotational transition frequencies and their differences for the VF...Ne cluster

Quantum numbers						Experimental frequencies (MHz)	Calculated frequencies (MHz)	Expt-Calc Frequencies (MHz)
J'	K_a'	K_c'	J''	K_a''	K_c''			
1	0	1	0	0	0	5147.5534	5147.5518	0.0016
3	0	3	2	1	2	7544.7198	7544.7227	-0.0029
2	1	2	1	1	1	9725.0600	9725.0613	-0.0013
2	0	2	1	0	1	10266.7500	10266.7470	0.0030
2	1	1	1	1	0	10810.0200	10810.0200	0.0000
1	1	1	0	0	0	13473.9810	13473.9820	-0.0010
3	1	3	2	1	2	14566.4400	14566.4400	0.0000
3	0	3	2	0	2	15329.4700	15329.4670	0.0030
3	1	2	2	1	1	16189.0000	16189.0000	0.0000
2	1	2	1	0	1	18051.4900	18051.4920	-0.0020

A possible structure for assigned VF...Ne cluster was found with the ABCluster force field approach (Fig. II.1).[6,7] The spectroscopic parameters of the assigned VF...Ne cluster and the predicted structure has been compared in Table II.2. When comparing the P_{cc} of these structures, both values are very small showing there is low mass distribution along the c axis of the molecule. Even though the P_{cc} agree, there are several mismatches

that can be seen among the parameters. Hence, more structural optimizations are needed to find the best structural match for the VF…Ne cluster.

Figure II.1: Predicted structure for VF…Ne dimer

Table II.2: Comparison of the experimental and predicted spectroscopic parameters for VF…Ne molecular cluster

Parameter	Experimental constants for VF…Ne	Predicted constants for VF…Ne
A / MHz	11041.5(8)	10579.1
B / MHz	2845.9077(21)	2625.2
C / MHz	2302.2822(21)	2146.2
Δ_J / MHz	0.15953(20)	
Δ_{JK} / MHz	5.9336(20)	
Δ_K / MHz	-142.52(74)	
δ_J / kHz	35.818(68)	
κ	-0.876	
P_{aa}/ amu Å^2	175.6612(37)	190.1
P_{bb}/ amu Å^2	43.8510(37)	45.4
P_{cc}/ amu Å^2	1.9197(37)	2.4
μ_a/ D	Strong	1.0
μ_b/ D	Strong	1.2
μ_c/ D	Weak	0.5
RMS/ kHz	1.8	
# of lines	10	

II. II). References

[1] Z. Kisiel, J. Kosarzewski, B. A. Pietrewicz, L. Pszczółkowski, Electric dipole moments of the cyclic trimers $(H_2O)_2HCl$ and $(H_2O)_2HBr$ from Stark effects in their rotational spectra. *Chem. Phys. Lett.* **2000**, 325, 523-530.

[2] Z. Kisiel, "PROSPE–Programs for Rotational Spectroscopy" available at http://info.ifpan.edu.pl/~kisiel/prospe.htm, accessed June **2009**.

[3] G. G. Brown, B. C. Dian, K. O. Douglass, S. M. Geyer, S. T. Shipman, B. H. Pate, A broadband Fourier transform microwave spectrometer based on chirped pulse excitation. *Rev. Sci. Instrum.* **2008**, 79, 053103.

[4] K. W. Hillig, J. Matos, A. Scioly, R. L. Kuczkowski, $(N_2O)_2{\cdot}SO_2$: Rotational spectrum and structure of the first van der Waals trimer containing sulfur dioxide. *Chem. Phys. Lett.* **1987**, 133, 359

[5] J. J. Newby, M. M. Serafin, R. A. Peebles, S. A. Peebles, Rotational spectrum, structure and modeling of the OCS–CS_2 van der Waals dimer. *Phys. Chem. Chem. Phys.* **2005**, 7, 487-492.

[6] J. Zhang, M. Dolg, ABCluster: The Artificial Bee Colony Algorithm for Cluster Global Optimization. *Phys. Chem. Chem. Phys.* **2015**, 17, 24173-24181.

[7] J. Zhang, M. Dolg, Global Optimization of Rigid Molecular Clusters by the Artificial Bee Colony Algorithm. *Phys. Chem. Chem. Phys.* **2016**, 18, 3003-3010.